

ABSTRACT

Title of dissertation: COUPLED OSCILLATOR ARRAYS:
DYNAMICS AND INFLUENCE
OF NOISE

ABDULRAHMAN ALOFI
2021

Dissertation directed by: Professor Balakumar Balachandran
Department of Mechanical Engineering

Coupled oscillator arrays can be used to model several natural systems and engineering systems including mechanical systems. In this dissertation work, the influence of noise on the dynamics of coupled mono-stable oscillators arrays is investigated by using numerical and experimental methods. This work is an extension of recent efforts, including those at the University of Maryland, on the use of noise to alter a nonlinear system's response. A chain of coupled oscillators is of interest for this work. This dissertation research is guided by the following questions: i) how can noise be used to create or quench spatial energy localization in a system of coupled, nonlinear oscillators? and ii) how can noise be used to move the energy localization from one oscillator to another? The coupled oscillator systems of interest were harmonically excited and found experimentally and numerically to have a multi-stability region (MR) in the respective frequency response curves. Relative to this region, it has been found that the influence of noise depends highly on the excitation frequency location in the MR. Near either end of the MR, the oscillator

responses were found to be sensitive to noise addition in the input and it was observed that the change in system dynamics through movement amongst the stable branches in the deterministic system could be anticipated from the corresponding frequency response curves. The system response is found to be robust to the influence of noise as the excitation frequency is shifted toward the middle of the MR. Also, the effects of noise on different response modes of the coupled oscillators arrays were investigated. A method for predicting the behavior is based on so-called basins of attractions of high dimensional systems. Through the findings of this work, many unique noise influenced phenomena are found, including spatial movement of an energy localization to a neighboring oscillator, response movement gradually up the energy branches, and generation of energy cascades from a localized mode.

COUPLED OSCILLATOR ARRAYS:
DYNAMICS AND INFLUENCE OF NOISE

by

Abdulrahman Alofi

Dissertation submitted to the Faculty of the Graduate School of the
University of Maryland, College Park in partial fulfillment
of the requirements for the degree of
Doctor of Philosophy
2021

Advisory Committee:

Professor Balakumar Balachandran, Chair and Advisor

Professor Amr Baz, Department of Mechanical Engineering

Professor Abhijit Dasgupta, Department of Mechanical Engineering

Professor Nikhil Chopra, Department of Mechanical Engineering

Professor Sung Lee, Department of Aerospace Engineering (Dean's Representative)

© Copyright by
Abdulrahman Alofi
2021

Dedication

To my parents, my wife and my two little kids

Acknowledgments

First and foremost, I would like to thank my advisor, Professor Balakumar Balachandran for providing me this special opportunity to pursue my Ph.D. and to work on this exciting project. He has always been there if I needed help and guided me throughout the whole years, and never hesitated to provide the help.

I would like to express my appreciation and deepest gratitude to Professor Amr Baz, Professor Abhijit Dasgupta, Professor Nikhil Chopra and Professor Sung Lee for accepting to be a part of the committee and taking the time to review my work. I have learned a lot from my interactions with them and the courses they have taught me.

I would like to thank my parents for all of the unconditional support provided over the years. They made me recognize my own potential and encouraged me to always have the ambition to be the best. Also, special thanks to my beloved wife for her patience and love. She always understood my circumstances and provided me the support that I needed. Thanks as well for my two little kids. They are simply creating happiness in my life. Thanks also to the rest of my family, who encouraged me and gave me their affection.

I would like to thank all of my friends and colleagues at UMD. I always received valuable help from them, and enjoyed the discussions on our free time. I would like to show my appreciation to them by listing their names: Gizem Acar; Xianbo Liu; Lautaro Cilenti; Xie Zheng; Vipin Agarwal; Guanjin Wang; Celeste Poley; Thomas Breunung; Preethi Ravula; Saliou Telly; Randall Kania; Abu Bockarie

Kebbie-Anthony; Nishant Nemani; and Samarpan Chakraborty. I would like to thank as well my friend Mohammed Fayed for his kind friendship and for the nice time spent with him.

Finally, I would like to thank King Fahd University of Petroleum and Minerals for sponsoring my Ph.D study. Also, I am grateful for the support received from NSF for the grant No. CMMI1760366..

Table of Contents

Dedication	ii
Acknowledgements	iii
Table of Contents	iii
List of Tables	v
List of Figures	vi
1 Introduction	1
1.1 Background and Motivation	1
1.1.1 Problem of Interest	1
1.1.2 Literature Review	3
1.2 Overall Goal and Specific Objectives	7
1.3 Organization of Proposal	7
2 Introduction and Background	9
2.1 System Modeling	9
2.2 Experimental Setup	11
2.3 Duffing Oscillator	12
2.4 Frequency Response Curves for Oscillator Arrays	19
2.5 Natural Frequencies and Mode Shapes	22
2.6 Nonlinear Modes	24
3 Effects of Noise in the Multi-stability Region of Coupled Oscillator Arrays	28
3.1 Experimental Setup	28
3.2 Numerical Scheme	31
3.3 Results and Discussion	33
3.3.1 Influence of Noise Near the Left Boundary of the Multi-Stability Region	33
3.3.2 Influence of Noise Near the Right Boundary of the Multi-Stability Region	38
3.3.3 Basins of Attraction	41

4	Effects of Noise on Different Response Modes of Coupled Oscillator Arrays	45
4.1	Experimental Setup	45
4.1.1	Two Oscillators	45
4.1.2	Three Oscillators	49
4.2	Effects of Noise on Different Modes of Coupled Oscillator Arrays . . .	53
4.2.1	Near the Left End of the Multi-Stability Region	53
4.2.1.1	Two oscillators	53
4.2.1.2	Three oscillators	58
4.2.2	Near the Right End of the Multi-Stability Region	62
4.2.2.1	Two Oscillators	62
4.2.2.2	Three Oscillators	64
4.3	Basins of Attraction	65
4.4	Effects of Coupling Strength on System Response	66
4.5	Effects of Increase in Number of Oscillators in an Array	69
5	Noise Based Control of System Energy of Coupled Oscillator Arrays	73
5.1	Influence of Noise Near MR Boundaries	73
5.2	Noise Induced Response Energy Level Increase	76
5.3	Noise Induced Spatial Movement of an Energy Localization	80
5.4	Influence of Noise on a Localized Mode and an Anti-localized Mode .	83
6	Summary and Recommendations for Future Work	88
6.1	Summary	88
6.2	Recommendations for Future Work	90
	Bibliography	92

List of Tables

2.1	Experimental results for system parameter values of a single oscillator.	16
3.1	Experimental results for the parameter values	30
4.1	First oscillator parameters obtained from experimental data given in Figure 4.2	48
5.1	First oscillator parameters obtained by matching the results from the quasi-static frequency sweep shown in Figure 5.3.	77

List of Figures

2.1	A coupled oscillator array in a free-free or in-line arrangement.	10
2.2	Experimental setup of in-line arrangement of coupled oscillators.	12
2.3	Potential energy of a representative softening Duffing oscillator obtained by using $E(x) = \frac{\omega_{n0}^2}{2}x^2 + \frac{\beta}{4}x^4$	13
2.4	Potential energy of a representative hardening Duffing oscillator obtained by using $E(x) = \frac{\omega_{n0}^2}{2}x^2 + \frac{\beta}{4}x^4$	13
2.5	Frequency response curve for a representative softening Duffing oscillator based on equation (2.3).	15
2.6	Frequency response curve for a representative hardening Duffing oscillator based on equation (2.3).	16
2.7	Basin of attraction of responses of a softening oscillator given by equation (2.3) for $\omega=34.86$ rad/s.	17
2.8	Basin of attraction of responses of a softening oscillator given by equation (2.3) for $\omega=35.39$ rad/s.	18
2.9	Basin of attraction of responses of a hardening oscillator given by equation (2.3) for $\omega=34.86$ rad/s.	18
2.10	Basin of attraction of responses of a hardening oscillator given by equation (2.3) for $\omega=36.72$ rad/s.	19
2.11	All solution branches for the array of equation (2.5).	21
2.12	Mode shapes of the coupled oscillators array	23
2.13	Nonlinear modes for the coupled oscillator array.	26
2.14	Localized nonlinear modes	27
3.1	Quasi-static frequency sweep for an array of two coupled oscillators.	29
3.2	Time series of the responses of the array system with two coupled oscillators.	31
3.3	Experimental results for harmonic excitation frequency near the left end of the MR.	35
3.4	Numerical results for harmonic excitation frequency near the left end of the MR.	36
3.5	Experimental results obtained when the harmonic excitation frequency is near the right end of the MR.	39

3.6	Numerical results obtained when the harmonic excitation frequency is near the right end of the MR.	40
3.7	Basin of attraction for the system near the left boundary of the MR .	42
3.8	Basins of attraction for the system near the right boundary of the MR.	43
4.1	Time series of the responses of the two coupled oscillators.	46
4.2	Frequency responses of the two coupled oscillators.	47
4.3	Matching of the experimental results of the first oscillator shown in Figure 4.2 (blue) with the analytical approximation for the parameters given in Table 4.1 (black).	49
4.4	Time series of the responses for the array with three coupled oscillators	51
4.5	Frequency response of the system with three coupled oscillators. . . .	52
4.6	System modes for (a) first oscillator and (b) second oscillator.	54
4.7	Experimental results for the effects of noise on different modes near the left boundary of MR of the two coupled oscillators arrays shown in Figure 4.2.	56
4.8	Numerical results for the effects of noise on different modes near the left boundary of MR for the array with two coupled oscillators shown in Figure 4.2.	57
4.9	Modes of interest of the system.	59
4.10	Experimental results for the effects of noise on different modes near the left boundary of MR for the array with three coupled oscillators shown in Figure 4.5.	60
4.11	Numerical results for the effects of noise on different modes near the left boundary of MR for the system with three coupled oscillators arrays. The parameter values are based on Table 4.1.	61
4.12	Experimental results for the effects of noise on different modes near the right boundary of MR for the system of two coupled oscillators shown in Figure 4.2.	63
4.13	Experimental results for the effects of noise on different modes near the right boundary of MR for the system of three coupled oscillators shown in Figure 4.5.	65
4.14	Basins of attraction for the system of three coupled oscillators.	67
4.15	Effects of coupling increase on the four response branches of the set of two coupled oscillators for the parameters provided in Table 4.1. . .	69
4.16	Bifurcation sets in the (ω, α) plane for the system of two coupled oscillators with the parameters listed in Table 4.1.	70
4.17	Effects of noise on an oscillator in a state of low amplitude oscillations.	72
4.18	Phase space plots for the selected modes in Figure 4.17.	72
5.1	Numerical results for the effects of noise on 21 hardening Duffing oscillators for the parameters listed in Table 2.1.	74
5.2	Numerical results for the effects of noise on 21 softening Duffing oscillators for the parameters listed in Table 2.1.	75

5.3	Experimental results for noise induced gradual energy increase in a set of two coupled oscillators.	78
5.4	Numerical results for noise induced gradual energy increase in a set of two oscillators.	79
5.5	Experimental results for noise induced spatial movement of energy in a set of two coupled oscillators.	81
5.6	Numerical results for noise inducing spatial movement of energy in a set of two coupled oscillators.	82
5.7	Influence of noise on a LM near the left boundary of MR ($\omega=34.90$ rad/s).	84
5.8	Noise is stopped at different time instants in Figure 5.7 inducing increase in the number of oscillators transitioning to a state of high amplitude oscillations.	85
5.9	Influence of noise on an ALM near the right boundary of MR ($\omega=36.72$ rad/s).	87

Chapter 1: Introduction

In this chapter, the author outlines the background and motivation for this work, the problem of interest, the literature review, the overall goals, and discusses the proposal organization.

1.1 Background and Motivation

1.1.1 Problem of Interest

It is of interest to this work to understand the influence of noise on the dynamics of coupled oscillator arrays. In the past, noise has been considered as an undesirable source of energy, and systems have been designed to overcome any possible negative outcomes due to noise. Thanks to the advances in understanding phenomena such as stochastic resonance [1], noise nowadays might be considered as a beneficial source of energy that helps in improving or controlling the system dynamics. In this work, the type of noise considered in the numerical study is a random process, white Gaussian noise, and in the experiments is a band-limited white noise.

Coupled oscillator arrays have rich nonlinear dynamics. For example, Papan-

gelo *et al.* [2] stated that for both linear and cyclic chain of coupled oscillator arrays, the response energy of such systems can be studied through clusters of branches in the corresponding frequency response. Then, each branch corresponds to a certain number of oscillators that have high amplitude oscillations. Previous efforts on introducing noise into such systems revealed the possibility for creating or destroying localization with noise [3, 4]. This work can be viewed as continuation in the spirit of the previous efforts. Here, for the first time, to the best of the author's knowledge, the influence of noise to induce a transition between different energy branches corresponding to high amplitude oscillations is discussed.

Here, the influence of noise on an array with two to three oscillators are first explored to get an insight into the behavior of an array with a large number of oscillators. As part of the study, a combination of numerical and experimental approach is used. Different phenomena of interest include response movement up or down in the response energy branches, and movement of the spatial localization from one oscillator to another. The building blocks for the array are monostable Duffing oscillators, and these oscillators are coupled through linear springs. The aforementioned phenomena are also numerically explored with arrays with a large number of oscillators.

This work is expected to be of interest to systems such as energy harvesting devices [5] and rotary systems [6].

1.1.2 Literature Review

In small scale devices, systems vibrate at low amplitudes, wherein any small disturbance may affect the system dynamics [7]. In these systems, one usually encounters noise that is either derived from the surrounding environment or inherent to the system [8]. Even though the noise levels may be low, they can alter the system dynamics in a noticeable way. For instance, small fluctuations have been shown to move systems with metastable states escape from a local stable state [9]. Also, the presence of noise may induce a transition between a limit cycle and a fixed point of a system [10]. Moreover, noise may induce a period doubling cascade, resulting in chaos [11]. If not designed or addressed properly, not only will the performance of these systems be affected [12] but there may be other undesirable consequences including system malfunction [13].

In previous studies [14–17], researchers have investigated the problem of interest from a different perspective. Instead of building systems that are robust to noise, they considered noise as a beneficial source of energy that could be exploited for enhancing the system dynamics. In recent studies with nonlinear systems, it has been shown that noise can be utilized to change dynamic system response. For example, noise has been used to stabilize nonlinear systems [18–20]. Also, Gao *et al.* [11] showed that noise can be used to control chaos in nonlinear systems. Moreover, through biological studies, it has been shown that introducing noise can be beneficial for human systems including heart function [21], human hearing [22, 23], and nervous system [24–26]. In addition, enhanced response features have been obtained

by utilizing noise in various mechanical [27–29] and chemical systems [30–32].

In the field of mechanical systems, as an atomic force microscope (AFM) operates in the tapping mode, a situation of interest occurs when there is zero normal speed contact, also known as grazing [33]. It has been reported that period doubling can exist and could be used as a new way to locate the grazing impacts [34,35]. Building on this work, Chakraborty and Balachandran [36] showed through experimental and numerical studies that the addition of white Gaussian noise can help the system to move from a no contact state to a contact state, wherein the associated response is close to that of a period-doubled orbit.

It is well known that for an inverted pendulum, the system has an unstable equilibrium point at the upright position [37]. A number of researchers have used control schemes [38, 39] or high-frequency excitations [40, 41] in their efforts for stabilizing the upright position. By using a different approach, Perkins and Balachandran [42] showed that noise can be used for stabilizing the upright position when combined with a harmonic excitation. In addition, noise can force the pendulum into rotation, which could be used for energy harvester applications [43].

With the Duffing oscillator, noise has been used to change the system dynamics [44, 45]; depending on the application, some of these changes can be useful for the system. Agarwal and Balachandran [46] showed that addition of noise can be used to move the system away from an aperiodic response, including the possibility to move the system from a chaotic motion into a fixed point of the unforced system. Furthermore, noise has been used to reduce the hysteresis region by moving the jump-up and the jump-down frequencies close to each other as well as for destroying

the hysteresis region [47].

In the 1980s, intrinsic localized modes (ILMs) were introduced as a new class of energy localization [48–51]. In contrast to the Anderson localization [52, 53], wherein the localization is due to the introduction of a defect or an impurity thus creating a near-periodic system, ILMs can occur in perfectly periodic lattices and the localization can potentially occur at any position [54]. Two important elements for creation of ILMs are nonlinearity and discreteness [55]. These elements along with weak coupling allow for the existence of ILMs in nonlinear systems [49]. Some examples of systems in which ILMs occur are photonic crystals [50, 56], antiferromagnet lattice [57], granular media [58–61], and coupled oscillator arrays [62–64].

Coupled oscillator arrays have received considerable interest during the last two decades. For example, Sato *et al.* [65] carried out a study on a micromechanical oscillator array, and they reported a localization locking effect. By adjusting the coupling between the oscillators, Kimura *et al.* [66] introduced a new means for manipulating ILMs. In a different study, Kimura *et al.* [67] created an experimental system to study ILMs.

The complexity of dynamics of coupled oscillator arrays makes these systems quite appealing to study. The building blocks for the array can be monostable Duffing oscillators [68, 69], wherein each oscillator has a single stable equilibrium position. The system can be more complex, if one were to consider the building blocks as bi-stable Duffing oscillators [70], in which case, each oscillator has two stable equilibrium points and an unstable one.

To provide a glimpse into the dynamics of arrays with monostable and bi-

stable oscillators, Papangelo *et al.* [2,71] studied coupled oscillator arrays comprised of monostable and bi-stable oscillators. In the case of an array with monostable oscillators, the system response state can go into spatially localized responses. The degree of localization ranges from being in one oscillator to the extreme case wherein all the oscillators vibrate at a high energy level. For the array with bi-stable oscillators, the researchers were able to mimic a snaking pattern in the solution structure, which is relevant to many continuous systems [72–74]. The response picture is complex, and it is composed of isolas (closed solution branches) and similar states that represent different energy levels.

Since coupled oscillator arrays have rich nonlinear dynamics that is sensitive to small perturbations, attractive results have been shown by utilizing noise in those systems. For instance, Ramakrishnan and Balachandran [75] showed that noise is capable of strengthening and attenuating localizations in coupled oscillator arrays. Also, Perkins *et al.* [3] carried out experimental and numerical investigations on coupled cantilever beam arrays. It was shown that localization can be destroyed, created or even shifted to a different spatial location under the influence of noise. While the results are appealing, the subject of interest is still in its infancy. One is still unclear on the level and/or duration of noise needed to change the system dynamics. Also, depending on the nonlinearity and interplay with noise, there can be new ways to positively use the noise to alter a system's response; these aspects remain to be explored. Moreover, even with recognition of the potential use of noise for control, additional studies are needed to make the best use of noise.

1.2 Overall Goal and Specific Objectives

The overall goal of this work is to continue the recent experimental and numerical efforts in the group's prior works on exploiting the interplay between noise and nonlinearity in mechanical and structural systems. The focus of this work is mainly on coupled oscillator arrays arranged in a linear or in-line configuration (free-free boundary conditions). These systems are excited by harmonic excitations and include noise inputs in some cases. There are four specific objectives for this dissertation work. They are as follows:

1. To understand how noise can be used to create a localization in a coupled array of nonlinear oscillators with different numbers of oscillators
2. To examine how noise can be used to quench a spatial energy localization in a coupled array of nonlinear oscillators with different numbers of oscillators
3. To investigating how to move a spatial localization from one oscillator to another in an array under the influence of noise
4. To develop appropriate means to analyze responses of arrays of different sizes

1.3 Organization of Proposal

The rest of the proposal is organized as follows. In Chapter 2, the system modeling is present along with the experimental setup. A background on the Duffing oscillator is presented as it represents important information for the coupled oscil-

lator arrays. The frequency response curve along with the natural frequencies and the nonlinear modes of the system are presented. In Chapter 3, when the harmonic excitation frequency is close to the boundaries of the multi-stability region of the coupled oscillators arrays, the influence of noise on the system response is discussed. A method for exploring how the oscillators respond to disturbances is presented using basins of attractions. Following that, in the next chapter, the effects of noise on different modes are investigated. In addition, the effects of coupling strength and the number of oscillators on how an oscillator responds to noise are explored. In Chapter 5, different phenomena are presented for the coupled oscillator arrays. To close, the work is summarized and recommendations for future work are outlined, in the last chapter.

Chapter 2: Introduction and Background

In this chapter, the author presents the model that is used for the study. In addition, a brief background on the Duffing oscillator is provided. The results are presented in the form of the frequency response curves, natural frequencies and mode shapes, and nonlinear modes.

2.1 System Modeling

In the considered model, there are N identical oscillators that are interconnected through linear springs. Each oscillator has a linear stiffness as well as a cubic stiffness. The oscillator array has free-free boundary conditions (i.e., the two oscillators at the boundary are only connected from one side and free from the other side). A schematic for the model is shown in Figure 2.1. The governing equations of motion for the system can be written as shown next:

$$\begin{aligned} m \frac{d^2 x_1}{dt^2} + c \frac{dx_1}{dt} + k_l x_1 + k_{nl} x_1^3 + k_c(x_1 - x_2) &= f_1(t) \\ m \frac{d^2 x_n}{dt^2} + c \frac{dx_n}{dt} + k_l x_n + k_{nl} x_n^3 + k_c(2x_n - x_{n+1} - & \\ x_{n-1}) &= f_n(t), \quad \text{for } 2 \leq n \leq N - 1 \\ m \frac{d^2 x_N}{dt^2} + c \frac{dx_N}{dt} + k_l x_N + k_{nl} x_N^3 + k_c(x_N - x_{N-1}) &= f_N(t) \end{aligned} \tag{2.1}$$

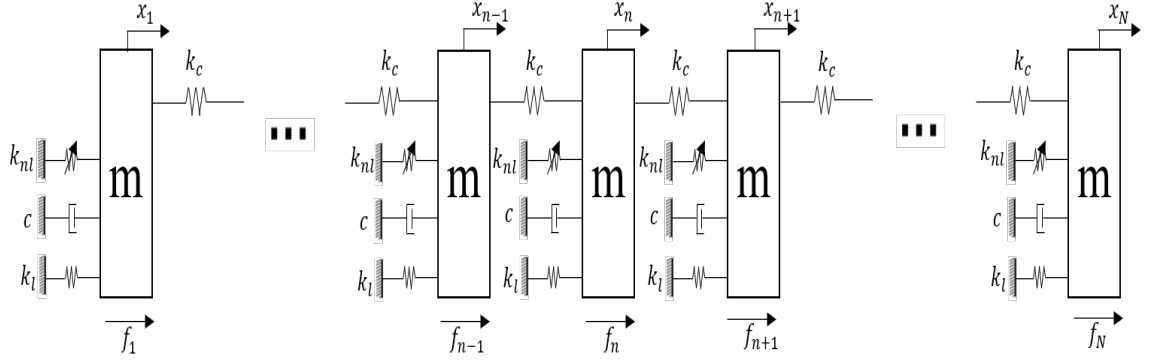


Figure 2.1: A coupled oscillator array in a free-free or in-line arrangement.

Here, x_n is the displacement of the n^{th} oscillator, m is the oscillator mass, c is the damping coefficient, k_l and k_{nl} are the linear and the nonlinear stiffness coefficients, respectively, k_c is the linear coupling coefficients, f_n is the force acting on the n^{th} oscillator. This forcing is composed of a deterministic component in the form of a harmonic excitation and a stochastic input. In the stochastic input, which is in the form of white Gaussian noise ($\hat{\sigma} \dot{W}(t)$), $\hat{\sigma}$ is the noise intensity, and $W(t)$ is the Wiener process. With the harmonic excitation given by $\hat{a} \cos(\omega t)$, \hat{a} is the forcing amplitude and ω is the forcing frequency. Introducing the following parameters

$$\zeta = \frac{c}{2\sqrt{mk_l}}, \quad \omega_{n0}^2 = \frac{k_l}{m}, \quad \beta = \frac{k_{nl}}{m}, \quad \alpha = \frac{k_c}{m}, \quad a = \frac{\hat{a}}{m}, \quad \text{and } \sigma = \frac{\hat{\sigma}}{m},$$

and assuming that the forcing on all the oscillators to have similar phase and amplitude values ($f_n = f$), equation (2.1) can be rewritten as follows:

$$\begin{aligned}
\ddot{x}_1 + 2\zeta\omega_{n0}\dot{x}_1 + \omega_{n0}^2x_1 + \beta x_1^3 + \alpha(x_1 - x_2) &= a \cos(\omega t) + \sigma \dot{W}(t) \\
\ddot{x}_n + 2\zeta\omega_{n0}\dot{x}_n + \omega_{n0}^2x_n + \beta x_n^3 + \alpha(2x_n - x_{n-1} - & \\
x_{n+1}) &= a \cos(\omega t) + \sigma \dot{W}(t), \quad \text{for } 2 \leq n \leq N - 1
\end{aligned} \tag{2.2}$$

$$\ddot{x}_N + 2\zeta\omega_{n0}\dot{x}_N + \omega_{n0}^2x_N + \beta x_N^3 + \alpha(x_N - x_{N-1}) = a \cos(\omega t) + \sigma \dot{W}(t)$$

Here, an overdot indicates the derivative with respect to time t . The parameters of the system are determined from the experimentally obtained frequency-response curves for the system shown in Figure 2.2, as done in the group's prior studies (e.g., [47]).

2.2 Experimental Setup

In Figure 2.2, the experimental setup that has been used to perform the study is shown. A spring coupled set of metallic cantilever oscillators is secured to a base, which is connected to an electrodynamic shaker used to generate the excitation. Permanent magnets are used to realize the nonlinear spring characteristics of each oscillator. For each cantilever oscillator, one of the magnets is located on top of the cantilever, while the other is fixed on a plate above the free end. The spacing between this pair of magnets can be adjusted to realize an oscillator with a hardening or softening characteristic. LabVIEW software is used to generate a combined excitation consisting of harmonic and noise components. The excitation input is filtered by using a low pass filter so that only frequencies that are below a chosen cutoff frequency are allowed. The transverse deflections of the cantilevers in the

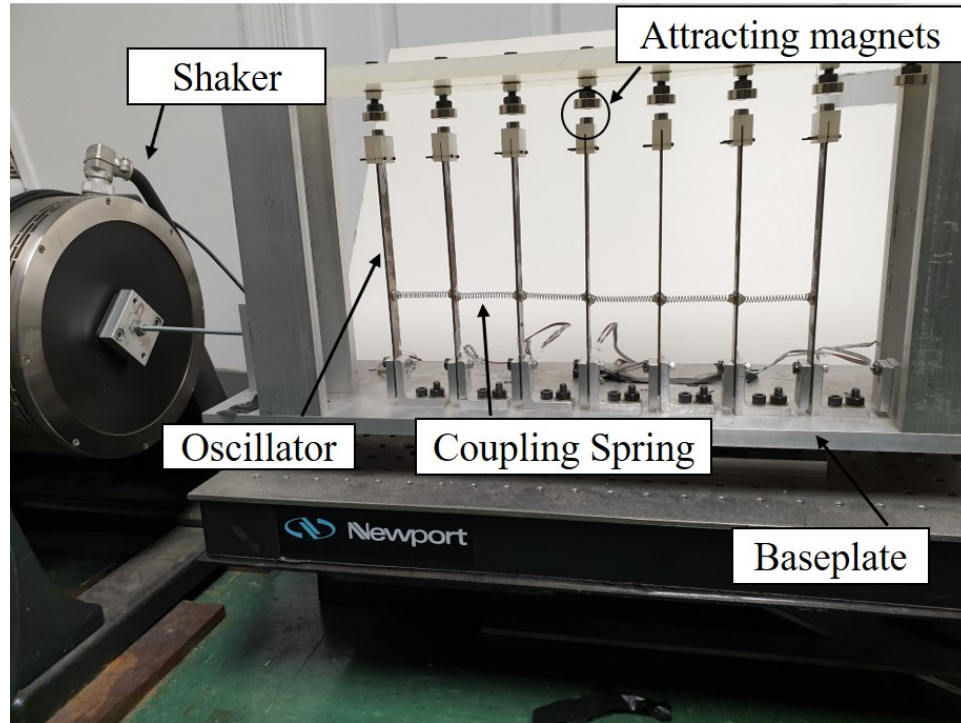


Figure 2.2: Experimental setup of in-line arrangement of coupled oscillators.

excitation direction are measured by using strain gauges that are attached close to each cantilever's base. LabVIEW software is also used for data acquisition of the strain gauge signals.

2.3 Duffing Oscillator

Since the Duffing oscillator represents the main oscillator component in equations (2.2), exploring the effects of parameter changes on the response of a single oscillator can give one a glimpse into the behavior of the full system. Considering only a single beam oscillator, the equation of motion reduces to the following Duffing equation:

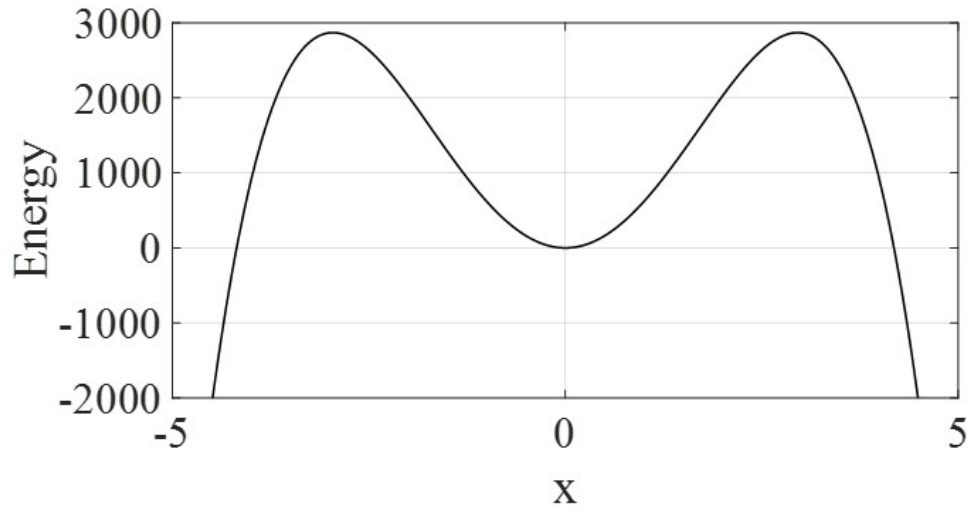


Figure 2.3: Potential energy of a representative softening Duffing oscillator obtained by using $E(x) = \frac{\omega_{n0}^2}{2}x^2 + \frac{\beta}{4}x^4$. The parameter values are similar to those given in Section 5.3 and listed in Table 2.1.

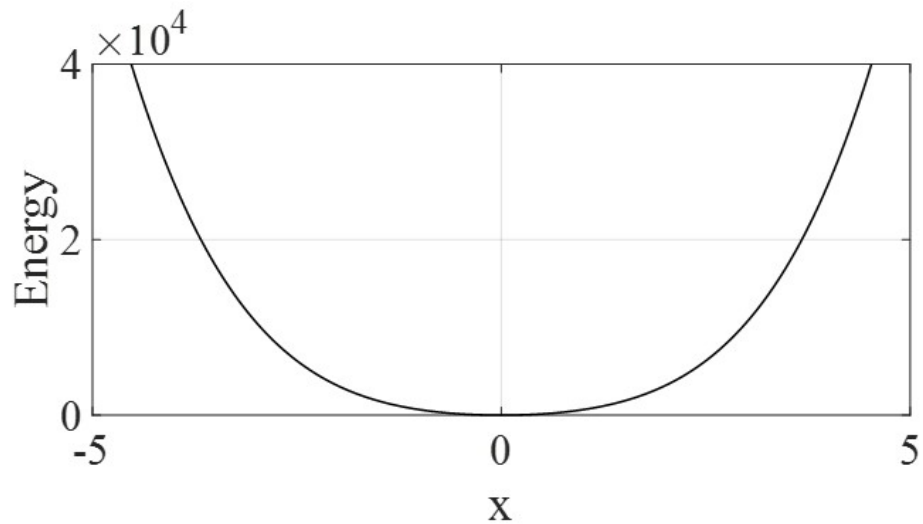


Figure 2.4: Potential energy of a representative hardening Duffing oscillator obtained by using $E(x) = \frac{\omega_{n0}^2}{2}x^2 + \frac{\beta}{4}x^4$. The parameter values are similar to those given in Section 5.3 and listed in Table 2.1.

$$\ddot{x} + 2\zeta\omega_{n0}\dot{x} + \omega_{n0}^2x + \beta x^3 = f(t), \quad (2.3)$$

Here, the forcing $f(t) = F \cos(\omega t)$.

In this work, the author considers mainly systems with a monostable hardening Duffing oscillator with a few cases of a softening monostable Duffing oscillator. For both configurations, the coefficients of x is positive; that is, > 0 . For monostable hardening case, the coefficients of x^3 is > 0 , while for a monostable softening case, this coefficient is < 0 . The energy of the unforced and undamped system for both configurations has a single potential well at the origin resulting corresponding to a stable equilibrium position, as shown in Figure 2.3 and 2.4 for the softening and hardening cases, respectively.

For the forced and damped system, the frequency response curves are shown in Figures 2.5 and 2.6, for the softening and hardening cases, respectively. The parameters are similar to those obtained from the experimental results given in Section 5.3 and summarized in Table 2.1. For certain forcing frequencies, the system has a region with three solutions, two stable periodic solutions (solid branches) and one unstable periodic solution (dashed branch). Due to the dissipation, each stable solution has a basin of attraction, in which trajectories are drawn towards this stable solution.

In order to gain an insight into the coupled oscillator array dynamics, the effects of system parameters on the basins of attraction of the periodic orbits of the single oscillator are studied. To obtain the basins of attraction, equation (2.3) is

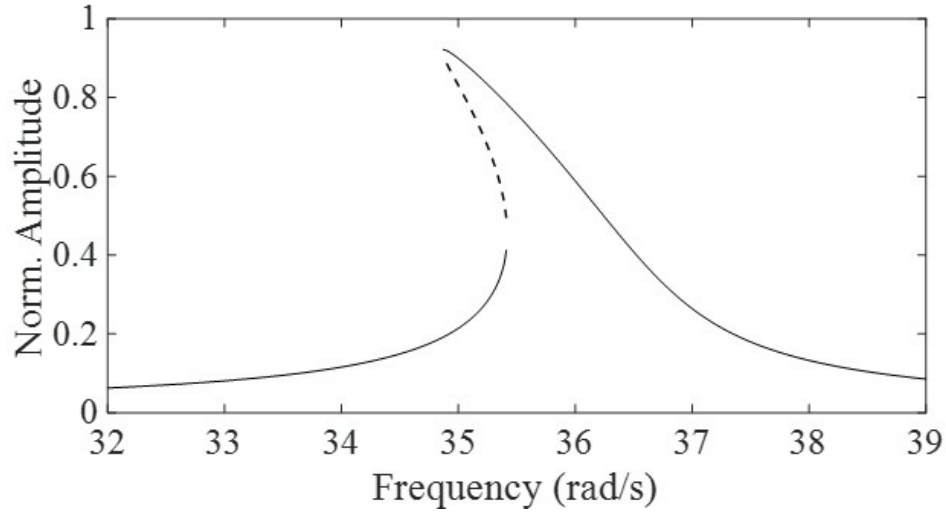


Figure 2.5: Frequency response curve for a representative softening Duffing oscillator based on equation (2.3). The parameters are similar to the obtained experimental values given in Section 5.3 and listed in Table 2.1. A normalized response amplitude is shown on the vertical axis and the excitation frequency is shown on the horizontal axis.

solved by using Matlab built-in function ode45 for a set of initial conditions. For each set of initial conditions, the steady state response ends up in either the high amplitude attractor or the low amplitude attractor. The corresponding results are plotted with a unique color specified for each corresponding attractor region. In Figures 2.7 and 2.8, the author has shown the effects of increasing the excitation frequency in a quasi-static manner on a softening Duffing oscillator, while keeping all of the other parameters fixed. In the figures, there are two attractors, one corresponding to the high amplitude response (small green point) and the other corresponding to the low amplitude response (small black point). Each attractor has an associated basin of attraction (shown in red for the high amplitude one and blue for the low amplitude one) wherein for trajectories initiated inside a basin,

Table 2.1: Experimental results for system parameter values of a single oscillator.

Oscillator 1 (Softening)		Oscillator 2 (Hardening)	
Parameter	Value	Parameter	Value
ω_{n0}	36.22 rad/s	ω_{n0}	33.76 rad/s
β	-150	β	270
F	18	F	18
ζ	0.00745	ζ	0.00717

they are attracted to the corresponding attractor. At $\omega = 34.86$ rad/s, the basin of attraction of the high amplitude response is relatively small compared to the basin of attraction of the low amplitude response, as illustrated in Figure 2.7. As the excitation frequency is increased, the basin of attraction of the high amplitude response increases in size while the basin of attraction of the low amplitude response decreases in size. This

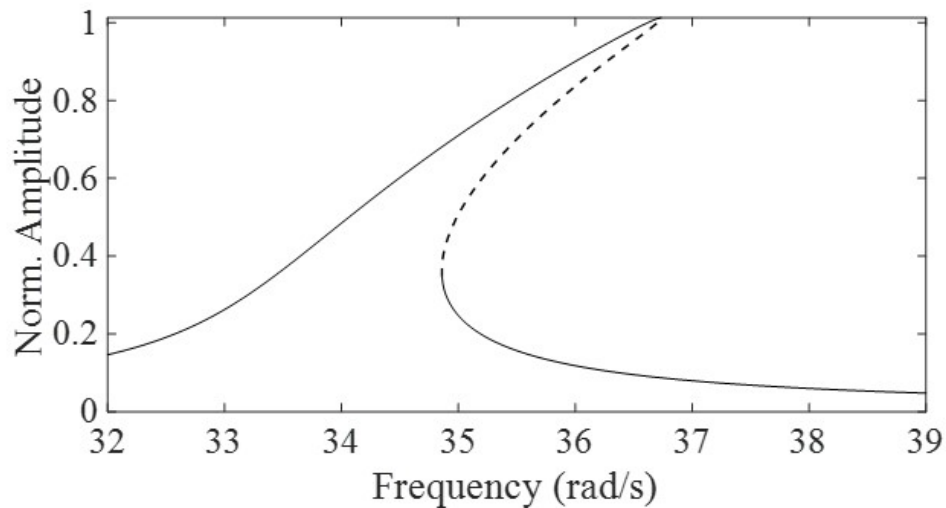


Figure 2.6: Frequency response curve for a representative hardening Duffing oscillator based on equation (2.3). The parameters are similar to the obtained experimental values given in Section 5.3 and listed in Table 2.1. A normalized response amplitude is shown on the vertical axis and the excitation frequency is shown on the horizontal axis.

trend continues until the basin of the high amplitude response reaches its largest size at the end of the hysteresis region, as shown in Figure 2.8 for $\omega = 35.39$ rad/s.

However for the hardening Duffing oscillator, an opposite behavior is observed. For $\omega=34.86$ rad/s , the basin of attraction of the high amplitude response is larger than the size of the basin of attraction of the low amplitude response. As one increases the forcing frequency, the basin of the high amplitude response shrinks in size until it reaches a minimum just before the jump down frequency, as shown in Figure 2.10 for $\omega=36.72$ rad/s.

The previous results are important for understanding the dynamics of the coupled oscillator array, as will be shown in the coming sections.

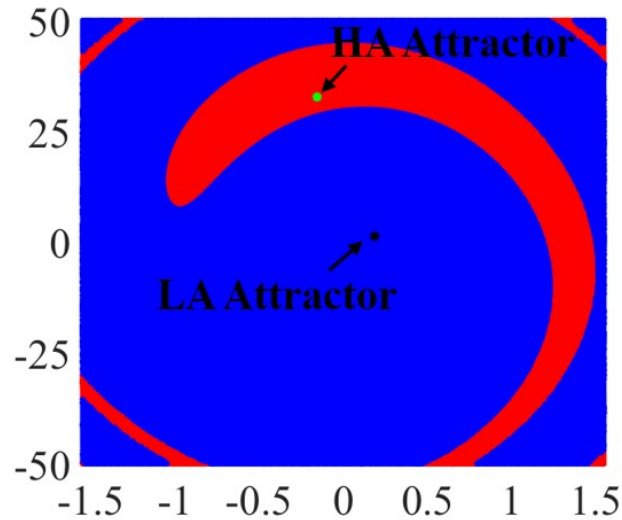


Figure 2.7: Basin of attraction of responses of a softening oscillator given by equation (2.3) for $\omega=34.86$ rad/s. The high amplitude stable response is labelled as the HA attractor and the low amplitude stable response is labelled as the LA attractor in this figure and other similar figures that follow.

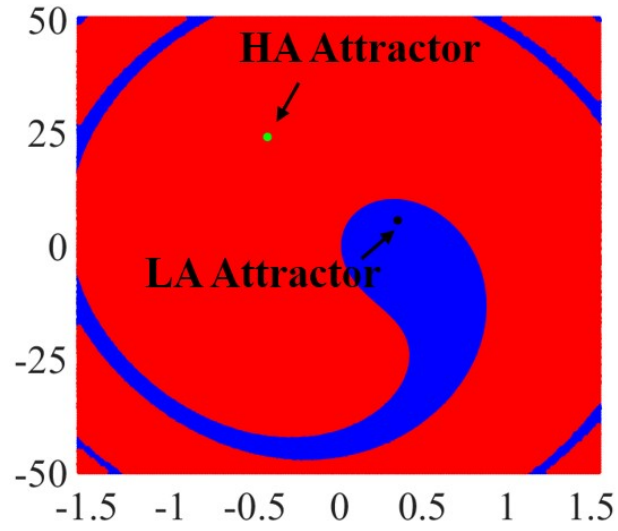


Figure 2.8: Basin of attraction of responses of a softening oscillator given by equation (2.3) for $\omega=35.39$ rad/s.

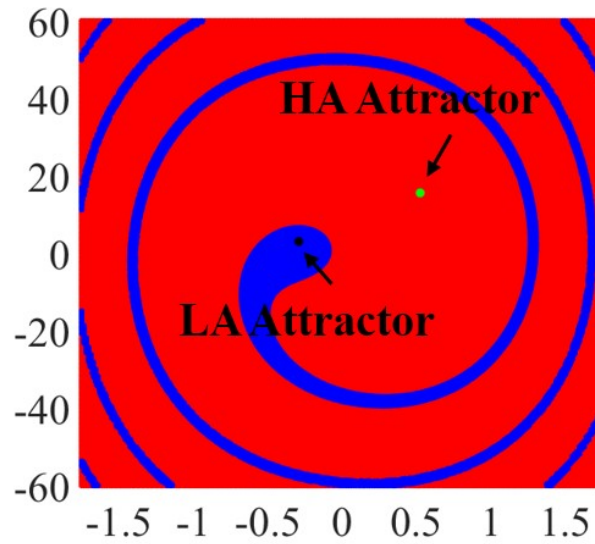


Figure 2.9: Basin of attraction of responses of a hardening oscillator given by equation (2.3) for $\omega=34.86$ rad/s.

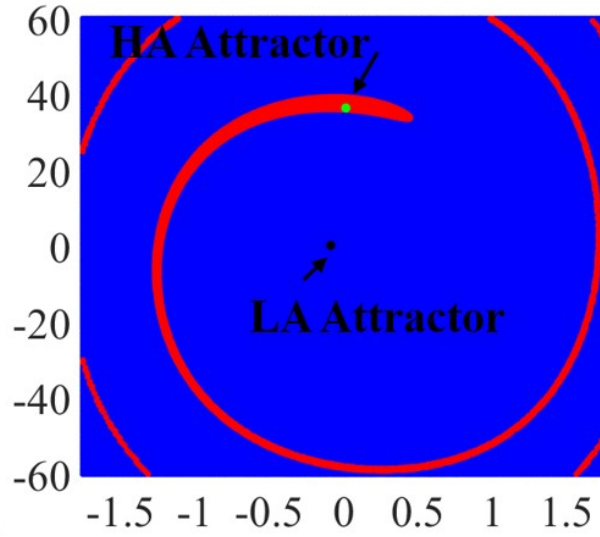


Figure 2.10: Basin of attraction of responses of a hardening oscillator given by equation (2.3) for $\omega=36.72$ rad/s.

2.4 Frequency Response Curves for Oscillator Arrays

To get a clear picture for all available solutions for equation (2.2), the author followed a similar procedure as in earlier work [2]. A harmonic balance method is first used to express the periodic solution of equation (2.2) as follows:

$$x_n = \sum_{m=0}^M [A_{n,m} \cos(m\omega t) + B_{n,m} \sin(m\omega t)] \quad (2.4)$$

Here, ω is the excitation frequency, M is the chosen number of harmonics, $A_{n,m}$ and $B_{n,m}$ are the amplitudes of cosine and sine terms, respectively. After substituting equation (2.4) with only the first harmonic in equation (2.2), the result is the following:

$$\begin{aligned}
(-\omega^2 + \omega_{n0}^2 + \frac{3}{4}\beta|B_1|^2 + \alpha)A_1 + 2\zeta\omega_{n0}B_1 + \frac{3}{4}\beta|A_1|^2A_1 - \alpha A_2 &= 0 \\
(-\omega^2 + \omega_{n0}^2 + \frac{3}{4}\beta|A_1|^2 + \alpha)B_1 - 2\zeta\omega_{n0}A_1 + \frac{3}{4}\beta|B_1|^2B_1 - \alpha B_2 &= a \\
(-\omega^2 + \omega_{n0}^2 + \frac{3}{4}\beta|B_n|^2 + 2\alpha)A_n + 2\zeta\omega_{n0}B_n + \frac{3}{4}\beta|A_n|^2A_n - \\
\alpha(A_{n-1} + A_{n+1}) &= 0, \quad \text{for } 2 \leq n \leq N-1 \\
(-\omega^2 + \omega_{n0}^2 + \frac{3}{4}\beta|A_n|^2 + 2\alpha)B_n - 2\zeta\omega_{n0}A_n + \frac{3}{4}\beta|B_n|^2B_n - \\
\alpha(B_{n-1} + B_{n+1}) &= a, \quad \text{for } 2 \leq n \leq N-1 \\
(-\omega^2 + \omega_{n0}^2 + \frac{3}{4}\beta|B_N|^2 + \alpha)A_N + 2\zeta\omega_{n0}B_N + \frac{3}{4}\beta|A_N|^2A_N - \alpha A_{N-1} &= 0 \\
(-\omega^2 + \omega_{n0}^2 + \frac{3}{4}\beta|A_N|^2 + \alpha)B_N - 2\zeta\omega_{n0}A_N + \frac{3}{4}\beta|B_N|^2B_N - \alpha B_{N-1} &= a
\end{aligned} \tag{2.5}$$

The obtained system of equation is in the form of N algebraic equations with $N + 1$ unknowns. To find all the frequency response branches of equation (2.2), Auto software [76] is used by considering the solution of equation (2.5) as an initial conditions and the excitation frequency ω as the continuation parameter. Equation (2.5) is solved for 5 coupled oscillators array by considering highly localized modes as initial conditions; for example, $(0, 1, 1, 1, 0)$ and $(1, 0, 1, 1, 1)$, where 1 corresponds to a high amplitude oscillator response and 0 corresponds to a low amplitude oscillator response. The system parameters are similar to the obtained experimental results given in Section 4.1.1 and summarized in Table 4.1. The solution branches are plotted in terms of the norm of all x solutions, which is defined by $L^2 = \sqrt{\sum_{n=0}^N A_n^2 + B_n^2}$. This norm is used as a measure of system energy. The frequency response curve for the oscillator array is shown in Figure 2.11. The energy of the system differs from one branch to another. On the upper branch (P5 Mode), the system has the

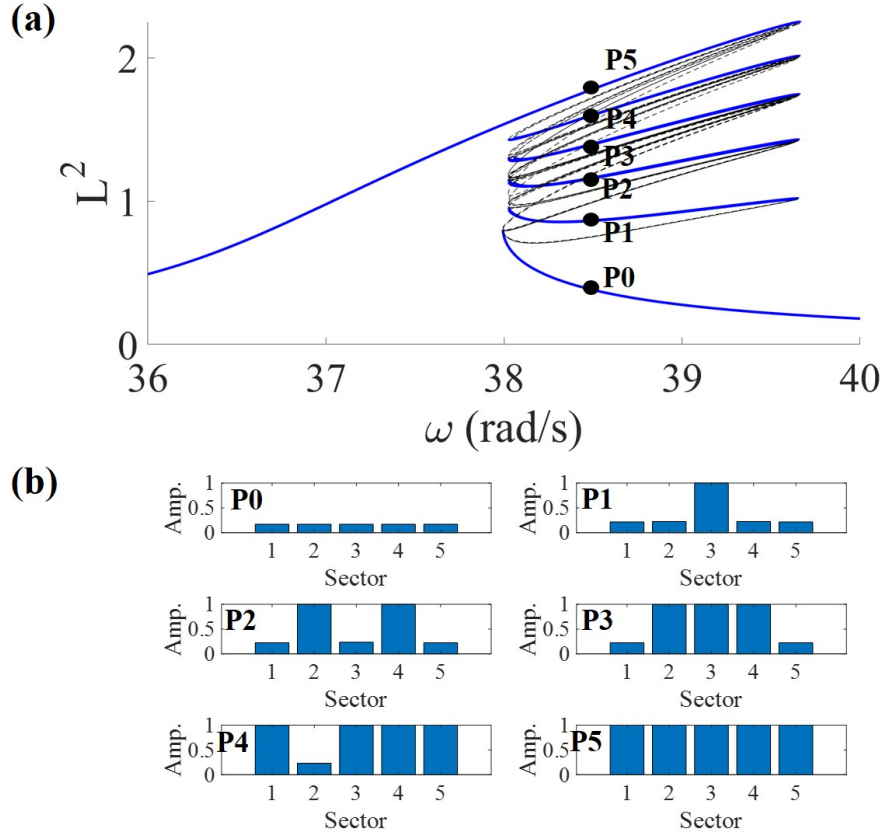


Figure 2.11: All solution branches for the array of equation (2.5): (a) all solution branches and (b) corresponding distribution of responses for branches P0-P5.

highest possible energy at the corresponding excitation frequency, and the energy is equally distributed between the oscillators. Moving to a lower solution branch (P4), one of the oscillators is in a low energy state, and the rest of them are in a high energy state. This pattern continues until one reaches the (P0) mode, in which the system energy has its minimum value, and each of the oscillators has a low amplitude response.

2.5 Natural Frequencies and Mode Shapes

Determining the linear natural frequencies of a system is helpful for characterizing the system responses. Toward this, the conservative, unforced linear system about the zero equilibrium position is first obtained from system (2.2) as follows

$$\begin{aligned} \ddot{x}_1 + \omega_{n_0}^2 x_1 + \alpha(x_1 - x_2) &= 0 \\ \ddot{x}_n + \omega_{n_0}^2 x_n + \alpha(2x_n - x_{n-1} - x_{n+1}) &= 0 \quad \text{for } n = 2, 3, \dots, N-1 \\ \ddot{x}_N + \omega_{n_0}^2 x_N + \alpha(x_N - x_{N-1}) &= 0 \end{aligned} \quad (2.6)$$

The solution of this system has an oscillatory behaviour. Thus, the solution is assumed to have the following trial functions

$$x_n(t) = X_n e^{i\omega t} \quad (2.7)$$

where X_n is the amplitude of the n^{th} oscillator and ω is the linear natural frequency. After substituting equation 2.7 into equation 2.6, the following eigenvalue problem can be obtained:

$$(\mathbf{K} - \omega^2 \mathbf{M})\mathbf{X} = 0 \quad (2.8)$$

where, \mathbf{M} is the $N * N$ identity matrix, \mathbf{X} is $N * 1$ vector of the unknowns X_n , \mathbf{K} is the stiffness matrix, which is defined by

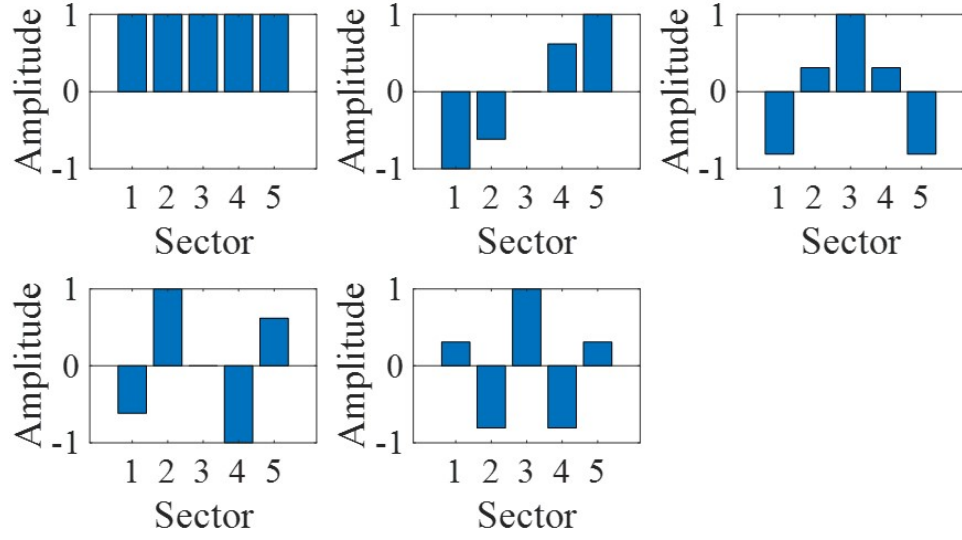


Figure 2.12: Mode shapes of the coupled oscillators array.

$$\mathbf{K} = \begin{bmatrix} \omega_{n_0}^2 + \alpha & -\alpha & 0 & 0 & 0 \\ -\alpha & \omega_{n_0}^2 + 2\alpha & -\alpha & 0 & 0 \\ 0 & -\alpha & \omega_{n_0}^2 + 2\alpha & -\alpha & 0 \\ 0 & 0 & -\alpha & \omega_{n_0}^2 + 2\alpha & -\alpha \\ 0 & 0 & 0 & -\alpha & \omega_{n_0}^2 + \alpha \end{bmatrix},$$

The experimental parameters that are shown in Table 4.1 are chosen for finding the solutions for a coupled array of five oscillators and parameters as in the previous subsection. The linear natural frequencies for the system are obtained as

$$\omega = 37.0000, 37.0052, 37.0187, 37.0354, \text{ and } 37.0489 \text{ rad/s}$$

The corresponding mode shapes are shown in Figure 2.12.

2.6 Nonlinear Modes

To find the nonlinear modes of the system, the concept of nonlinear modes is considered [77, 78] following a procedure that is similar to that used for a cyclic coupled oscillator array [2]. To start the analysis, the unforced conservative system of equation (2.2) is first considered

$$\begin{aligned} \ddot{x}_1 + \omega_{n0}^2 x_1 + \alpha(x_1 - x_2) + \beta x_1^3 &= 0 \\ \ddot{x}_n + \omega_{n0}^2 x_n + \alpha(2x_n - x_{n-1} - x_{n+1}) + \beta x_n^3 &= 0 \quad \text{for } n = 2, 3, \dots, N-1 \\ \ddot{x}_N + \omega_{n0}^2 x_N + \alpha(x_N - x_{N-1}) + \beta x_N^3 &= 0 \end{aligned} \quad (2.9)$$

The solution of equation (2.9) is expressed using only one harmonic as

$$x_n = X_n \exp(i\omega t) + c.c., \quad (2.10)$$

where X_n is a complex valued amplitude and ω is the the nonlinear natural frequency. After substituting equation (2.10) into equations (2.9) and neglecting the higher order terms, the following set of algebraic equations is obtained

$$\begin{aligned} (-\omega^2 + \omega_{n0}^2 + \alpha)X_1 + 3\beta X_1^3 - \alpha X_2 &= 0 \\ (-\omega^2 + \omega_{n0}^2 + 2\alpha)X_n + 3\beta X_n^3 - \alpha(X_{n-1} - & \\ X_{n+1}) &= 0 \quad \text{for } n = 2, 3, \dots, N-1 \\ (-\omega^2 + \omega_{n0}^2 + \alpha)X_N + 3\beta X_N^3 - \alpha X_{N-1} &= 0 \end{aligned} \quad (2.11)$$

The nonlinear modes of the system can be obtained by solving equation (2.11).

The solution of equation (2.11) is found using MANLAB package [79]. The details of which are summarized in [80]. As it can be seen from equations (2.11), the nonlinear modes of the system show the dependence between the amplitude and frequency of the system. For frequency values close to the linear frequencies of the system, the linear modes are considered good initial conditions for equations (2.11). The obtained solution branches are shown in Figure 2.13 with solid blue lines. No bifurcations are detected in all of the five branches. For low amplitudes, the shapes of the nonlinear modes resembles the shapes of the corresponding linear modes. However, as the amplitude increases, the energy gets focused in only a subgroup of the oscillators, while the other oscillators lose the energy gradually. For sufficiently high amplitudes, the energy of the system is completely localized in only a subgroup of the oscillators. The only exception for this scenario happens for the in-phase mode, wherein all the oscillators keep the homogeneity of the mode shape as the amplitude increases. The final shape for the nonlinear modes corresponding to the five linear modes are shown in Figure 2.14 .

To obtain the other nonlinear modes of the system, highly localized solution at high frequency values are considered. Since the oscillators should vibrate at the same frequency at the highly localized modes, the oscillators will either have similar non-zero amplitudes or zero amplitudes. Thus, the three possibilities for each oscillator are $X_n = (-1, 0, 1)$. Toward this, there are $3^5 = 243$ possible mode outcomes. Many of these modes belong to the same family due to the axial symmetry or a change in sign. After reducing the similar modes and the five corresponding modes of the linear modes, only 65 different modes are left. These remaining modes are plotted

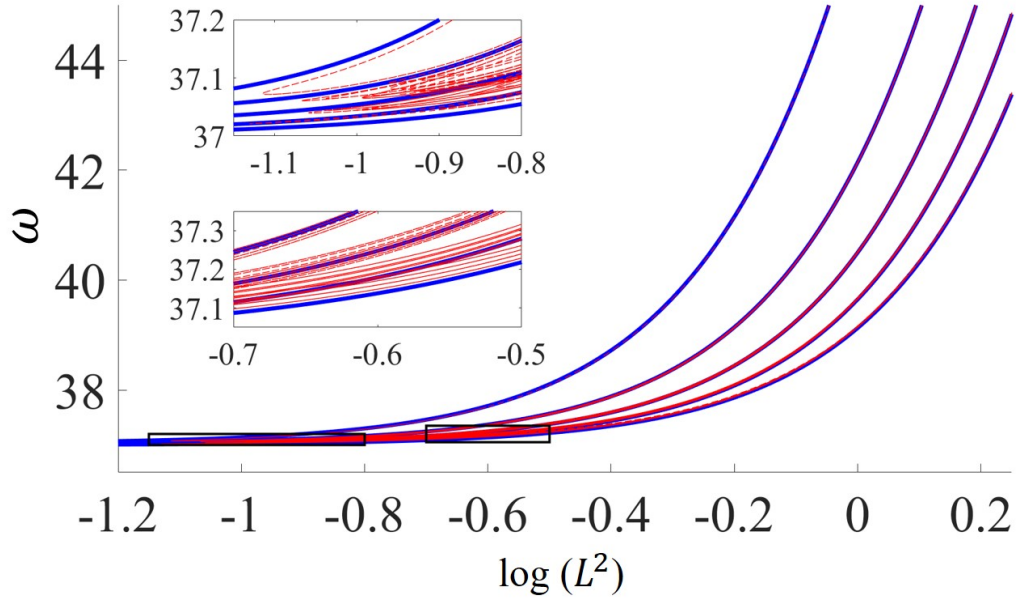


Figure 2.13: Nonlinear modes for the coupled oscillator array. The solid blue lines are the nonlinear modes that are obtained from the linear modes. The dashed red lines are the remaining modes obtained from the localized modes. The starting points of different branches are shown in the top inset. The majority of the branches are shown in the bottom inset.

in Figure 2.13 with dashed red lines. As it can be seen from the top zoomed portion, there is no presence of those modes at low amplitudes. As the amplitude increases more branches are born. Also, the majority of these branches bifurcate into one or more than one branches. The bottom zoomed portion shows the majority of these branches. Seven samples of the obtained localized solutions are shown in Figure 2.14.

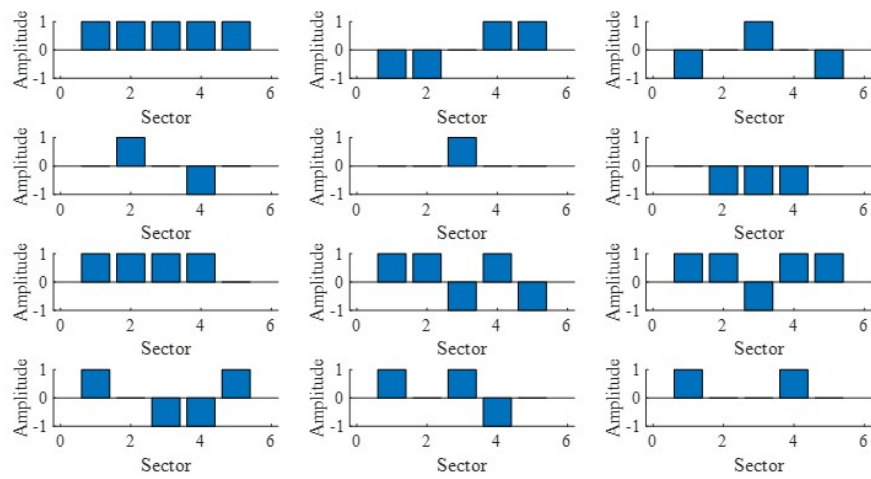


Figure 2.14: The localized nonlinear modes obtained from solving equation (2.11). The first five modes correspond to the linear modes of the system. The other seven modes are representative examples of the 65 modes.

Chapter 3: Effects of Noise in the Multi-stability Region of Coupled Oscillator Arrays

In this chapter, the effects of noise on the system response in the multi-stability region of coupled oscillator arrays are discussed. The considered systems are subjected to harmonic excitations with and without noise additions. First, the influence of noise is experimentally studied with an array of two coupled oscillators for harmonic excitation values in the hysteresis region. The experimental results are compared qualitatively to the numerical results obtained by using Euler Maruyama simulations. The findings help understand the level of noise and the duration of noise required to induce a change in the system dynamics as well as whether one can create or destroy a response for frequency values in the multi-stability region.

3.1 Experimental Setup

An array consisting of two coupled oscillators is considered here. The experimental setup is similar to the one shown in Figure 2.2, with only two oscillators in the present case. The beam oscillator on the left is called the first oscillator and the other one is called the second oscillator. The oscillators are tuned to realize a multi-stability region in the same frequency range.

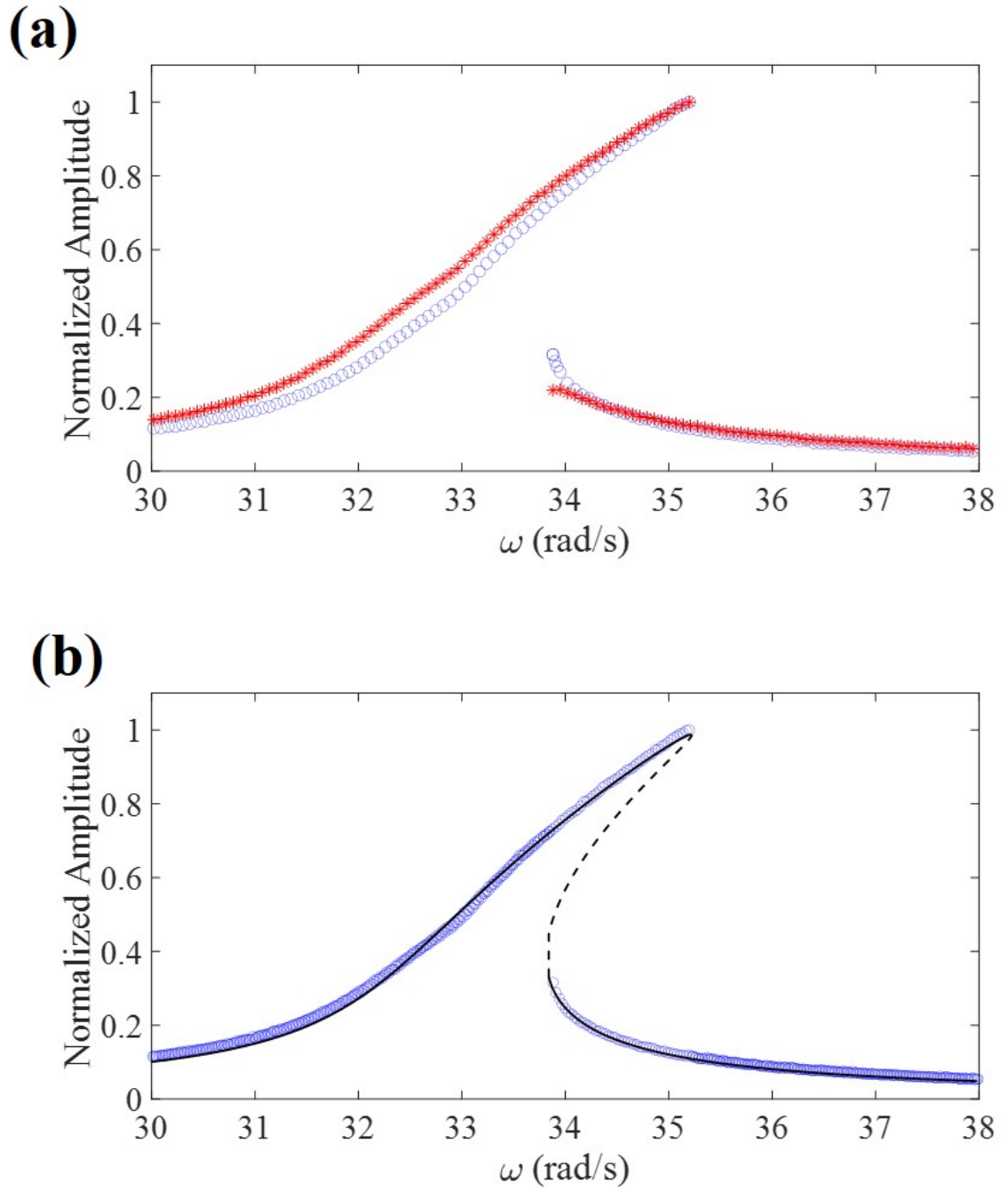


Figure 3.1: Quasi-static frequency sweep for an array of two coupled oscillators: (a) the quasi-static frequency sweep of the first (blue) and second (red) oscillators and (b) matching of the experimental results of the first oscillator (blue) with the numerical solution (black) obtained for the parameters given in Table 3.1. The unstable branch is depicted with dashed lines.

Table 3.1: Experimental results for the parameter values

Parameter	Value	Parameter	Value
ω_{n0}	32.78 rad/s	β	225.5
F	17.95	ζ	0.00787
α	1	—	—

Each oscillator's response is normalized with the maximum response amplitude value. A quasi-static frequency sweep is conducted with the system shows that the responses of both of the oscillators to have multi-stability region for the range of $\omega = 33.86$ rad/s to $\omega = 35.22$ rad/s as illustrated in Figure 3.1 (a). Localized modes (LMs), in which the system response is localized in which the responses of one of the two beam oscillators is on the high amplitude branch while the response of the other beam oscillator is on the low amplitude branch exist within this range; however, they are only obtainable when a certain disturbance is applied to the beam oscillators. For simplicity, both oscillators are assumed to have similar properties, as the first oscillator, when carrying out the numerical studies. The matching of the first oscillator's response from the experiments to the numerical solution of the Duffing oscillator [81] with the parameters provided in Table 3.1 is shown in Figure 3.1 (b). In Figure 3.2, the time series of the beam oscillator responses for a quasi-static frequency sweep up (i.e., increasing excitation frequency) and a quasi-static frequency sweep down (i.e., decreasing excitation frequency) are shown. No LMs are found during these sweeps.

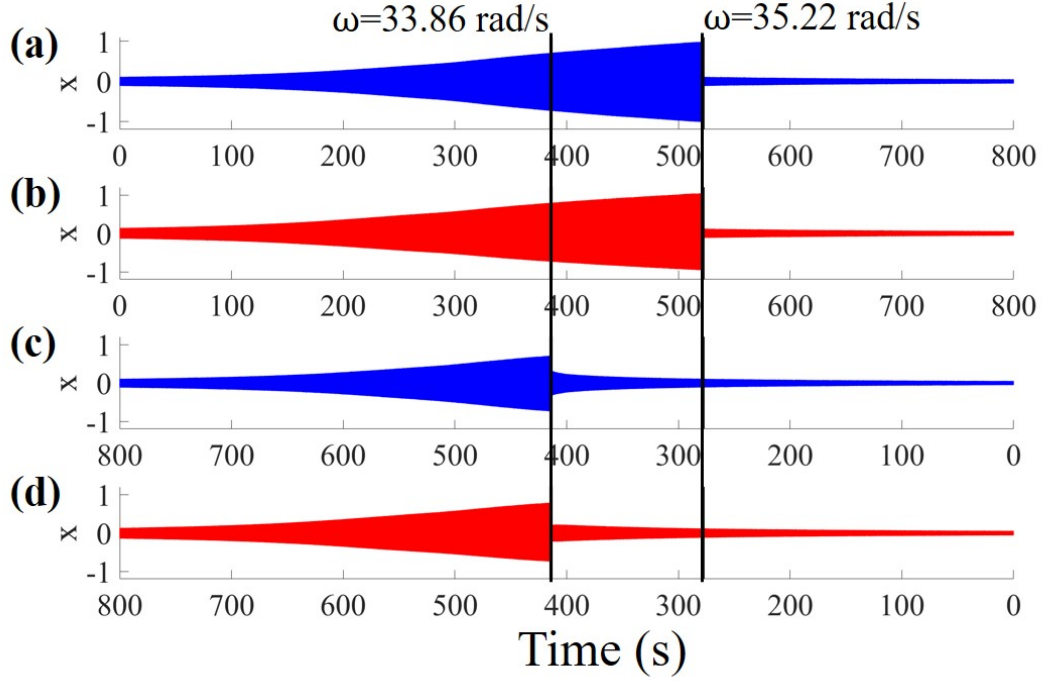


Figure 3.2: Time series of the responses of the array system with two coupled oscillators: (a) quasi-static frequency sweep up for the first oscillator, (b) quasi-static frequency sweep up for the second oscillator, (c) quasi-static frequency sweep down for the first oscillator, and (d) quasi-static frequency sweep down for the second oscillator. The window where the system has multiple stable responses is marked in this figure.

3.2 Numerical Scheme

Here, the scheme used for numerical simulations is described. In equations (2.2), the derivative of Wiener process does not exist and to carry out the simulations, these equations are converted to a Langevin form, which has an incremental noise dW with zero mean and a standard deviation \sqrt{dt} . The result is

$$\begin{aligned}
dz_1 &= z_2 dt \\
dz_2 &= (-2\zeta\omega_{n_0}z_2 - \omega_{n_0}^2 z_1 - \beta z_1^3 - \alpha(z_1 - z_3) + a \cos(\omega t))dt + \sigma dW(t) \\
dz_{n^*2-3} &= z_{n^*2-2} dt, \quad \text{for } 2 \leq n \leq N-1 \\
dz_{n^*2-2} &= (-2\zeta\omega_{n_0}z_{n^*2-2} - \omega_{n_0}^2 z_{n^*2-3} - \beta z_{n^*2-3}^3 - \alpha(2z_{n^*2-3} - z_{n^*2-1} - z_{n^*2-5}) + \\
&\quad a \cos(\omega t))dt + \sigma dW(t), \quad \text{for } 2 \leq n \leq N-1 \\
dz_{N^*2-1} &= z_{N^*2} dt dz_{N^*2} = (-2\zeta\omega_{n_0}z_{N^*2} - \omega_{n_0}^2 z_{N^*2-1} - \beta z_{N^*2-1}^3 - \alpha(z_{N^*2-1} - z_{N^*2-3}) + \\
&\quad a \cos(\omega t))dt + \sigma dW(t)
\end{aligned} \tag{3.1}$$

For two oscillators, equations (3.1) are reduced to

$$\begin{aligned}
dz_1 &= z_2 dt \\
dz_2 &= (-2\zeta\omega_{n_0}z_2 - \omega_{n_0}^2 z_1 - \beta z_1^3 - \alpha(z_1 - z_3) + a \cos(\omega t))dt + \sigma dW(t) \\
dz_3 &= z_4 dt \\
dz_4 &= (-2\zeta\omega_{n_0}z_4 - \omega_{n_0}^2 z_3 - \beta z_3^3 - \alpha(z_3 - z_1) + a \cos(\omega t))dt + \sigma dW(t)
\end{aligned} \tag{3.2}$$

The solution is obtained by numerically integrating system (3.2) by using the Euler-Maruyama scheme [82]. To obtain the localized modes, the authors have used the anti-continuous limit based method (e.g., [83]). With this method, the uncoupled system is considered first and the initial conditions are determined for the high amplitude and the low amplitude responses of an individual oscillator. Then, after introducing coupling and increasing the coupling strength gradually, and using the shooting method with an initial guess determined from the uncoupled system, the

periodic solutions for the coupled system are found.

3.3 Results and Discussion

In this section, the influence of noise on system responses are explored for different excitation frequency values, for which jumps between different solution branches may occur. Two regions of interest, which are at either end of the multi-stability region are explored.

3.3.1 Influence of Noise Near the Left Boundary of the Multi-Stability Region

When the harmonic excitation frequency is close to the left side or the low frequency end of the multi-stability region (MR), the experimental results obtained are shown in Figure 3.3. At each frequency, the experiment has been run for twelve times for 100 s time window for different noise intensities, starting from the low-low mode, a mode in which both beam oscillators have a low response amplitude when noise is not present. The root mean square (RMS) value over each period in each run is calculated for the whole interval. The RMS value for the 12 runs is then averaged and plotted for the chosen noise input and excitation frequency. The averaged RMS value for each oscillator's response is represented in color over the corresponding time window with the blue color corresponding to low amplitude oscillations and the red color corresponding to high amplitude oscillations. The horizontal black and white bar on the top is used to show the time windows over which noise is applied.

In the present case, noise has been applied over the whole interval shown.

The two oscillators are set to vibrate at the low-low mode in the beginning of the experiments. Then, noise has been applied and the two oscillators tend to move toward the high-high mode, which is a mode in which each of the beam oscillators have a high amplitude response in the absence of noise. Close to the left boundary of the MR ($\omega=33.82$ rad/s), for $\sigma = 0.5$ units, the oscillator responses jumped to the high-high mode eight times with the average time being 77.5 s. In Figure 3.3 (a), the author shows the experimental results for this case. As it can be seen, the color gradient for both oscillators tend to the red color at the end of the time interval. However, the responses still do not clearly reach a red color, indicating that jumps did not occur in all runs. At the same frequency value, when the noise intensity is increased to $\sigma = 0.8$ units, the responses in all of the cases were found to have moved to the high-high mode except in one occasion with the average time being 50.5 s. The results are plotted in Figure 3.3 (b), and it is clearly evident that the response gradient color for both oscillators becomes red indicating almost all runs induced the jump. As the noise intensity is increased, an observation is that the time required to induce jumps is reduced. While the change in the response color gradient for $\sigma = 0.5$ units is limited in the first 50 s, there is a significant change for $\sigma = 0.8$ units.

Another experiment was conducted at $\omega=33.84$ rad/s for two different noise intensities, namely $\sigma = 0.8$ units and $\sigma = 1.2$ units, and the results are shown in Figures 3.3 (c) and (d), respectively. While the noise intensity $\sigma = 0.8$ units is found to have a pronounced impact on the response for $\omega=33.82$ rad/s, there is almost

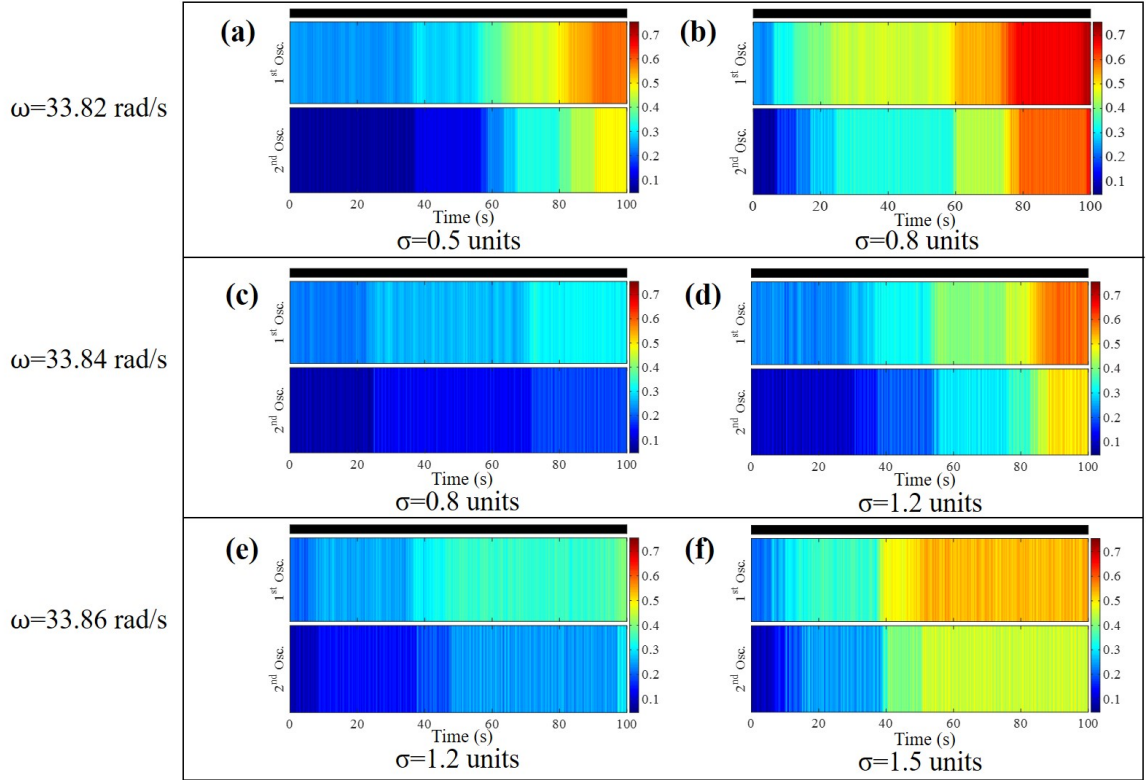


Figure 3.3: Experimental results for harmonic excitation frequency near the left end of the MR.

no impact on the response for $\omega=33.84$ rad/s. Only in two out of the 12 runs, the introduction of noise is found to induce jumps. However, for $\sigma = 1.2$ units, the responses of the oscillators jumped into the high-high mode for 8 cases, indicating a noticeable effect on the low-low mode. The test are run further on $\omega=33.86$ rad/s for two noise intensities $\sigma = 1.2$ units and $\sigma = 1.5$ units, and these results are shown in Figures 3.3 (e) and (f), respectively. As it can be seen from the response color gradient, for $\sigma = 1.2$ units only a small number of responses cases (4) have moved into the high-high mode. On the other hand, for $\sigma = 1.5$ units more number of runs reveal a change in the system response dynamics (7 in this case).

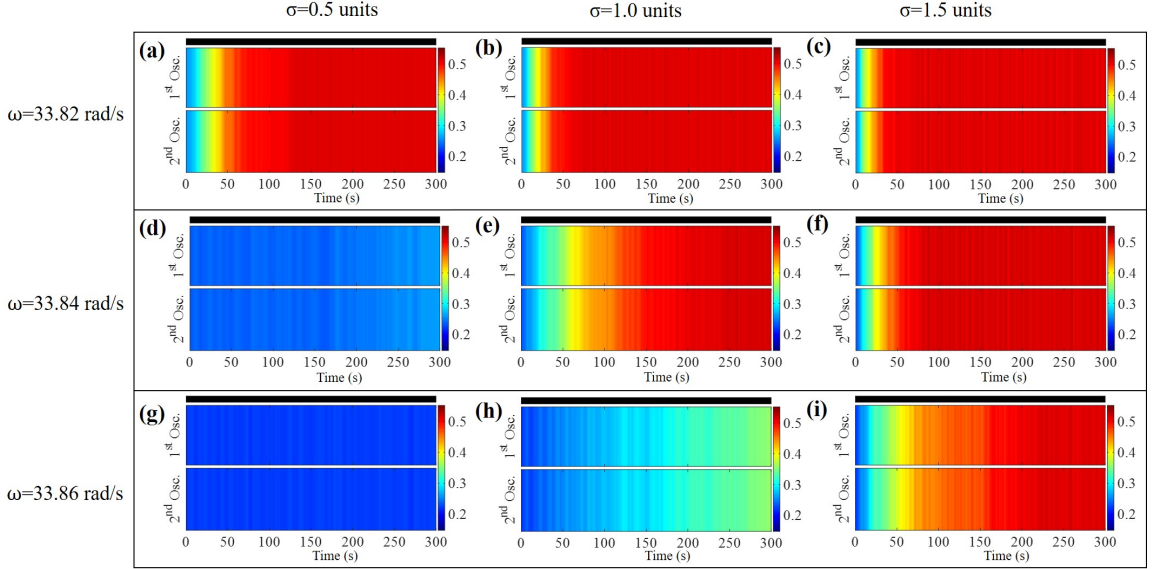


Figure 3.4: Numerical results for harmonic excitation frequency near the left end of the MR.

The numerical results are obtained by solving equation (3.2) using Euler-Maruyam simulations. The average RMS value for the numerical simulation is obtained by considering the RMS average over 50 runs by using a different noise vector for each run. Similar ω values to the experimental tests are considered ($\omega=33.82$, 33.84 , and 33.86 *rad/s*) for three different noise intensities ($\sigma = 0.5, 1.0$, and 1.5 *units*) for each ω value. For the first frequency $\omega=33.82$ *rad/s*, successful jumps are observed to be induced for all noise intensities with the differences in the time required to induce that jump decreasing as the noise intensity was increased. For $\omega=33.84$ *rad/s*, a low noise intensity almost has no impact on the system dynamics, but the intermediate and high noise levels being sufficient to induce a mode change with a transition time for the high noise level case being less than that for the medium level. For the last ω value ($\omega=33.86$ *rad/s*), again no effect on the re-

sponse was observed when a low noise level was used. For the medium noise level, the change in responses occurred in less trials than the observed for the previous ω value. Only the high noise level was found to have a discernible impact on the low-low mode for this excitation frequency.

From the previous experimental and numerical results, one can note that the level of noise and the required time to move the system from the low-low mode to the high-high mode depend on the excitation frequency. Close to the left boundary or low frequency end of the MR, the low-low mode is sensitive to disturbances. Small disturbances move the system response from the low-low mode to the high-high mode in a small amount of time. When the harmonic excitation frequency was moved towards the center of the MR, the low-low mode was found to become robust to disturbances. High noise intensities are found to be needed to induce a response jump. The average time to induce a jump was found to increase as one moves toward the center of the MR and this time needed was found to decrease when the noise intensity was increased. It is clear that the experimental and numerical results agree qualitatively. It is worth mentioning that when starting from the high-high mode and applying comparable noise intensities no change was observed in the system response dynamics.

3.3.2 Influence of Noise Near the Right Boundary of the Multi-Stability Region

In Figure 3.5, the author has shown the experimental results obtained when the harmonic excitation frequency is near to right end of the MR. Three different ω values are chosen for the study, which are 35.2, 35.12, and 35.0 rad/s. Similar to the previous experimental studies, for each parameter set, the test was run for twelve times in 100 s time windows and the average of the RMS value over the 12 runs is plotted. All runs are set to start from the high-high mode to explore the possibility for changing the system dynamics to the low-low mode.

At $\omega=35.2$ rad/s, the high-high mode was found to be quite sensitive for a low level noise disturbance. For a low noise intensity ($\sigma = 0.25$ units), in eleven of the twelve cases, the system response collapsed to the low-low mode with the average time being 44.17 s. The associated dynamics is illustrated in Figure 3.5 (a). When the noise intensity is increased to $\sigma = 0.5$ units, in all of the twelve cases, the system response collapsed within an average time of only 5.17 s, as illustrated in Figure 3.5 (b) . Moving toward the center of the MR, the effects of two noise intensities are explored at $\omega=35.12$ rad/s. These intensities are $\sigma = 0.5$ units and $\sigma = 0.8$ units, and the corresponding results are depicted in Figures 3.5 (c) and (d), respectively. For $\sigma = 0.5$ units, only in two of the twelve cases, the chosen noise input induced a transition from the high-high mode to the low-low mode, but by increasing the intensity further to $\sigma = 0.8$ units, in all the twelve cases, the response collapsed to the low-low mode within an average time of 14.67 s. At the last chosen ω value

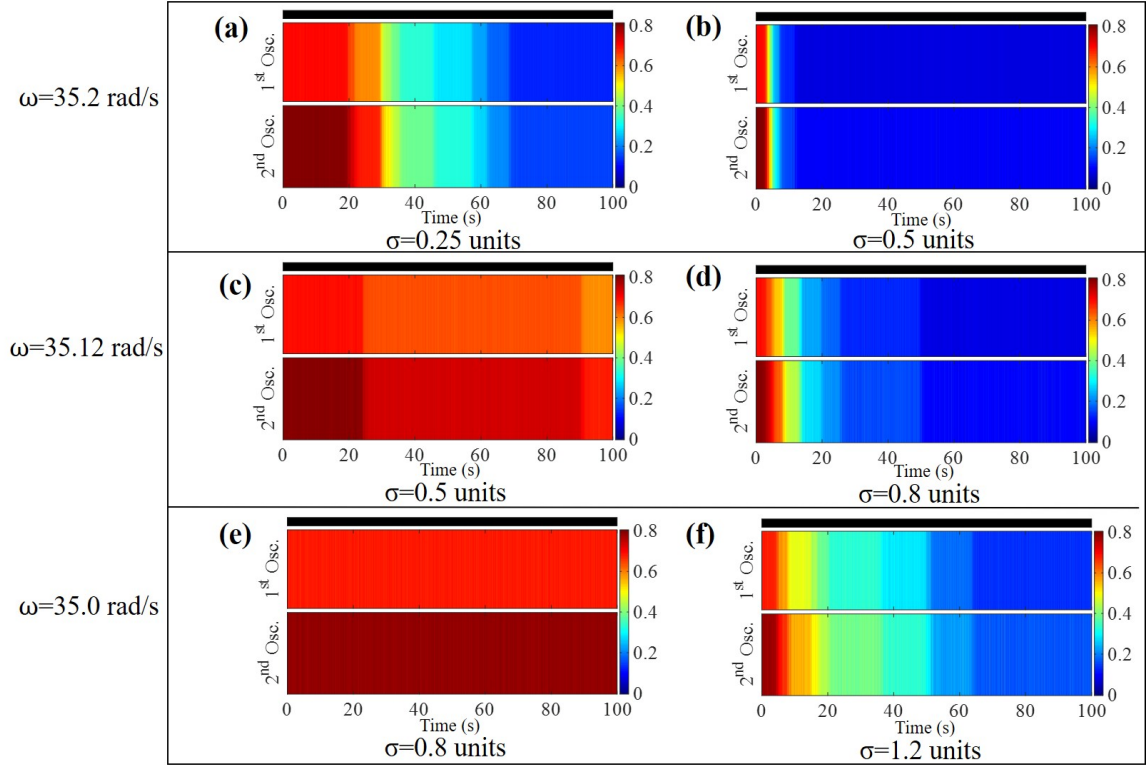


Figure 3.5: Experimental results obtained when the harmonic excitation frequency is near the right end of the MR.

($\omega=35.0$ rad/s), the high-high mode was found to become more robust to noise. When applying noise with $\sigma = 0.8$ units, almost no effect on the response mode was observed. In none of the twelve cases, there was a change in the system dynamics, as shown in Figure 3.5 (e). In order to have response jump downs occur, higher noise intensity needed to be applied, as shown in Figure 3.5 (f) for $\sigma = 1.2$ units.

It is clear that at the right side of the MR of identical oscillators, the oscillator responses tend to move toward the low amplitude responses. Applying sufficient noise can alter the system dynamics and move each oscillator's response to the low-amplitude response. On the other hand, at the left side of the MR, the oscillator

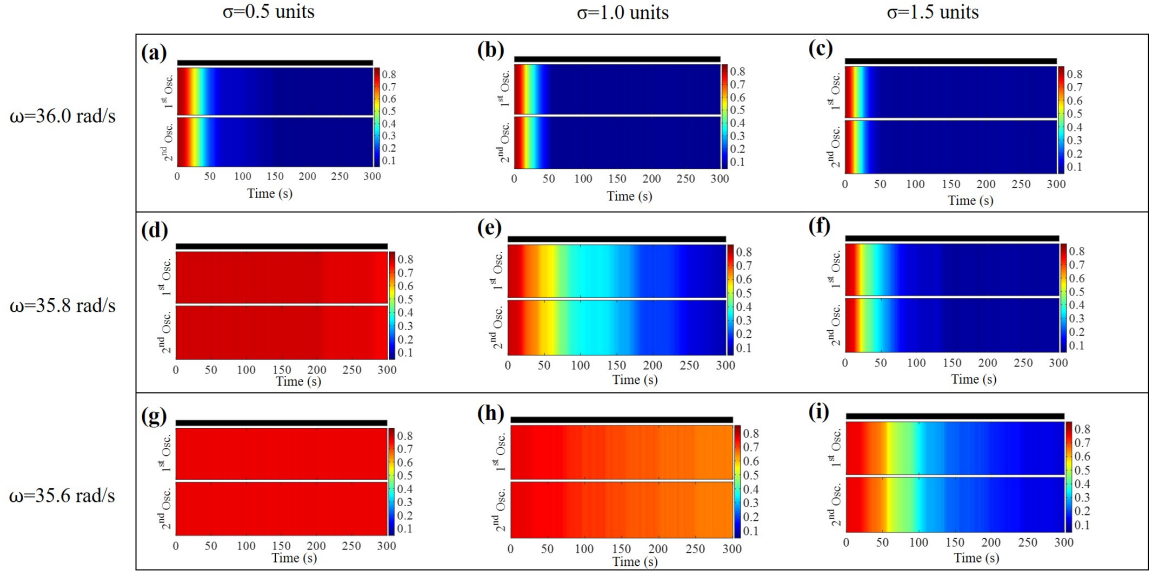


Figure 3.6: Numerical results obtained when the harmonic excitation frequency is near the right end of the MR.

responses tend to move toward the high amplitude oscillations. Applying noise can change the system dynamics and induce more high amplitude oscillations. Another observation based on the results from Figures 3.3-3.6 is that the sensitivity of the oscillators to disturbances for the right region of the MR is higher than the left region. As a result, when moving from one frequency value to another in the right of the hysteresis region, less noise intensity was found to be required than when is at the left region and considering similar increment for the frequency. The reason for this might related to the basin of attraction of an uncoupled oscillator; that is the single Duffing oscillator. It is well known that for the Duffing oscillator the ratio of the high amplitude attractor basin to the low amplitude attractor basin close to the jump down frequency is much smaller than the ratio of the low amplitude attractor basin to the high amplitude attractor basin close to the jump up frequency.

3.3.3 Basins of Attraction

To better understand the influence of disturbances on the system, the basin of attractions near the left and right boundaries of MR are obtained and shown in Figure 3.7. While the basins of attraction are usually illustrated for two-dimensional systems, they can be found for a four-dimensional system. The procedure is similar to the one used in the work of Ikeda *et. al.* [68]. To find the basins, the initial conditions for a mode of interest (L-L, H-L, L-H and H-H) is selected as the starting point for the numerical integration of equation by using the ode45 solver in Matlab [84]. Next, a grid of 250*250 with (0,0) as the center point is defined as a disturbance for the system. For each point, the first value is added for each displacement (x_1 and x_2) and the second point is added for each velocity (\dot{x}_1 and \dot{x}_2) to represent deviations for the system. Equation (2.2) is then solved for two oscillators for each point and the solution is traced after reaching the steady state solutions. Depending on the final state, each point is colored as red (H-H), green (H-L), magenta (L-H) or blue (L-L). In Figures 3.7 (a)-(c), the basins of attraction corresponding to Section 3.3.1 are shown for the three previously considered ω values,; that is, $\omega=33.82$, 33,84 and 33.86 rad/s. The initial state for the system is on the L-L mode, and it is represented by the black point and this is the state at which no deviations have been applied. For $\omega=33.82$ rad/s, when small deviations are applied, the system response is found to return to the original state of the L-L mode, and this is represented by the small blue region. However, if the deviation is relatively higher, the response no longer return to the L-L mode but to the H-H mode. This is illustrated by the red

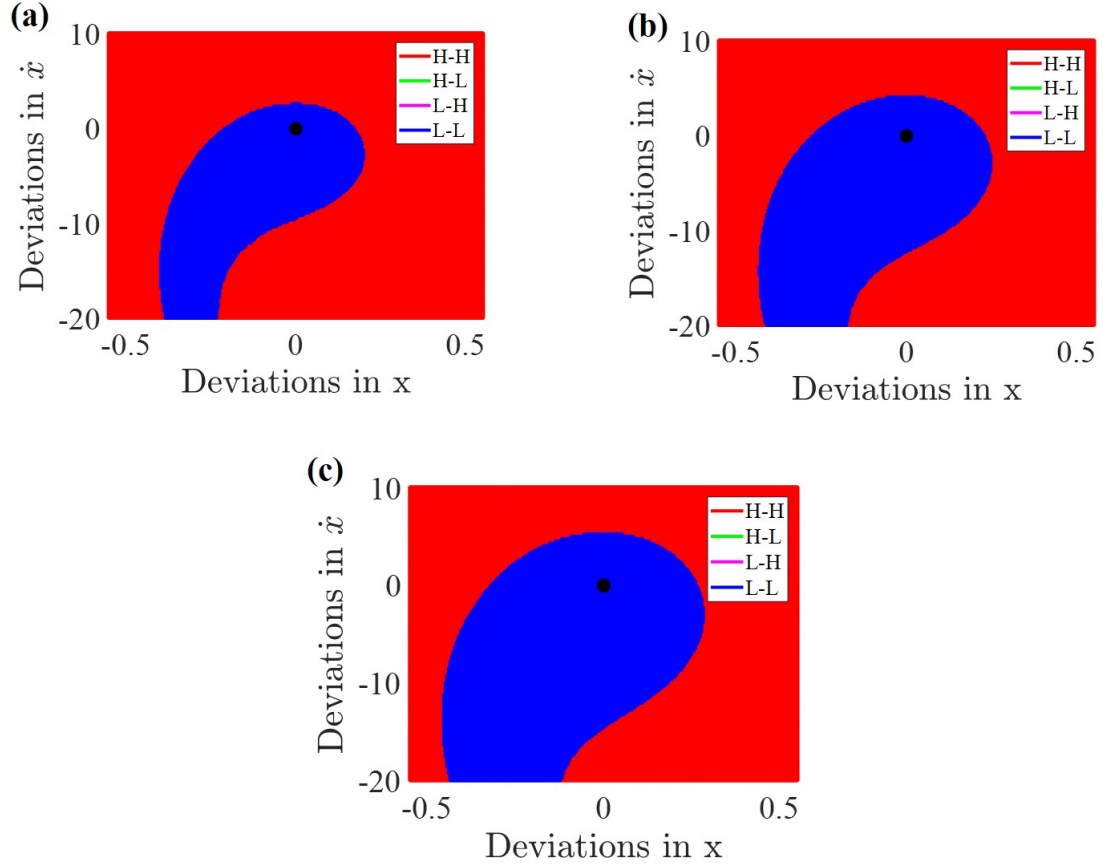


Figure 3.7: Basin of attraction for the system near the left boundary of the MR starting from the L-L mode: (a) $\omega=33.82$ rad/s, (b) $\omega=33.84$ rad/s, and (c) $\omega=33.86$ rad/s.

region. When one moves towards the center of the MR, the blue region is found to expand further and the black dot is found to move more inside of the L-L mode, as shown in Figures 3.7 (b) and (c). The previous results might give an indication for what to expect in the response change after applying noise to the coupled oscillator arrays. For ω values close to the left boundary, the L-L mode region is small in size indicating how sensitive this mode is to a noise disturbance. As a result, small disturbances might be enough to move the response mode into the H-H response

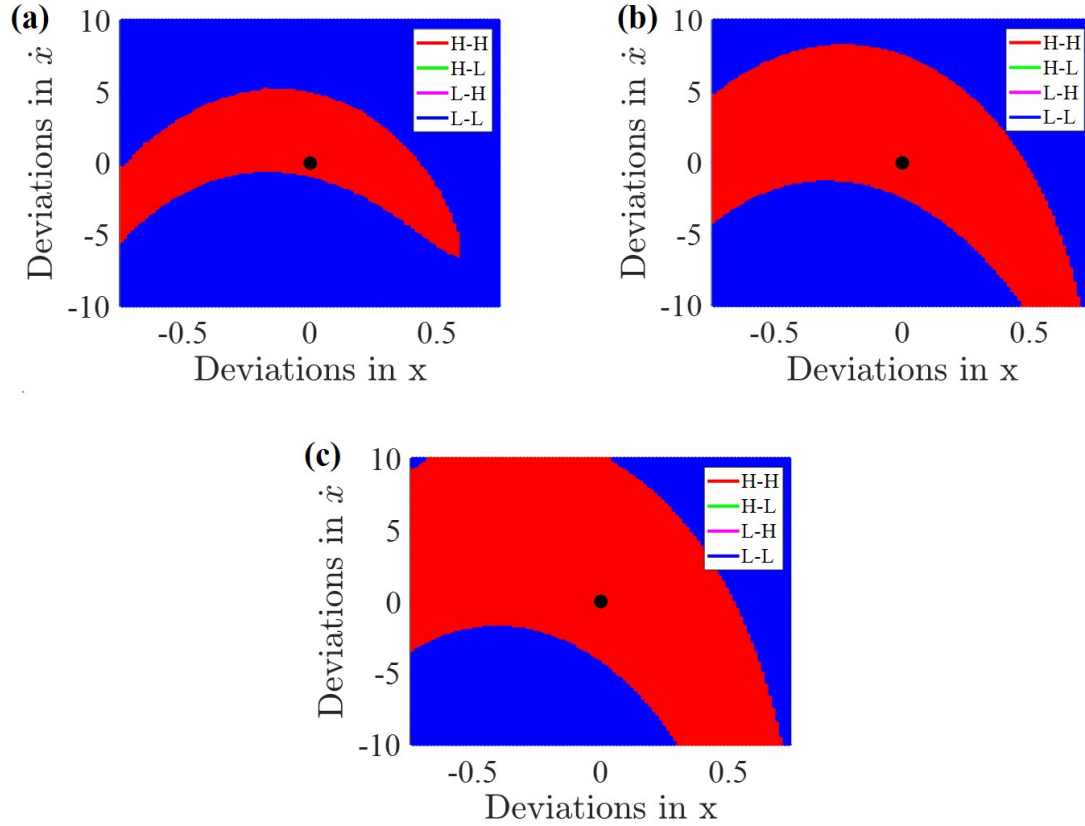


Figure 3.8: Basins of attraction for the system near the right boundary of the MR starting from the H-H mode: (a) $\omega=35.2$ rad/s, (b) $\omega=35.12$ rad/s, and (c) $\omega=35.0$ rad/s.

mode. As one moves toward the center, the blue region expands in size and higher noise intensities would be needed to induce a change in the system dynamics.

For the right side of the MR, three ω values are considered as in Section 3.3.2, which are: 35.2, 35.12 and 35.0 rad/s. The basins of attraction for this region are shown in Figures 3.8 (a)-(c). For $\omega=35.2$ rad/s, the H-H mode has a small basin that is shown as a small red stripe in Figure 3.8 (a). When one moves towards the center of the MR region, the red area expands in size as shown in Figures 3.8 (b) and (c). These plots might give an indication for how robust the H-H mode is to a

disturbance in this region. When the red area is small in size, it is expected that the H-H mode is vulnerable to a disturbance and the system response can change with a low intensity disturbance. However, as one moves toward the center, the red region is found to expand in size, and high noise intensities are needed to alter the system dynamics. In the considered basin sets, there is no presence of basins of the LMs responses. As a result, it is considered less likely to obtain LMs by introducing noise to the system for the chosen initial conditions.

Chapter 4: Effects of Noise on Different Response Modes of Coupled Oscillator Arrays

In this chapter, the influence of noise on different response modes of coupled oscillator arrays is investigated. In the experimental part, arrays of two and three coupled oscillators are investigated. The results are then compared with results from numerical simulations obtained by using the Euler-Maruyama scheme. Furthermore, the effects of coupling and changing the number of oscillators on the system responses are discussed, in the presence of noise.

4.1 Experimental Setup

4.1.1 Two Oscillators

An array composed of two coupled-oscillators is set to have similar properties. The time series for the system responses obtained by performing a quasi-static frequency sweep is shown in Figure 4.1. For the quasi-static frequency sweep up, the system response is on the H-H branch as shown for the first and second oscillators in Figures 4.1 (a) and (b), respectively. When the critical excitation frequency of $\omega=38.97$ rad/s is reached, the responses of both oscillators collapse in amplitude val-

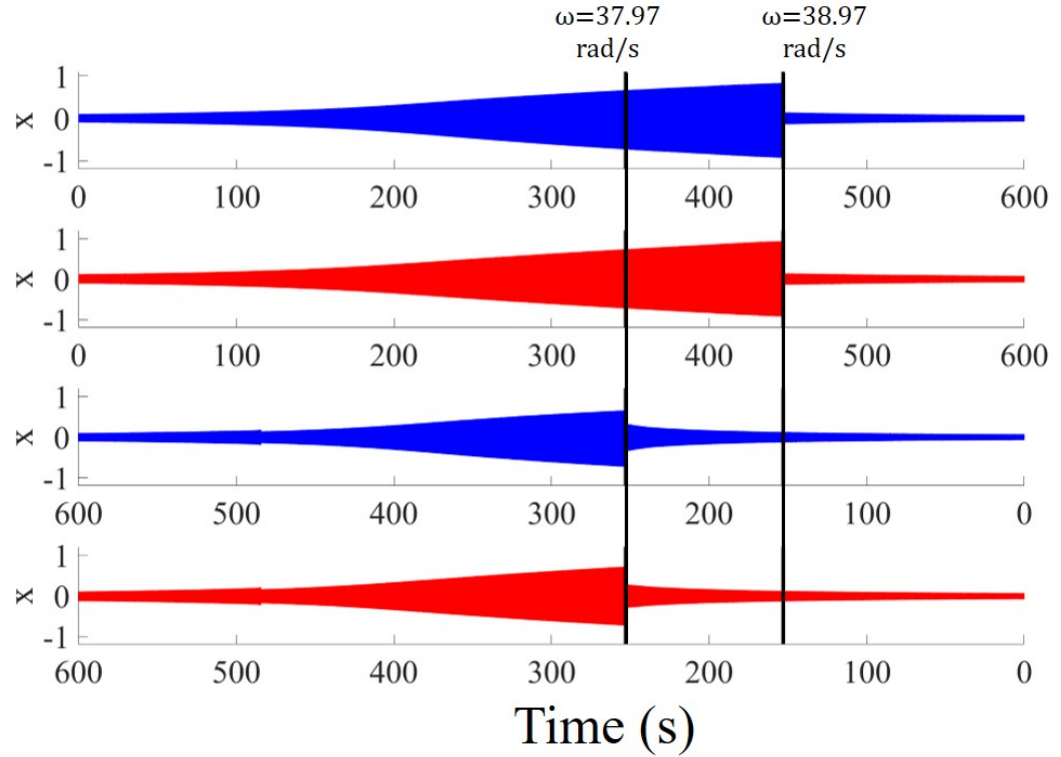


Figure 4.1: Time series of the responses of the two coupled oscillators: responses to quasi-static frequency sweep up for (a) first oscillator and (b) second oscillator, and responses to quasi-static frequency sweep down for (c) first oscillator and (d) second oscillator.

ues. During the quasi-static frequency sweep down, the system response is initially on the L-L branch. As the frequency is swept down, the system response continues on the L-L branch until one reaches the critical frequency value of $\omega=37.97$ rad/s, at which location, the response of both oscillators jump to higher amplitude values, as shown in Figures 4.1 (c) and (d) for the first and second oscillators, respectively.

Localized modes within the considered frequency region exist, but they are not attainable using the quasi-static frequency sweep for the system. In Figure 4.2, all the possible solution branches for the system are shown. To obtain the

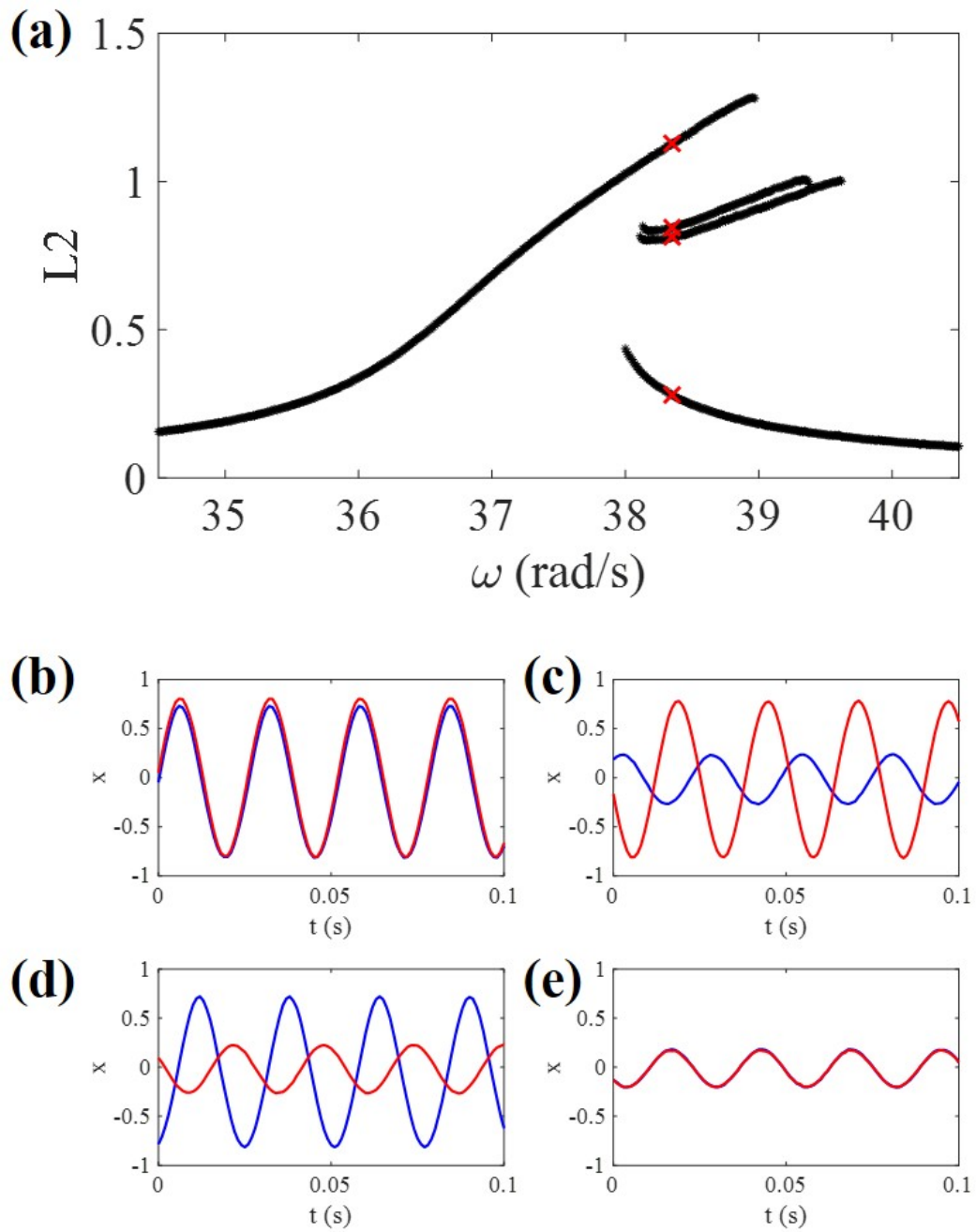


Figure 4.2: Frequency responses of the two coupled oscillators: (a) all the four branches of the four modes H-H, L-H, H-L and L-L arranged from top, (b)-(e) time series of the first (blue) and second (red) oscillators at the marked red location (X) in (a) for the different: (b) H-H, (c) L-H, (d) H-L, and (e) L-L.

Table 4.1: First oscillator parameters obtained from experimental data given in Figure 4.2

Parameter	Value	Parameter	Value
ω_{n0}	37.0 rad/s	β	270
F	18.5	ζ	0.0063
α	1	—	—

L-H mode, the experiment is first set to run in the middle of the MR on the H-H branch. Next, a disturbance is applied to the first oscillator to change its dynamics from high amplitude oscillations to low amplitude oscillations. Then, a quasi-static frequency sweep up is performed to obtain the right side of the branch. Next, the same procedure is performed but with a quasi-static frequency sweep down to obtain the left side of the branch. A similar procedure can be applied to obtain the H-L mode, but with a disturbance applied to the second oscillator. Four possible branches exist, which are H-H, L-H, H-L and L-L modes as arranged from the top to bottom in Figures 4.2 (a). Here, the localized modes (L-H and H-L modes) have different branches due to the imperfections in matching the two oscillators, which is the case in real-life situations. These imperfections between the two beam oscillators might appear due to the difference in the beam properties, magnets characteristics or the boundary conditions. The time series obtained for the four possible modes at $\omega=38.35$ rad/s are plotted in Figures 4.2 (b) to (e).

From the experiment results, it is noted that the H-H branch is destroyed when one reaches to the end of the high amplitude branch at $\omega= 38.97$ rad/s and jumps to the L-L branch, even though the LMs exist beyond this frequency, as shown in

Figure 4.1. For the numerical study, both oscillators are assumed to have the same properties as the first oscillator. The matching of the experimental results with the analytical approximation based on the parameters given in Table 4.1 is shown in Figure 4.3.

4.1.2 Three Oscillators

For the experimental setup for three oscillators, an additional oscillator is added next to the second oscillator. The first and third oscillators are each free at one end and coupled with the second oscillator from the other end. The oscillators are set to have comparable properties, since this helps to better understand the

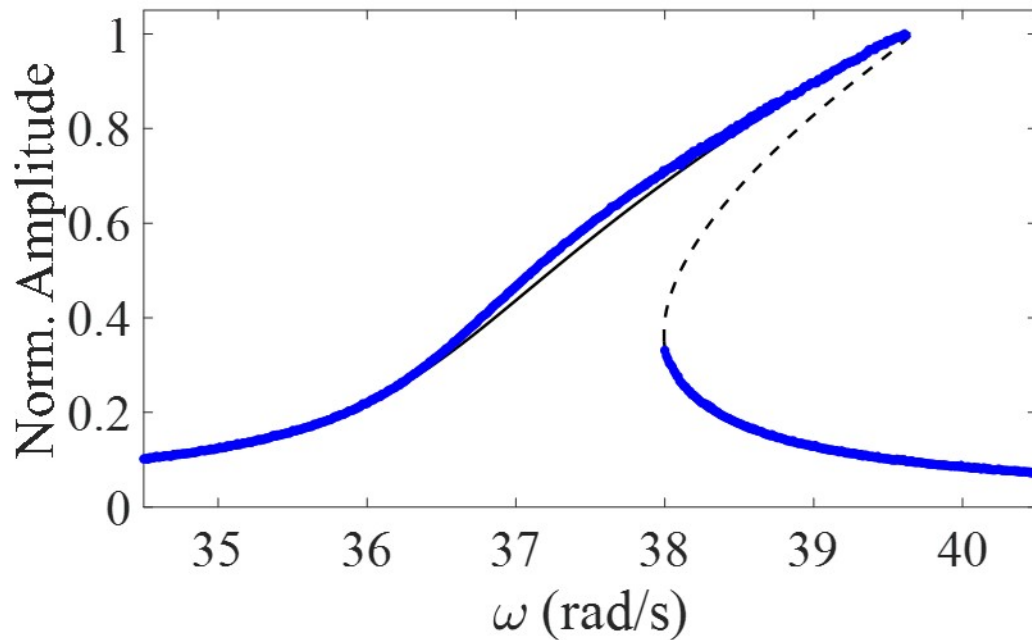


Figure 4.3: Matching of the experimental results of the first oscillator shown in Figure 4.2 (blue) with the analytical approximation for the parameters given in Table 4.1 (black). Dashed lines are used for the unstable branch.

transition of energy in the MR. The time series for the responses obtained during the quasi-static frequency sweep up and down are shown in Figures 4.4 (a)-(c) and (d)-(e), respectively. When performing the quasi-static frequency sweep up, the system response follows the H-H-H branch. At $\omega=38.40$ rad/s, the first oscillator collapses to a state of low amplitude oscillations while the other two oscillators responses remain in a state of high amplitude oscillations. As the frequency sweep up is continued, the second oscillator response falls to a state of low amplitude oscillations at $\omega=38.87$ rad/s. The remaining (third) oscillator response moves to a state of low amplitude oscillations at $\omega=39.83$ rad/s. During the quasi-static frequency sweep down, the system response starts on the L-L-L branch, and continues without change until one reaches $\omega=37.58$ rad/s, wherein all of the responses of the oscillators jump to a state of high amplitude oscillations simultaneously.

All the solution branches for the system are shown in Figure 4.5 (a). As it can be seen, responses on all LMs branches are not observed during the quasi-static frequency sweep. Applying different disturbances, as explained in the two oscillators case, and running the experiments with frequency sweep in the forward and backward directions lead to obtaining of all the system response branches. Based on the system energy, the response branches can be classified into four different levels. The highest energy level is the one wherein all of the oscillators vibrate in a state of high amplitude oscillations. The next level is when two oscillators vibrate in high amplitude states, containing three different energy branches, which are H-L-H, L-H-H, and H-H-L as arranged from top to bottom in Figure 4.5 (a). The next level is when only one oscillator vibrates in a high amplitude state. This

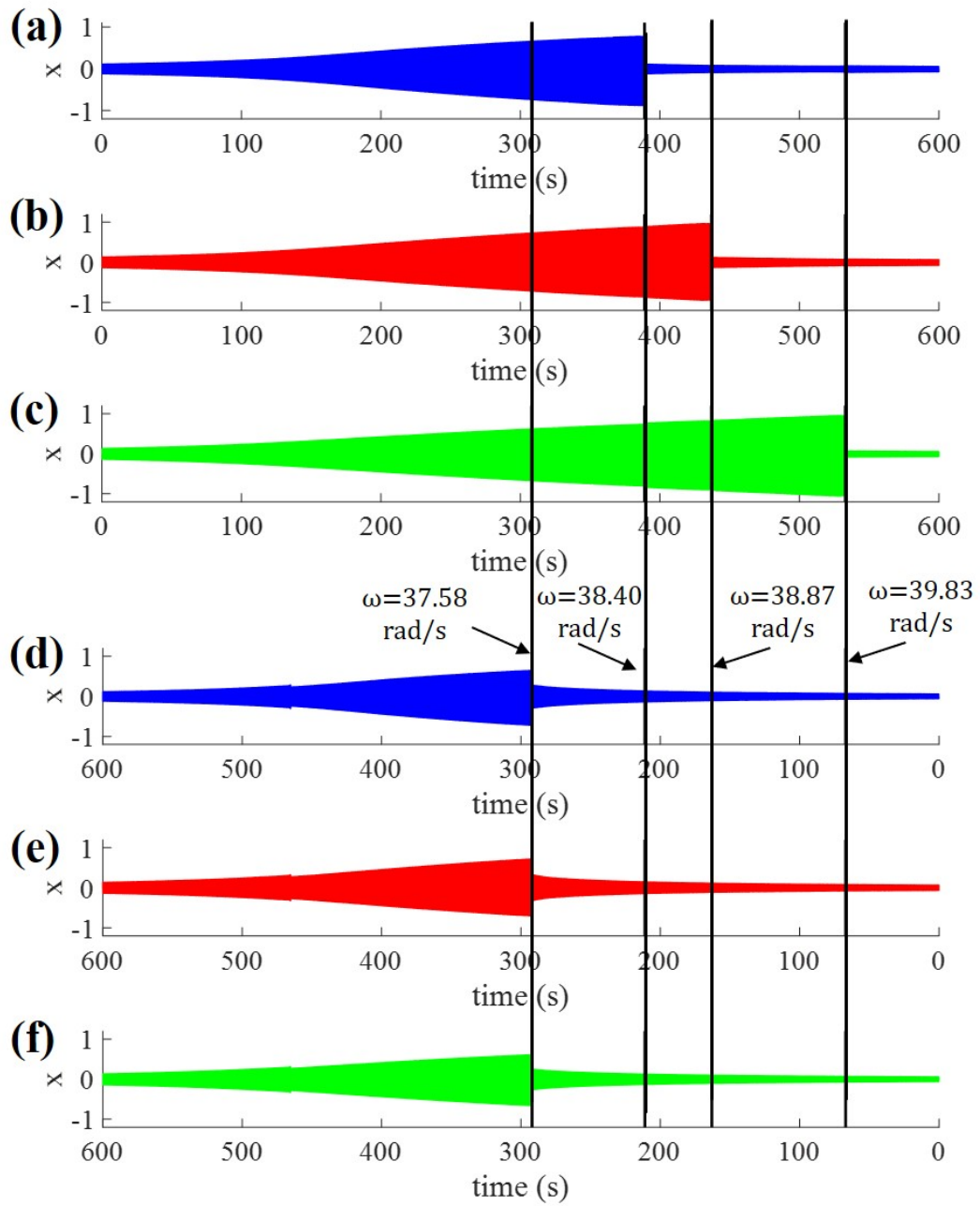


Figure 4.4: Time series of the responses for the array with three coupled oscillators: responses to quasi-static frequency sweep up for (a) first oscillator, (b) second oscillator, and (c) third oscillator, and responses to quasi-static frequency sweep down for (d) first oscillator, (e) second oscillator, and (f) third oscillator.

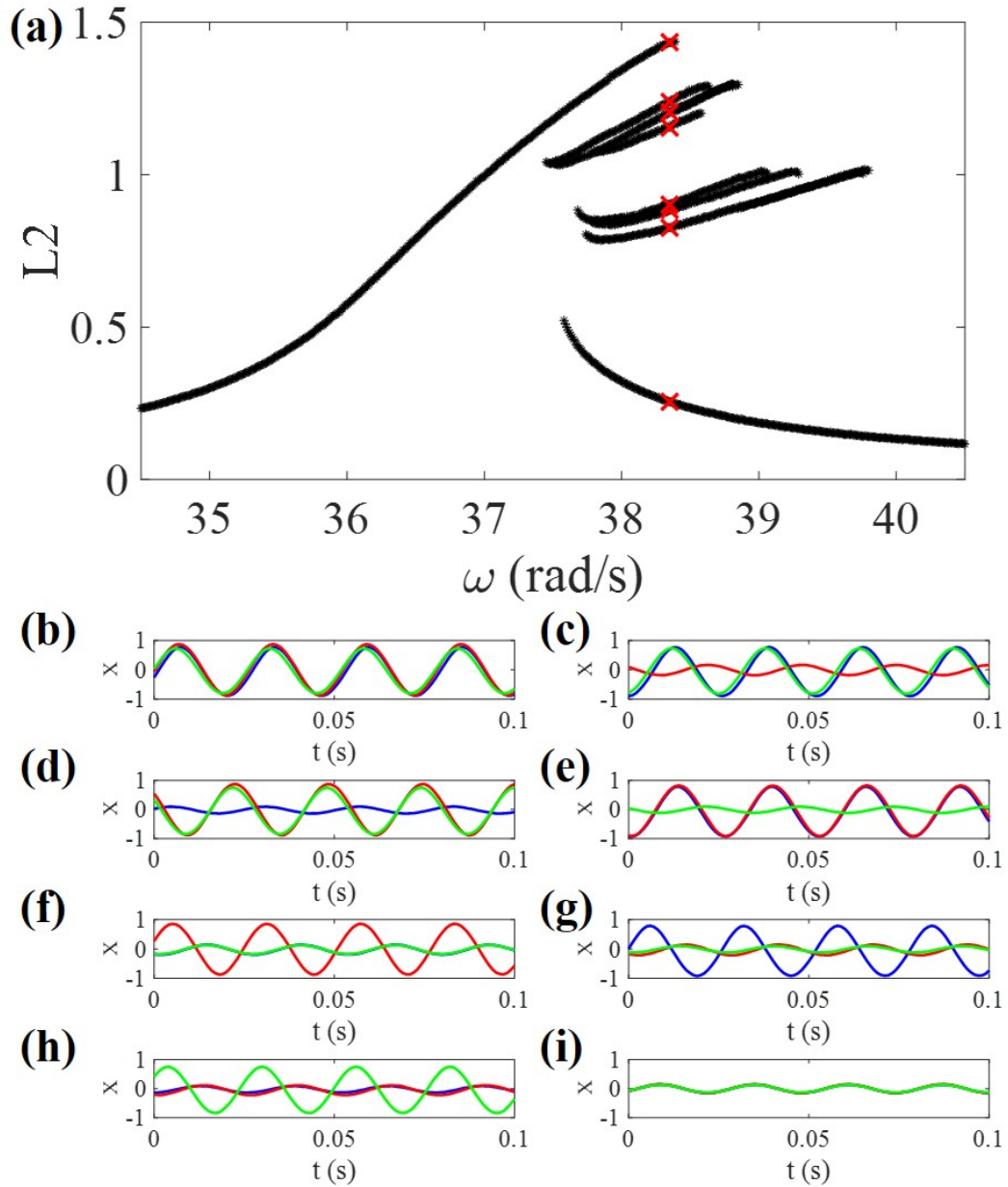


Figure 4.5: Frequency response of the system with three coupled oscillators: (a) Eight branches of the eight modes H-H-H, H-L-H, L-H-H, H-H-L, L-H-L, H-L-L, L-L-H, and L-L-L as arranged from top, (b)-(e) Time series of the responses of the first (blue), second (red) and third (green) oscillators at the marked red location (X) in (a) for: (b) H-H-H, (c) H-L-H, (d) L-H-H, (e) H-H-L, (f) L-H-L, (g) H-L-L, (h) L-L-H, and (i) L-L-L. In plot (a), the L2 norm based on the response amplitudes is plotted on the y-axis.

corresponds to the three branches L-H-L, H-L-L, and L-L-H as arranged from the top. The last branch is for the lowest energy level, which is the L-L-L branch. Due to the experiment imperfections, as explained in the two oscillators case, a difference between the L-H-H and H-H-L modes branches is observed as well as between the H-L-L and L-L-H modes branches. The time series for each response branch at $\omega=38.35$ rad/s is shown in Figures 4.5 (b)-(i).

4.2 Effects of Noise on Different Modes of Coupled Oscillator Arrays

4.2.1 Near the Left End of the Multi-Stability Region

4.2.1.1 Two oscillators

Here, noise has been applied on the system of two coupled oscillators system of Figure 4.2 on different modes. The study is first run near the left end of the MR to investigate the increase of system energy, and then near the right end to investigate the decrease of energy. Black arrows are included in Figures 4.6 (a) and (b), to show the transition locations on the branches, for the responses of the first and second oscillators, respectively.

To start the investigation, $\omega=38.2$ rad/s is chosen, since it is close enough to the left boundary of the MR and all response branches are present at this frequency; that is, L-H, H-L, L-L, and H-H modes. For the L-H mode, applying noise at $\sigma = 0.75$ units is enough to alter the system dynamics from the L-H mode to the H-H mode, as can be seen from Figure 4.7 (a). However, applying a similar noise

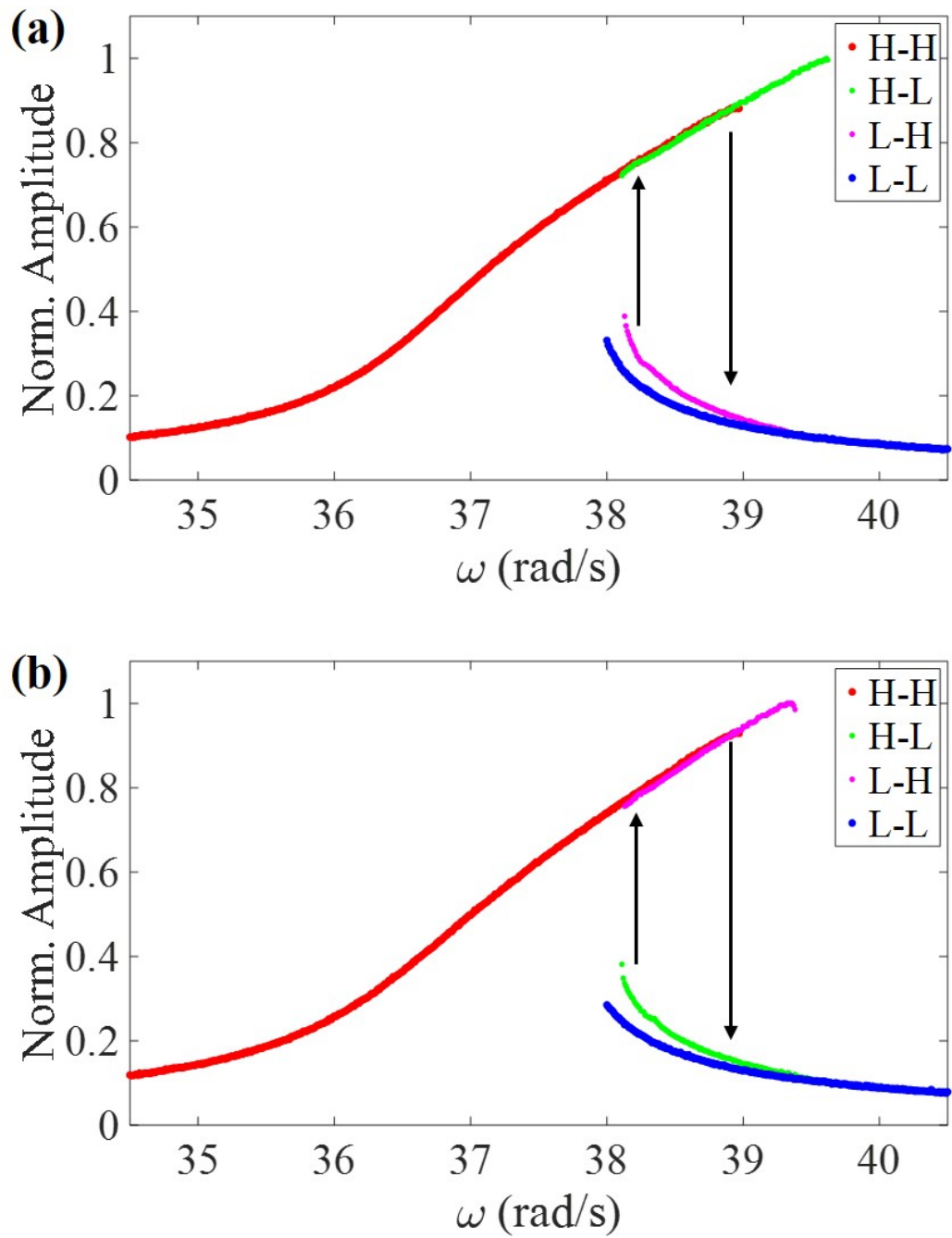


Figure 4.6: System modes for (a) first oscillator and (b) second oscillator. The black arrows indicate the expected transition in the response of an oscillator under the influence of noise.

intensity to the H-L mode has almost no effects. To induce a change on this mode, higher noise intensity needs to be considered such as $\sigma = 1.5 \text{ units}$, as can be seen from Figure 4.7 (b). For the L-L mode, the dynamics is robust to noise, and no change is found to occur for $\sigma = 1.5 \text{ units}$, see Figure 4.7 (c). It is expected that noise can induce a change for high noise intensities, but this could not be pursued due to the experimental limitations in applying noise intensities ($\sigma > 1.5 \text{ units}$), which could damage the experimental setup. However, this mode becomes more sensitive to perturbations for ω values closer to the MR boundary, and moving to the high amplitude oscillations is possible, as can be seen in Figure 4.7 (d) for $\omega=38.1 \text{ rad/s}$ and $\sigma = 1.2 \text{ units}$.

Numerical studies were also conducted. To obtain the numerical results, equation (3.2) is solved by using the Euler-Maruyama simulations for 50 different noise vectors and the resulting RMS displacement average is plotted in Figure 4.8. Due to the homogeneity of the two oscillators, the H-L mode is similar to the L-H mode. As a result, only two modes are considered for the test, which are the H-L and the L-L modes. When considering similar noise intensities ($\sigma = 2.5 \text{ units}$) at the same frequency value ($\omega=38.2 \text{ rad/s}$), the H-L mode is found to be more sensitive to the noise perturbation. With the H-L mode, in 49 tests, there was a successful transition to the H-H mode compared to transitions observed in 34 tests with the L-L mode. The summary of the results is plotted in Figures 4.8 (a) and (b) for the H-L and L-L modes, respectively.

Through The results, it is shown that the influence of noise on the different modes near the left boundary of the MR can be anticipated from the end of each

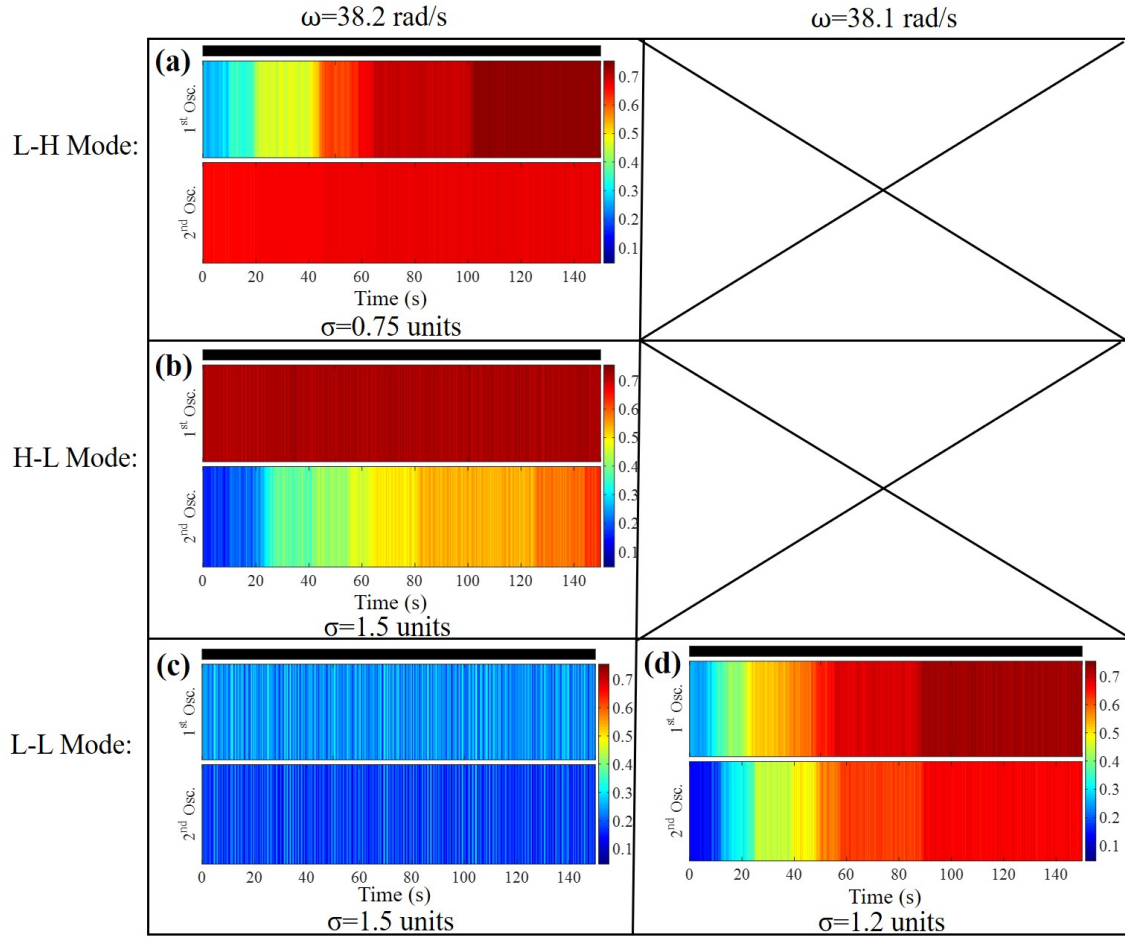


Figure 4.7: Experimental results for the effects of noise on different modes near the left boundary of MR of the two coupled oscillators arrays shown in Figure 4.2.

response branch. The branch that has an end longer than the others is expected to be more robust to noise. As can be seen from Figure 4.2 (a), the L-L mode has an end at $\omega=37.97$ rad/s compared to the frequency values of $\omega=38.18$ rad/s and $\omega=38.19$ rad/s for the H-L and the L-H modes, respectively. As a result, the modes that are more vulnerable to change in system dynamics under the influence of noise can be arranged in order as L-H mode, H-L mode, followed by the L-L mode.

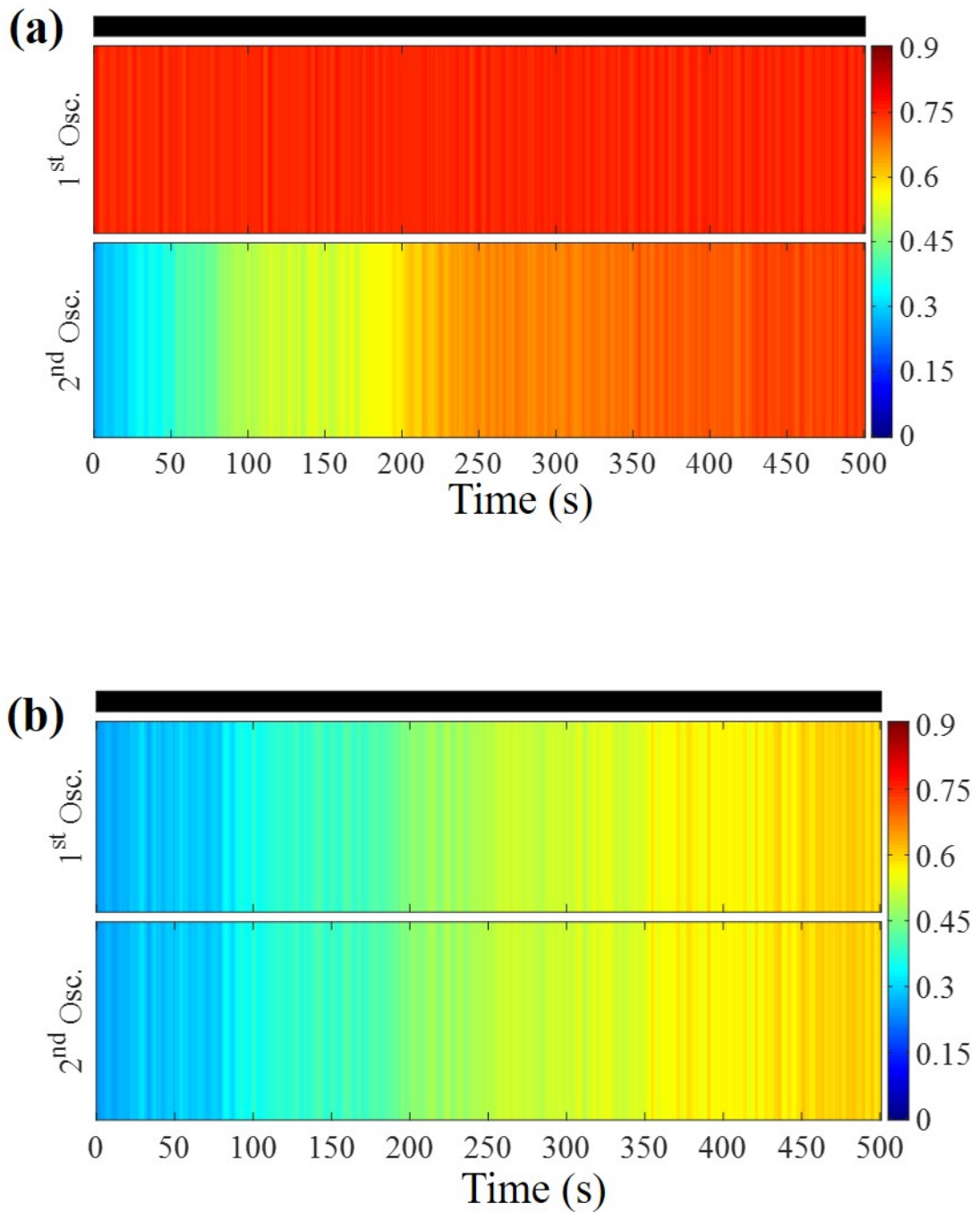


Figure 4.8: Numerical results for the effects of noise on different modes near the left boundary of MR for the array with two coupled oscillators shown in Figure 4.2: (a) starting point is H-L mode and (b) starting point is L-L mode. The horizontal bar on the top is indicative of the duration over which noise is applied. Here, noise is applied throughout the window shown.

4.2.1.2 Three oscillators

A similar type of study has been made with a system consisting of three coupled oscillators. Four different modes near the left boundary of the MR are considered. These modes are H-L-H, L-L-H, H-L-L, and L-L-L, and they are depicted in Figure 4.9 (a).

At $\omega=38.2$ rad/s, the H-L-H and the H-L-L modes are found to be influenced by noise, with the H-L-H mode requiring lesser noise intensity than the H-L-L mode, as shown in Figures 4.10 (a) and (b). The other two modes are found to remain robust to noise, even when high noise intensity is applied; that is, $\sigma = 1.5$ units. As with the two oscillators array, the mode that has a longer end in the MR is found to be more robust to noise, as shown in the zoomed in portion of Figure 4.9 (a). As noise intensities (σ) > 1.5 units might damage the experiment, the other two modes are tested for another frequency value ($\omega=37.8$ rad/s) that is closer to the left end of the MR. While the L-L-H mode responds to noise and a change is observed in the resulting system dynamics, the L-L-L mode is found to be not responsive to noise; the results are illustrated in Figures 4.10 (c) and (d). The L-L-L mode is found to become sensitive to noise very close to the end of the L-L-L branch, as shown in Figure 4.10 (g) at $\omega=37.61$ rad/s .

In the numerical simulations, the system is studied at $\omega=38.2$ rad/s with a noise input of $\sigma = 2.5$ units. Due to the homogeneity of the chosen oscillators, only three modes are considered, namely, the H-L-H, H,L,L, and the L-L-L modes. As observed in the experiments, the mode that has a shorter branch end in the MR is

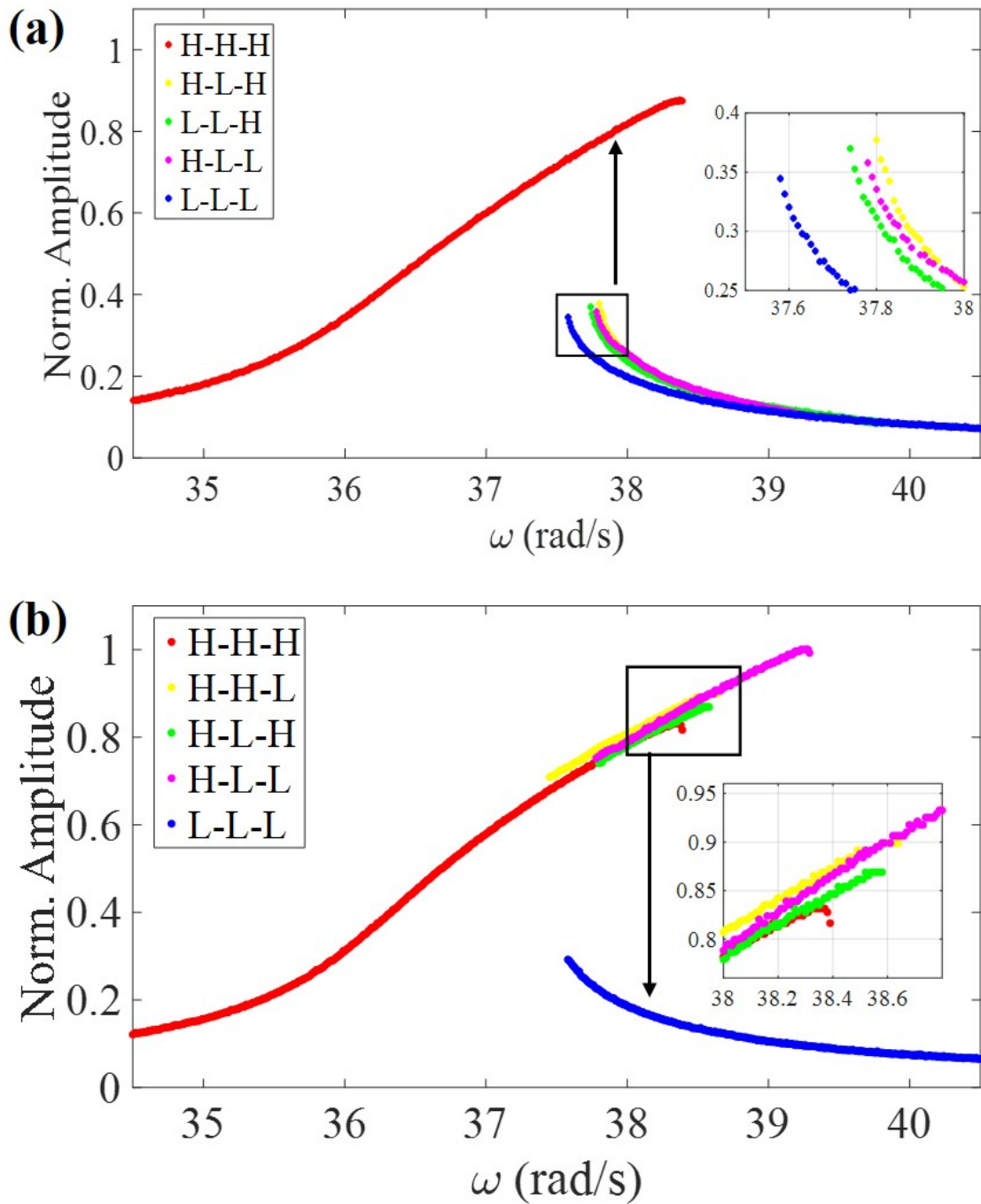


Figure 4.9: Modes of interest of the system: (a) creation of response in the second oscillator and (b) attenuation of response in the first oscillator. The black arrows indicate the expected transition for each oscillator to follow under the influence of noise.

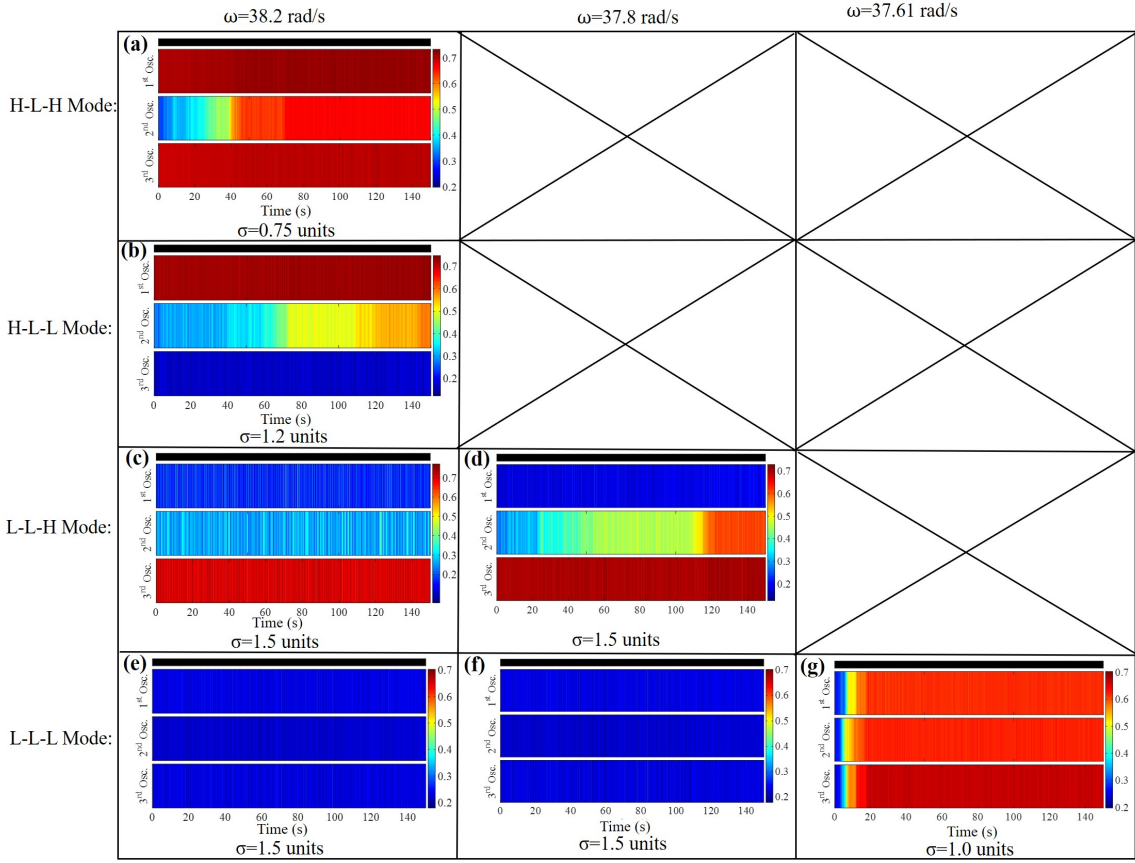


Figure 4.10: Experimental results for the effects of noise on different modes near the left boundary of MR for the array with three coupled oscillators shown in Figure 4.5.

found to respond quicker than the other modes. In most of the runs starting with the H-L-H mode, a change is noted in the system dynamics within the first 100 s, as shown in Figure 4.11 (a). With the H-L-L mode, the second oscillator response jumps to a state of high amplitude oscillations in the most runs within about 300 s. With regard to the results of Figure 4.11 (c), when noise is applied to the L-L-L mode over a similar time window, the system dynamics is found to be altered in only 34 runs, which is the lowest among all the mode cases. This can be explain

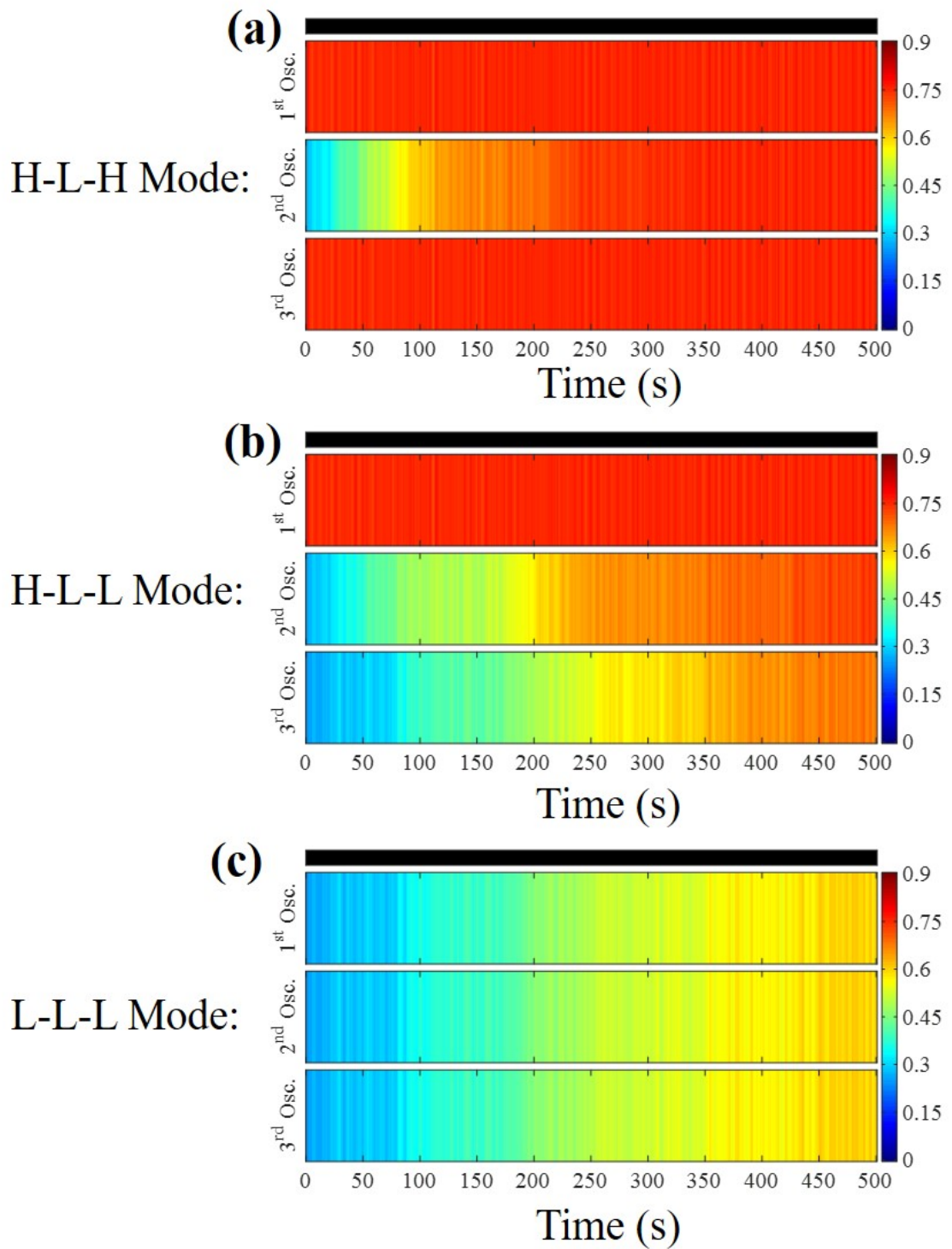


Figure 4.11: Numerical results for the effects of noise on different modes near the left boundary of MR for the system with three coupled oscillators arrays. The parameter values are based on Table 4.1.

by noting that with this mode, one has the longest end in the frequency response curve.

4.2.2 Near the Right End of the Multi-Stability Region

4.2.2.1 Two Oscillators

For the system in Figure 4.2, the results obtained by applying noise when the harmonic excitation frequency is near the right side of the MR in the frequency response curve are shown in Figure 4.12. Three modes are considered, namely, the H-H, L-H, and H-L modes. From Figure 4.12 (a), the H-H mode at $\omega=38.96$ rad/s is found to be vulnerable even when noise with a low intensity is applied, such as, $\sigma = 0.25 \text{ units}$. The L-H mode is found to be responsive to a moderate noise intensity, as shown in Figure 4.12 for $\sigma = 1.2 \text{ units}$. With regard to the H-L mode, no change in the system dynamics is observed for all noise intensities less than $\sigma = 1.5 \text{ units}$. This mode can collapse when noise with a strong noise intensity is applied. However, this is not safe for the experiment. Alternatively, this can also happen when one moves closer to the branch end, such as the excitation frequency of 39.15 rad/s. The results obtained for this mode are shown in Figures 4.12 (c) and (d). As with the previous study, a quasi-static frequency sweep can be used to get a clue to how robust this system mode is. A response branch, which has a longer end, is supposed to be more robust to disturbances.

Through the numerical studies, the author is not able to capture similar qualitative behavior as that observed in the experiments. This can be reasoned by

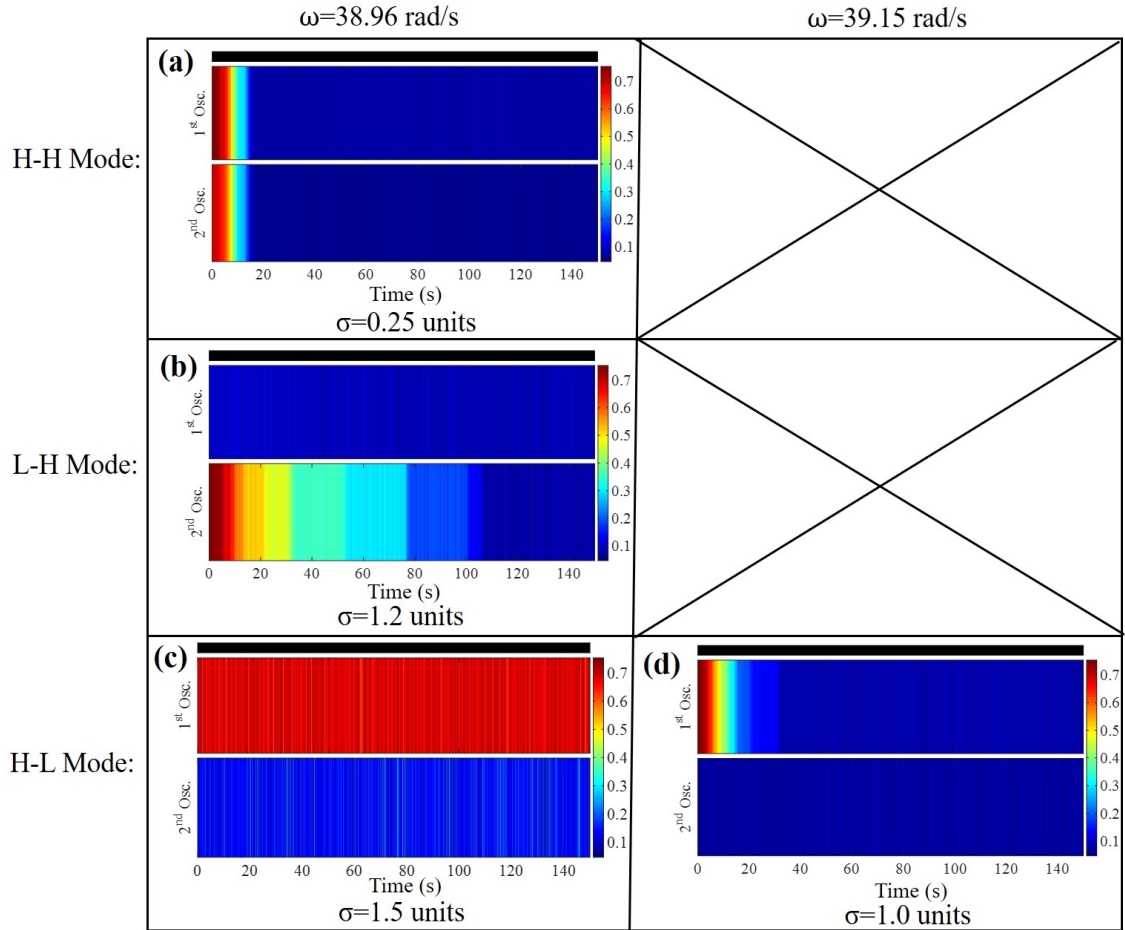


Figure 4.12: Experimental results for the effects of noise on different modes near the right boundary of MR for the system of two coupled oscillators shown in Figure 4.2.

comparing the frequency response curves obtained from the experiments and the numerical work. The LMs observed in the experiments have longer ends compared to the response state in which all oscillators are in a high mode. However, in the numerical results, they have shorter ends than that of the all high mode. As a result, in the numerical study, the LMs are more vulnerable to a change under the influence of noise, which is not in agreement with the experimental results. A better system

model is needed to predict the qualitative behavior within this region.

4.2.2.2 Three Oscillators

For the array with three coupled oscillators, four different modes are chosen near to the right end of the MR, which are H-H-H, H-H-L, H-L-H, and H-L-L modes, as shown in Figure 4.9 (b). The influence of noise on these modes is shown in Figure 4.13. The results show that the H-H-H mode is the the most vulnerable mode to perturbations. In Figure 4.13 (a), applying $\sigma = 0.5 \text{ units}$ at $\omega=38.29 \text{ rad/s}$ is sufficient to induce a change in the system dynamics. As one moves down in the energy branches, the modes become more robust to noise. A change in the H-L-H mode is possible for higher noise intensities, as shown in Figure 4.13 (b). For the last two modes, no change is noticed when applying noise at $\sigma = 1.5 \text{ units}$. One needs to either apply higher noise intensities or move closer to the two modes ends for a change to happen, as shown in Figures 4.13 (c)-(g).

The results agree well with the previous findings obtained with two oscillators. The mode that has the longest branch is found to be the most robust one to disturbances. In the numerical part, the the author is not able to capture the mode response change for the same reason as described in the previous section for the case with two coupled oscillators.

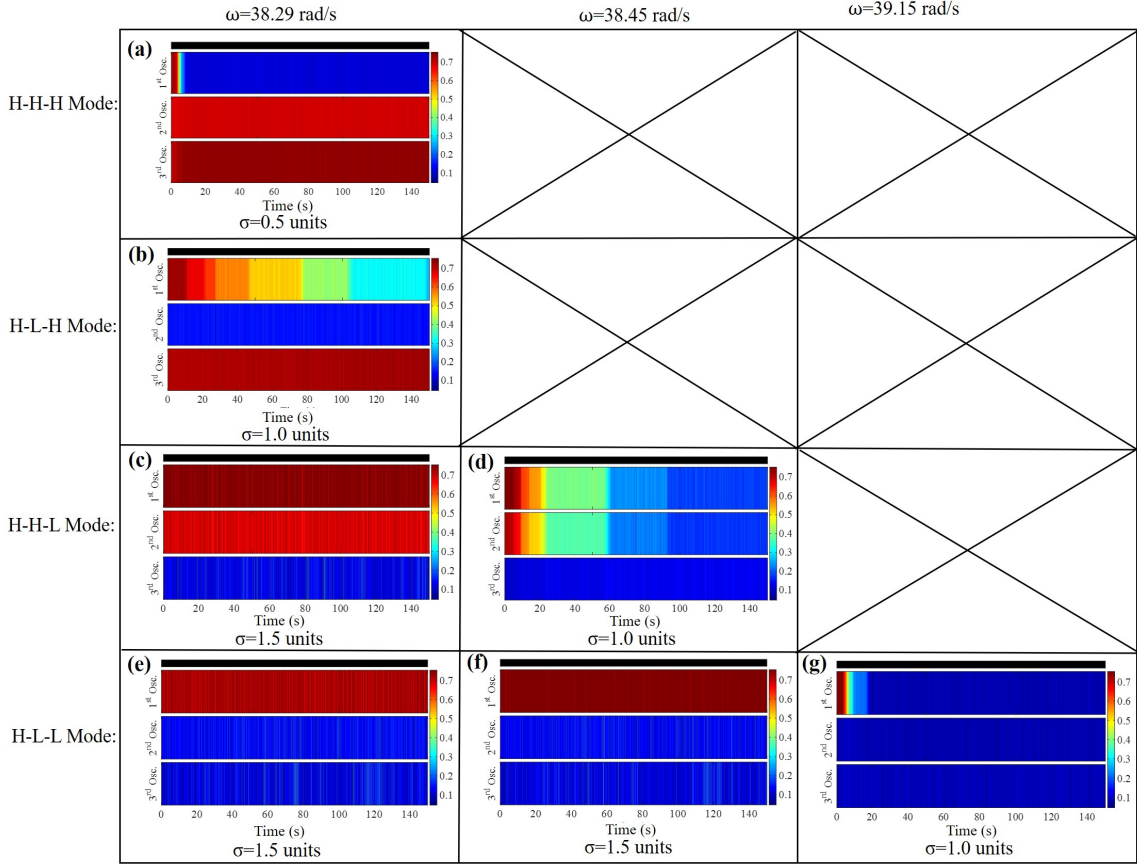


Figure 4.13: Experimental results for the effects of noise on different modes near the right boundary of MR for the system of three coupled oscillators shown in Figure 4.5.

4.3 Basins of Attraction

The basins of attraction for the three previous oscillators starting from H-H-H, H-L-H, H-L-L, and L-L-L are generated as described in Chapter 2 and shown in Figures 4.14 (a), (b), (c), and (d), respectively. For an initial condition in the H-H-H mode, a large basin of the H-H-H mode is found surrounding the original initial condition with only a relatively small sized basin for the L-L-L mode. This

result indicates the robustness of the H-H-H mode to noise at this frequency. For a start from the H-L-H mode, it is found that the basin of this mode is surrounded by the basin of the H-H-H mode in mostly all directions. Thus, if noise is applied to response in the H-L-H mode, the middle oscillator response is most likely to jump from a low amplitude state to a high amplitude state. For dynamics initiated from the H-L-L mode, a small sized basin is found for the H-H-L mode surrounding the basin of the H-L-L mode, and a large sized basin for the H-H-H mode covering mostly the whole remaining region. This would mean that when noise is applied, a transition from the H-L-L mode into the H-H-L mode, followed by a transition to H-H-H is possible. For the last case, when the dynamics is initiated from the L-L-L mode, the H-H-H mode basin is found to cover the whole region, which is expected as one jumps from the L-L-L mode immediately to the H-H-H mode after application of noise.

4.4 Effects of Coupling Strength on System Response

For low coupling strength to zero coupling, the system dynamics is similar to that of individual Duffing oscillators discussed in Chapter 2. As the coupling strength increases, the coupling between the oscillators is expected to influence the system dynamics. Understanding how the coupling influences the dynamics could be helpful in better utilizing noise to change the system dynamics. To that end, the Van der Pol's method is used to obtain the steady state solutions for different coupling values [68]. To begin with, the solution of equation (2.2) for a set of two

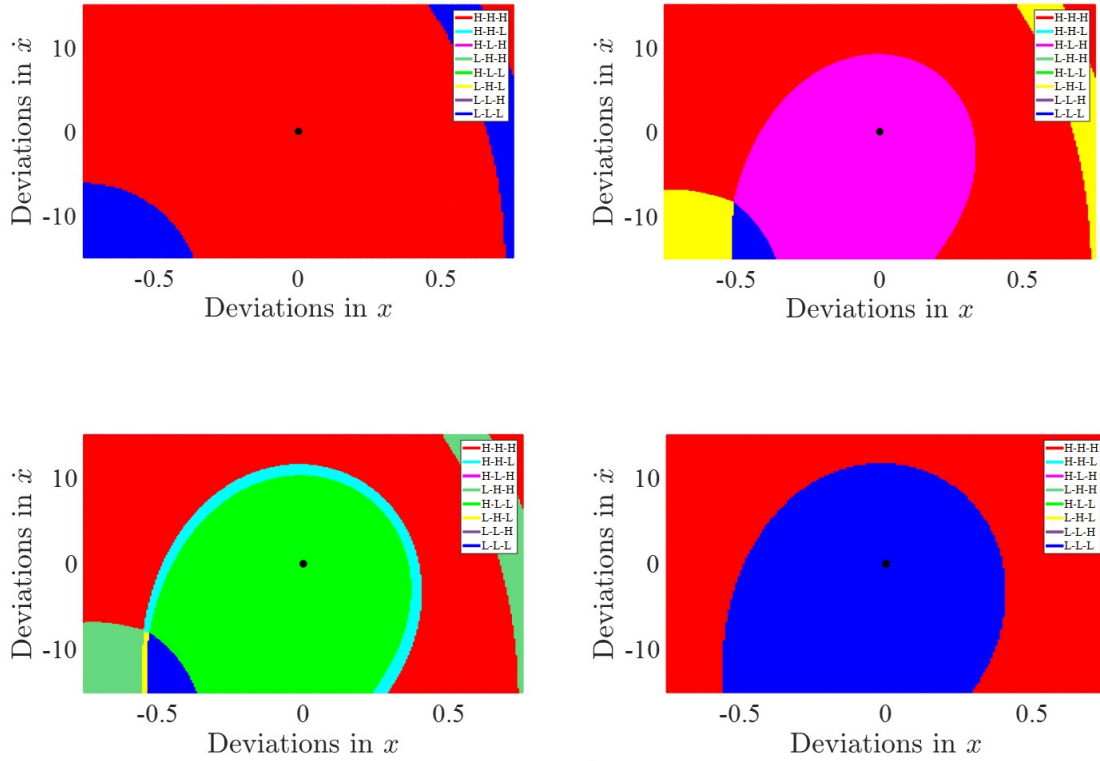


Figure 4.14: Basins of attraction for the system of three coupled oscillators, when starting from the following response modes: (a) H-H-H, (b) H-L-H, (c) H-L-L, and (d) L-L-L.

coupled oscillators is assumed to have the following form:

$$x_i = u_i \cos \omega t - v_i \sin \omega t \quad \text{for } i = 1 \text{ and } 2 \quad (4.1)$$

where, u_i and v_i are unknown variables of time. The amplitude and phase of each oscillator are represented by $A_i = \sqrt{u_i^2 + v_i^2}$ and $\theta = v_i/u_i$, respectively. The system parameters are scaled using a book keeping parameter ϵ as follows:

$$u_i, v_i = O(1), \quad \zeta, \beta, a = O(\epsilon) \quad \dot{u}_i, \dot{v}_i = O(\epsilon^2), \quad \ddot{u}_i, \ddot{v}_i = O(\epsilon^4) \quad (4.2)$$

After substituting equation (4.1) into equation (2.2) with consideration of the scaling provided in equation (4.2), the governing equation for the approximate steady solutions can be found, up to the accuracy of $O(\epsilon^2)$, as follows:

$$\begin{aligned}
2\omega\dot{u}_1 &= -2\zeta\omega\omega_{n0}u_1 + \alpha v_2 + (\omega^2 - \omega_{n0}^2 - \alpha)v_1 - \frac{3}{4}\beta v_1(u_1^2 + v_1^2) \\
2\omega\dot{v}_1 &= -2\zeta\omega\omega_{n0}v_1 - \alpha u_2 + (-\omega^2 + \omega_{n0}^2 + \alpha)u_1 + \frac{3}{4}\beta u_1(u_1^2 + v_1^2) - a \\
2\omega\dot{u}_2 &= -2\zeta\omega\omega_{n0}u_2 + \alpha v_1 + (\omega^2 - \omega_{n0}^2 - \alpha)v_2 - \frac{3}{4}\beta v_2(u_2^2 + v_2^2) \\
2\omega\dot{v}_2 &= -2\zeta\omega\omega_{n0}v_2 - \alpha u_1 + (-\omega^2 + \omega_{n0}^2 + \alpha)u_2 + \frac{3}{4}\beta u_2(u_2^2 + v_2^2) - a
\end{aligned} \tag{4.3}$$

To obtain the solutions for the different response branches from equation (4.3), the initial condition of (1,0) is first assigned for each oscillator based on the H or L amplitude assumptions. The solutions are then used in Auto software to continue the solution along each branch. In Figures 4.15 (a)-(d), the solution of equation (4.3) for the parameters shown in Table 4.1 for the first oscillator with the coupling parameters $\alpha = 1$, $\alpha = 3$, $\alpha = 5$, and $\alpha = 20$ are presented, respectively. Since the numerical results do not show accurate results for the right boundary of the MR, the focus will be only on the left boundary. For small coupling ($\alpha = 1$), the ends of the two LMs are just before the ends for the unison modes, wherein all oscillators have the same response amplitudes. As the coupling strength is increased, the amplitude gap between the LMs and the unison modes is found to increase. Increasing the coupling strength further will make this gap larger with the inducement of a Hopf bifurcation as shown for $\alpha = 20$.

In Figure 4.16, the bifurcation sets are shown in the $\alpha - \omega$ space. The solid

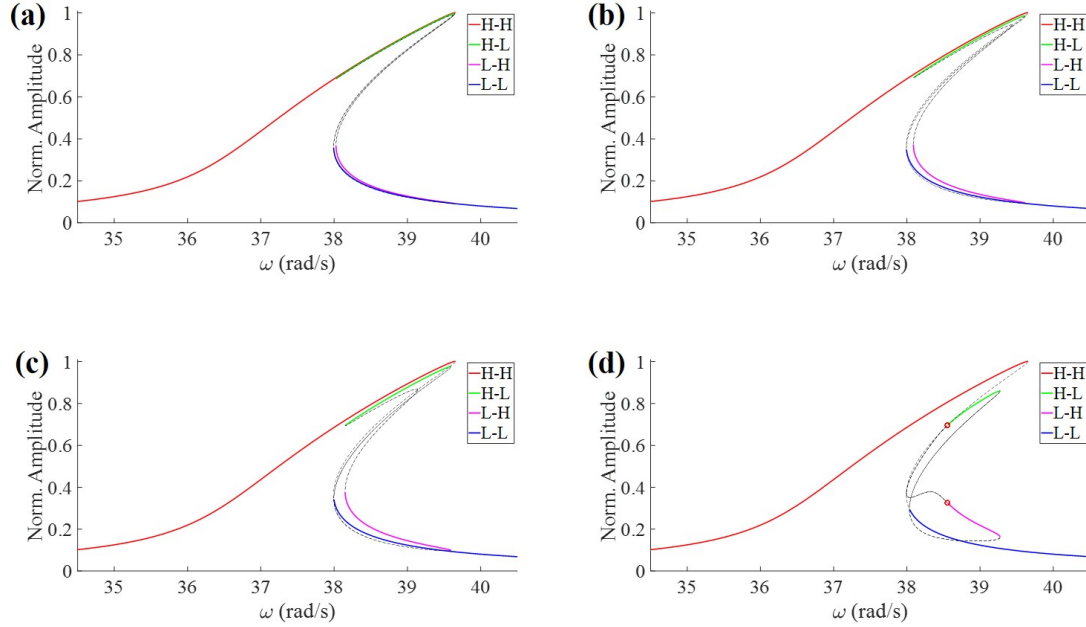


Figure 4.15: Effects of coupling increase on the four response branches of the set of two coupled oscillators for the parameters provided in Table 4.1: (a) $\alpha = 1$, (b) $\alpha = 3$, (c) $\alpha = 5$, and (d) $\alpha = 20$.

black lines are the boundary of the unison mode with the region for the H-H and the L-L modes illustrated by the black arrow. These modes are not affected by the increase in the coupling strength. The LMs are bounded by the two green curves, which is illustrated by the red arrow. For a high coupling strength, a Hopf bifurcation is induced, and the loci of the Hopf instability points is shown by using the red curve.

4.5 Effects of Increase in Number of Oscillators in an Array

In this section, numerical simulations are used to study how the increase the number of oscillators affects the noise influenced responses. Arrays of one to five

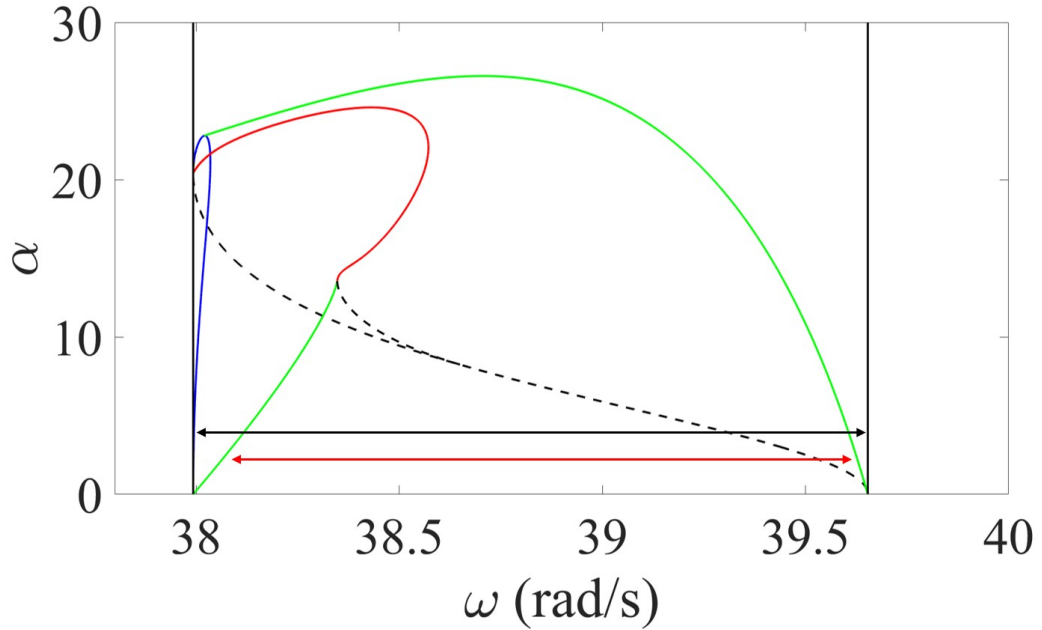


Figure 4.16: Bifurcation sets in the (ω, α) plane for the system of two coupled oscillators with the parameters listed in Table 4.1. The black lines are the boundaries of the MR, the green curves are the boundaries of the LMs, the red curve is the loci of Hopf bifurcation points, the blue curve is a stable branch near the left boundary and the black dashed curves are unstable saddle points. The black and red arrows represent the range for the MR and LMs, respectively.

oscillators are considered near to the left boundary ($\omega=38.3$ rad/s) of the MR of the system with parameters as listed in Table 4.1. The corresponding modes are are L, H(L), H(L)H, HH(L)HH and HHH(L)HHH. The goal is to track how the responses of the low amplitude oscillators induce a transition to a state of the high amplitude oscillations. The average RMS displacements, which were obtained with 50 noise vectors for all the selected modes at $\sigma = 2.5$ units, are shown in Figures 4.17 (a)-(e). For a single oscillator, it is clear that over a time window of 500 s, in only a few trials (8 out of 50), the addition of noise is successful in inducing a

jump. When another oscillator in a state of high amplitude oscillations is coupled to a low amplitude state oscillator, the number of trials in which a noise induced jump occurs increases significantly. For the same time window, in only 8 of the 50 trials, a jump did not occur. Next, two neighboring oscillators with a high amplitude state are coupled to an oscillator in a low amplitude state. Within almost no time, the responses of all of the oscillators jumped to a state of high amplitude oscillators. When increasing the number of oscillators further, no significant change is observed in the responses of the three oscillators. Through the numerical results, it is shown that the two neighboring oscillators have a high impact on the middle oscillator's response sensitivity to noise. When they have different amplitude oscillations they facilitate the transition of the middle oscillator's response to another state. The plots for all of the low amplitude oscillations in the previous cases as well as the final state of the high amplitude oscillations are shown in Figure 4.18. From these results, it can be noted that when an oscillator has neighboring oscillators with different amplitude responses, the addition of noise gets the response closer to the final H state, wherein all oscillators are in a high amplitude state. Beyond three oscillators, the phase space plots are found to not change, and this is reflected in the previous results.

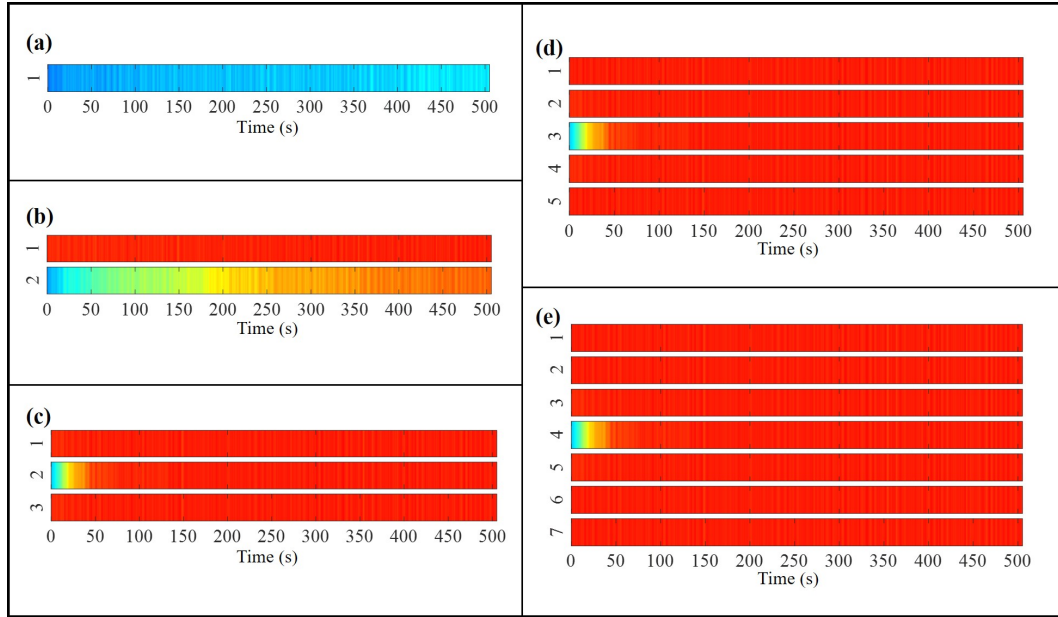


Figure 4.17: Effects of noise on an oscillator in a state of low amplitude oscillations: (a) L, (b) H-L, (c) H-L-H, (d) H-H-L-H-H, and (e) H-H-H-L-H-H-H

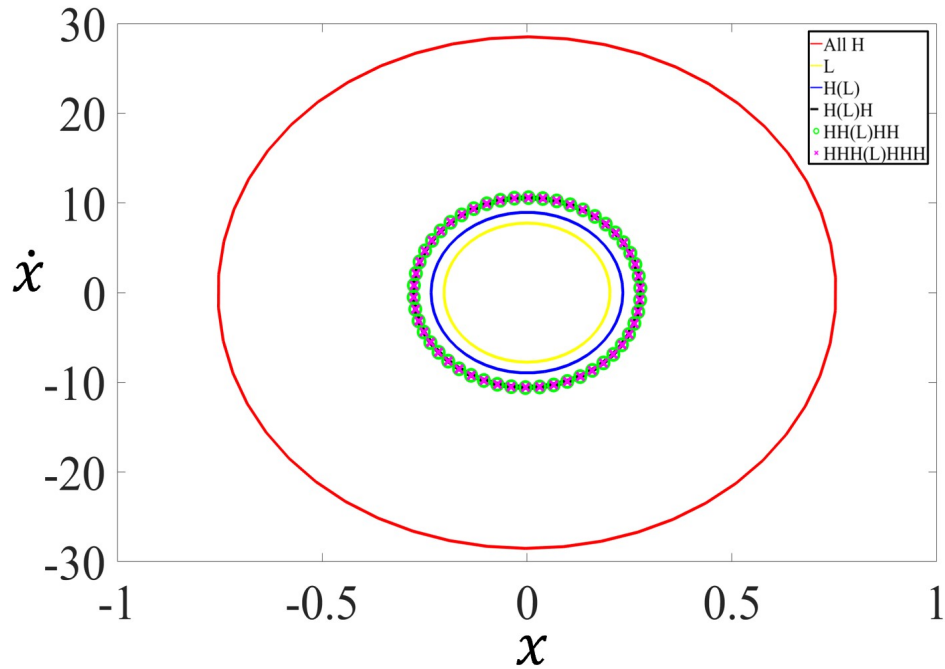


Figure 4.18: Phase space plots for the selected modes in Figure 4.17.

Chapter 5: Noise Based Control of System Energy of Coupled Oscillator Arrays

In this chapter, possible noise based methods for controlling the system energy of coupled oscillator arrays are discussed. Different responses are generated under the influence of noise. Both experimental and numerical efforts are used here.

5.1 Influence of Noise Near MR Boundaries

The results of Chapter 2 are used as a clue to test a large array size. Hardening and softening oscillators in arrays, each composed of 21 oscillators, are considered for the study. All of the oscillators are assumed to be identical with the properties of an oscillator as listed in Table 2.1. For the hardening case, the qualitative results obtained for the influence of noise on a large oscillator array agree well with those provided in Chapter 2 for a set of two coupled oscillators. Near the left boundary or the low frequency end of the MR, all of the oscillators tend to move towards a state of high amplitude oscillations under the influence of noise, while near the right boundary or the high frequency end of the MR, the oscillators tend to move toward towards a state of low amplitude oscillations, as can be seen from Figure 5.1. For the case with softening oscillators, the opposite is true. Near the left boundary of

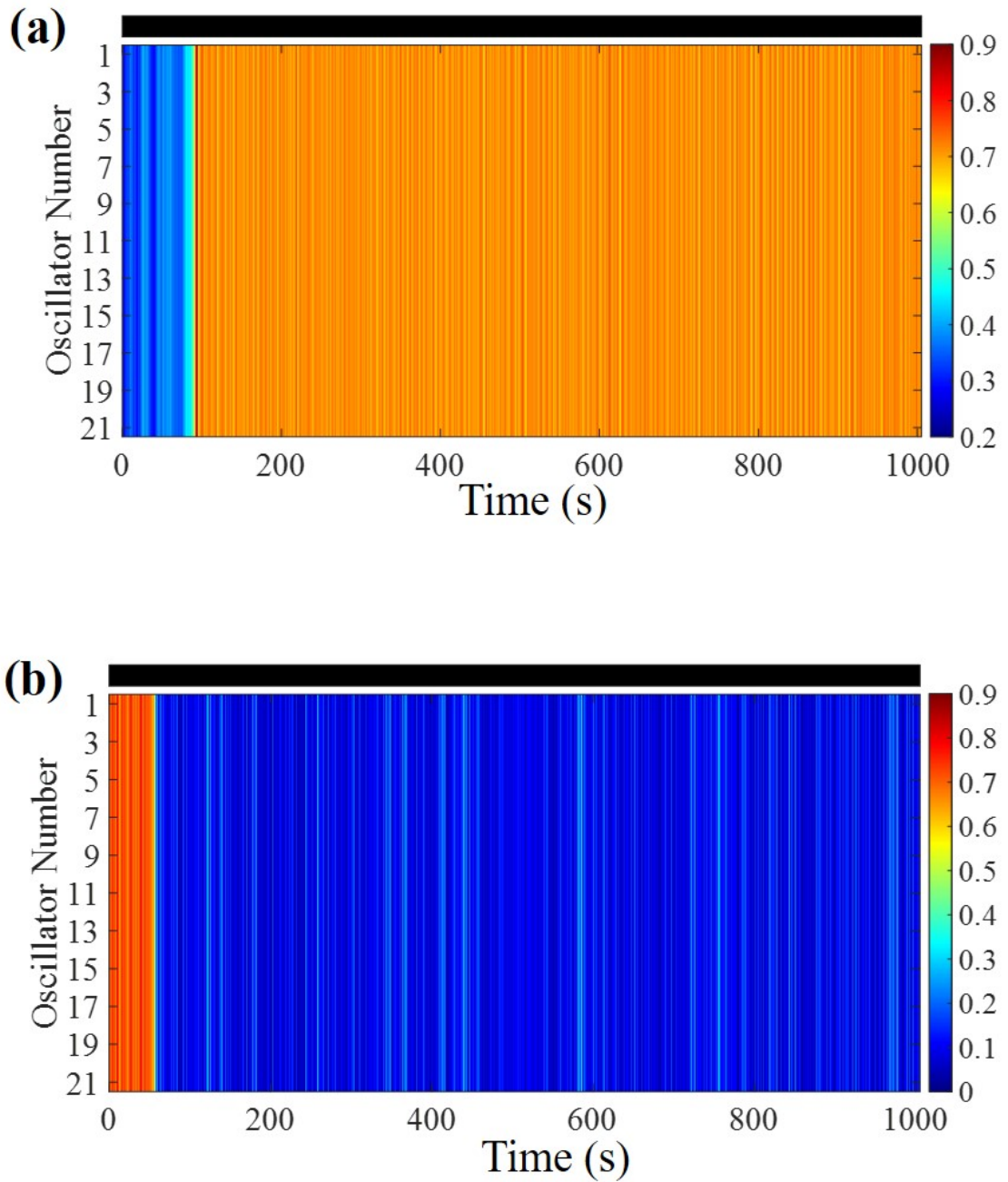


Figure 5.1: Numerical results for the effects of noise on 21 hardening Duffing oscillators for the parameters listed in Table 2.1: (a) near left boundary of MR ($\omega=34.86$ rad/s) and (b) near right boundary of MR ($\omega=36.72$ rad/s). The dark horizontal bar on the top is used to indicate that noise is applied throughout the chosen duration.

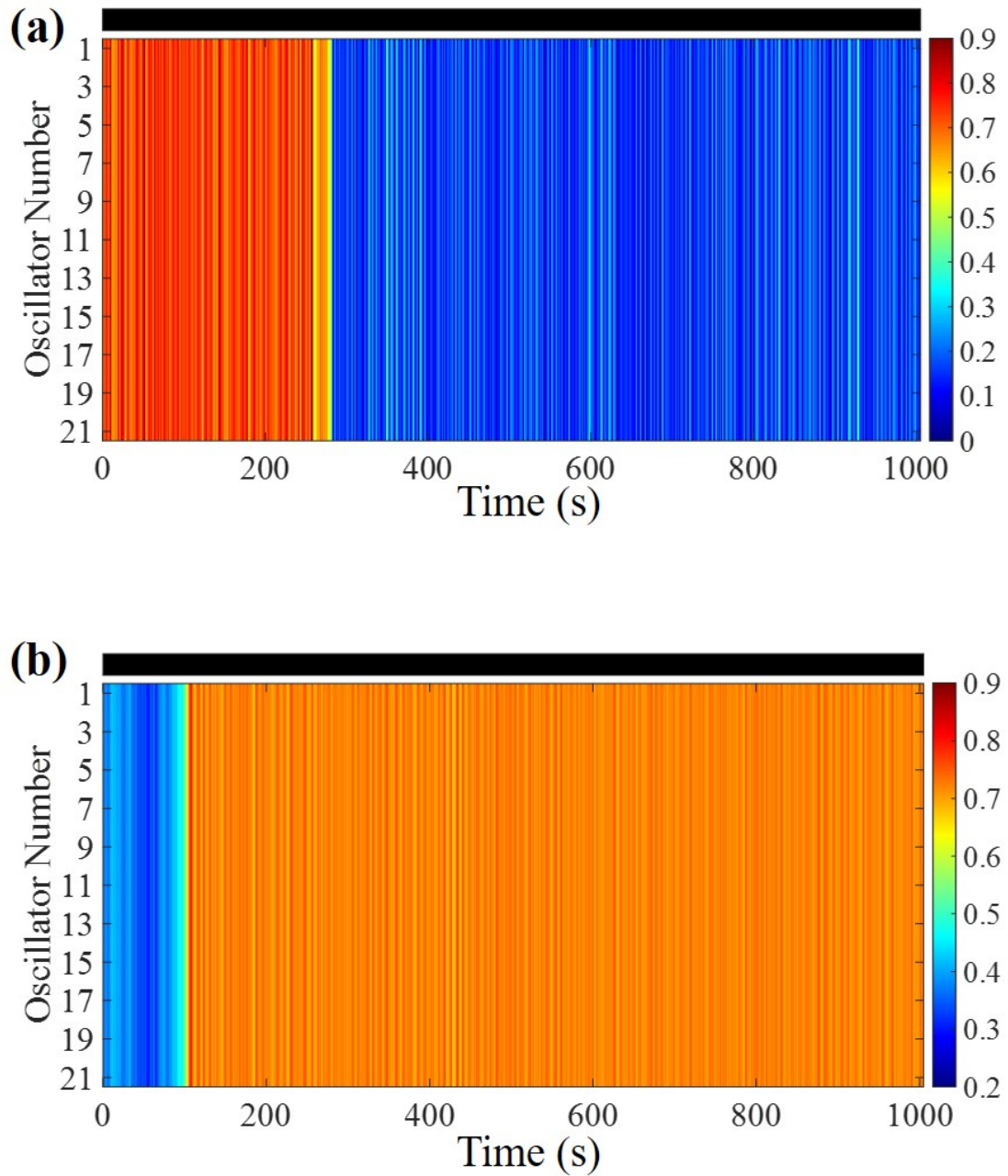


Figure 5.2: Numerical results for the effects of noise on 21 softening Duffing oscillators for the parameters listed in Table 2.1: (a) near left boundary of MR ($\omega=34.86$ rad/s) and (b) near right boundary of MR ($\omega=35.39$ rad/s). The dark horizontal bar on the top is used to indicate that noise is applied throughout the chosen duration.

the MR, the oscillators tend to move towards a state of low amplitude oscillations, whereas near the right boundary, the oscillators tend to move towards a state of high amplitude oscillations, as can be seen from Figure 5.2.

These findings can be understood by studying the basins of attractions for the single Duffing oscillators, since they represent the building blocks for the oscillator arrays. For the hardening type of oscillators, near the left boundary of the MR, the basins of attraction of the high amplitude oscillations is larger in size than that of the basin of the low amplitude oscillations. As perturbations are applied, the system in all likelihood transitions to a state of high amplitude oscillations. Near the right boundary of the MR, the basin of attraction for the high amplitude oscillations is small in size compared to the basin of the low amplitude oscillations. Thus, it is expected that the coupled oscillator arrays move from a state of high amplitude oscillations to a state of low amplitude oscillations under the influence of noise. For a system composed of softening type oscillators, the opposite behavior is expected.

5.2 Noise Induced Response Energy Level Increase

In all of the previous findings, applying noise for unison modes (all high or all low) of homogeneous oscillators results in a system response wherein all of the oscillators either jump to high amplitude oscillations or drop to low amplitude oscillations simultaneously. The oscillators could have different transition times from one response to another, if there are imperfections/non-uniformity in the coupling between the oscillators. To that end, two coupled oscillators are tuned experimen-

Table 5.1: First oscillator parameters obtained by matching the results from the quasi-static frequency sweep shown in Figure 5.3.

Parameter	Value	Parameter	Value
ω_{n01}	33.25 rad/s	ω_{n02}	33.15 rad/s
β	205	F	18.0
ζ	0.0075	α	1

tally such that the oscillators have different jump up frequencies in the coupled system. From the corresponding results shown in Figure 5.3 (a), it is clear that during a quasi-static frequency sweep down the first oscillator jumps to a state of high amplitude oscillations at $\omega=34.24$ rad/s, whereas the second oscillator jumps at $\omega=34.19$ rad/s. The system is first set to the L-L mode at $\omega=34.26$ rad/s, as can be seen from Figure 5.3 (b). Noise is applied at $t=113$ s for about 13 s. Since this frequency is close to the jump up frequency of the first oscillator, a localized mode is created when the first oscillator response is induced a jump to a state of high amplitude oscillations. Stopping noise input at this time shows that the localized mode persists as long as no further disturbances are applied. Noise is reapplied at $t=210$ s for about 190 s. Due to the influence of noise, the second oscillator response jumps as well to a state of high amplitude oscillations. As a result, noise can be used to jump between the energy branches of the oscillator arrays when nonhomogeneities exist.

Similar qualitative results are obtained by using numerical simulations. The oscillator in the arrays are assumed to have properties close to that of first oscillator in Figure 5.3 with the natural frequencies being the only difference between the two

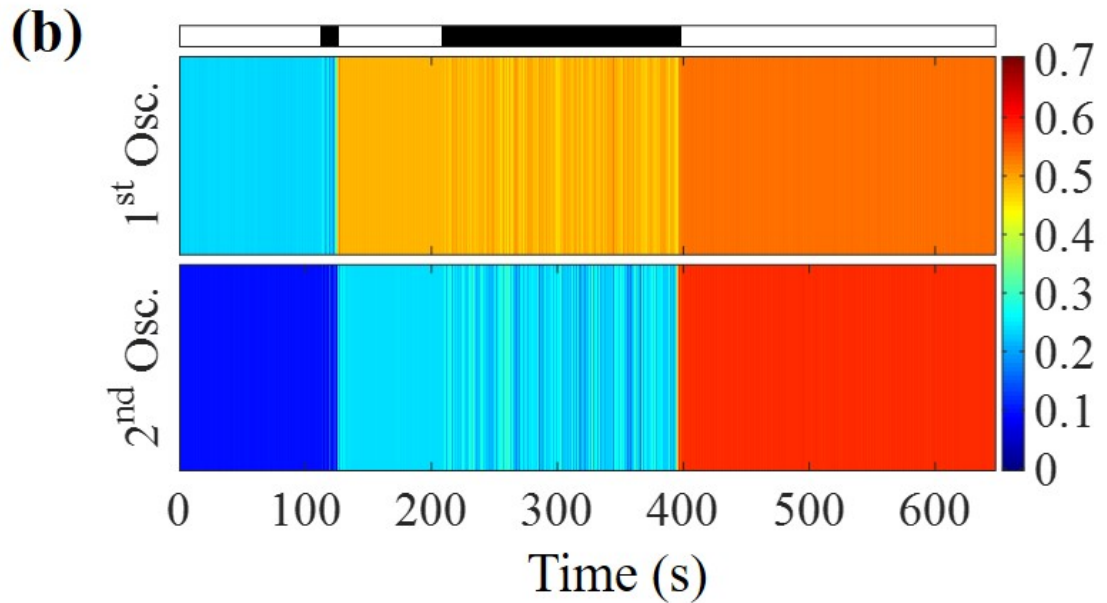
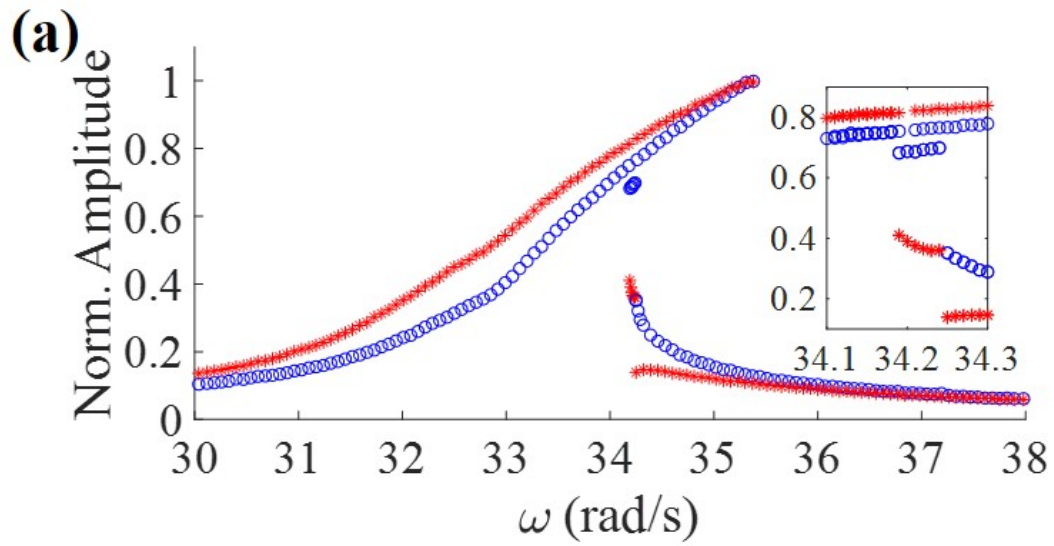


Figure 5.3: Experimental results for noise induced gradual energy increase in a set of two coupled oscillators: (a) a quasi-static frequency change for the system and the responses for the first (blue) oscillator and second (red) oscillator and (b) increase of energy in the first oscillator followed by that in the second oscillator. The dark regions in the horizontal bar on the top in (b) are regions where noise is applied.

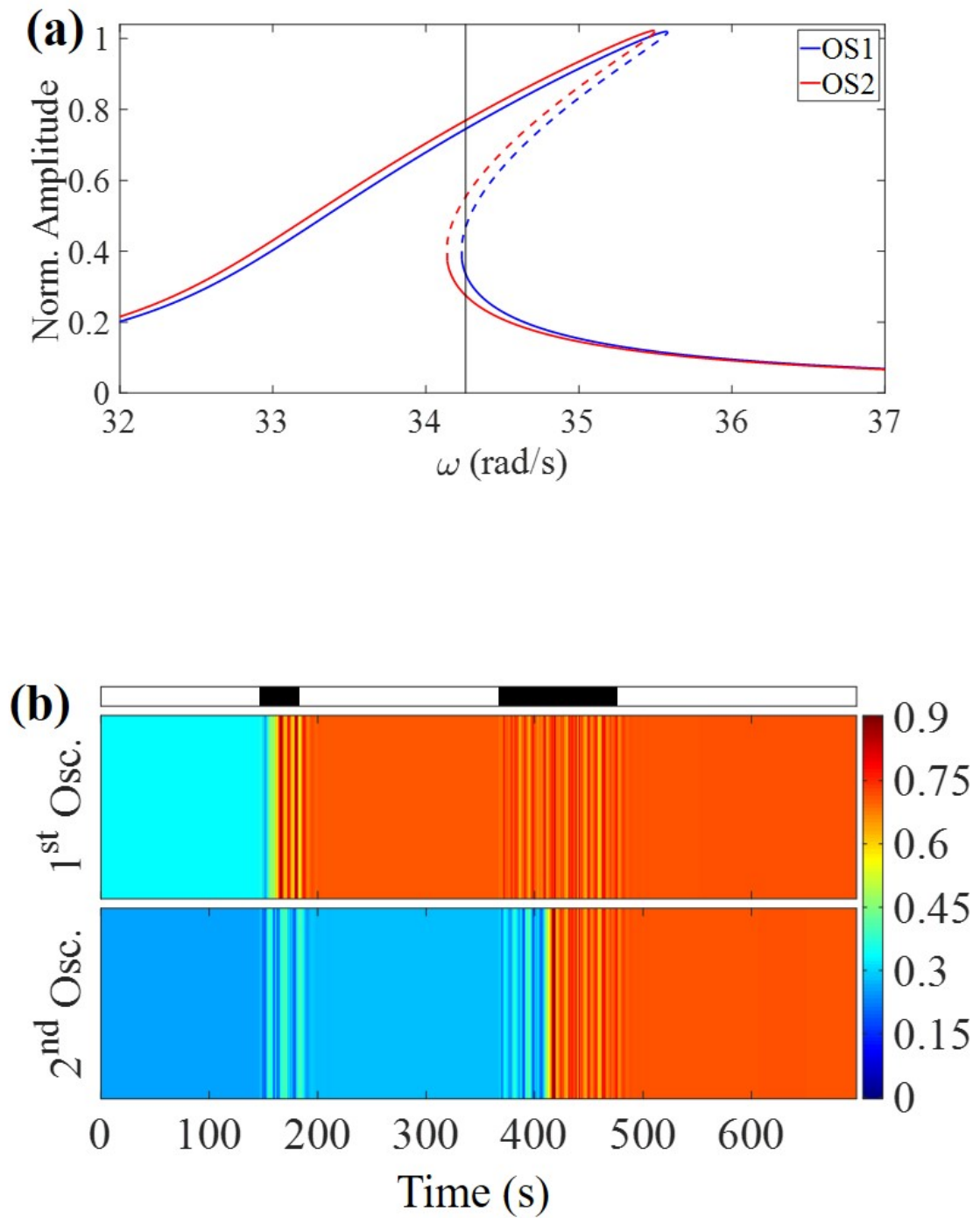


Figure 5.4: Numerical results for noise induced gradual energy increase in a set of two oscillators: (a) quasi-static frequency sweep for the system and the responses for the first (blue, OS1) oscillator and second (red, OS2) oscillator and (b) increase of energy in the first oscillator followed by that in the second oscillator. The dark regions in the horizontal bar on the top in (b) are regions where noise is applied.

oscillators, as shown in Table 5.1. The analytical approximations for the responses of the uncoupled oscillators are shown in Figure 5.4 (a). Similar to the experiments, noise is used to induce energy transition from the L-L response mode to the H-L response mode and then to the H-H response mode.

5.3 Noise Induced Spatial Movement of an Energy Localization

As discussed previously, the hardening and softening oscillators arrays have opposite properties. For this section, two oscillators are coupled together, with the first oscillator having a softening character and the second oscillator having a hardening character. The two oscillators are tuned so that the jump down in the first oscillator's response is near the jump up in the second oscillator's response. Results from the experimental quasi-static frequency sweep for the array is shown in Figure 5.5 (a). At $\omega=34.86$ rad/s, the oscillators are set to have a localized mode in the first oscillator, as shown in Figure 5.5 (b). Noise is then applied for a time duration of about 70 s. Due to the application of noise, the first oscillator response is collapsed to a state of low amplitude oscillations, and the energy of the system is decreased. Since the considered harmonic excitation frequency is close to the jump up frequency for the second oscillator, a continued application of noise induces the second oscillator to move to a state of high amplitude oscillations. Thus, noise has been used to induce a spatial movement of energy in the considered coupled oscillator array.

Similar results were obtained during numerical simulations. The properties of

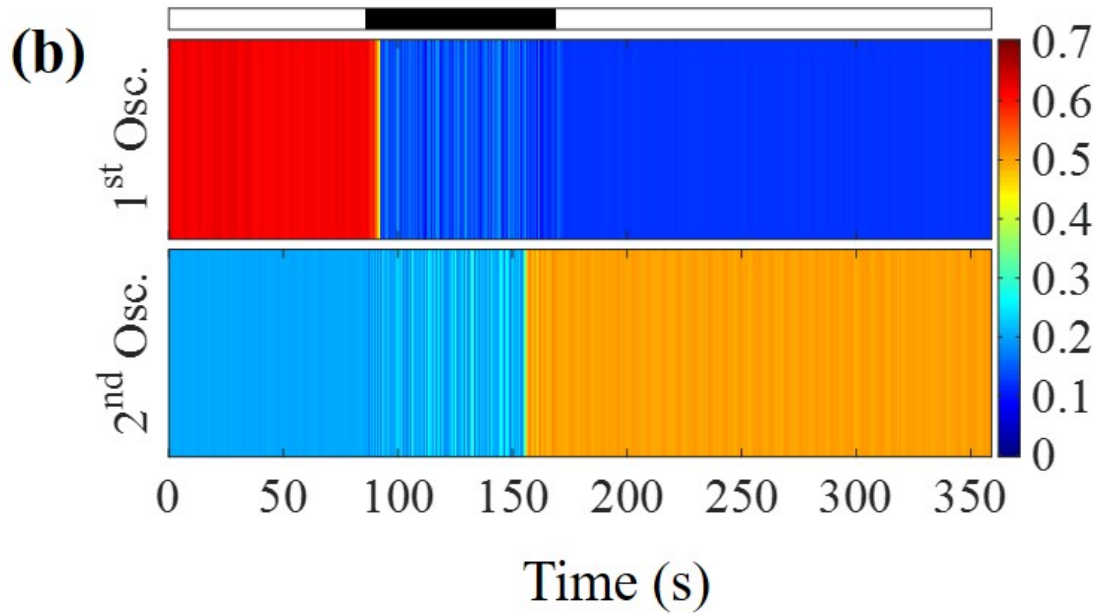
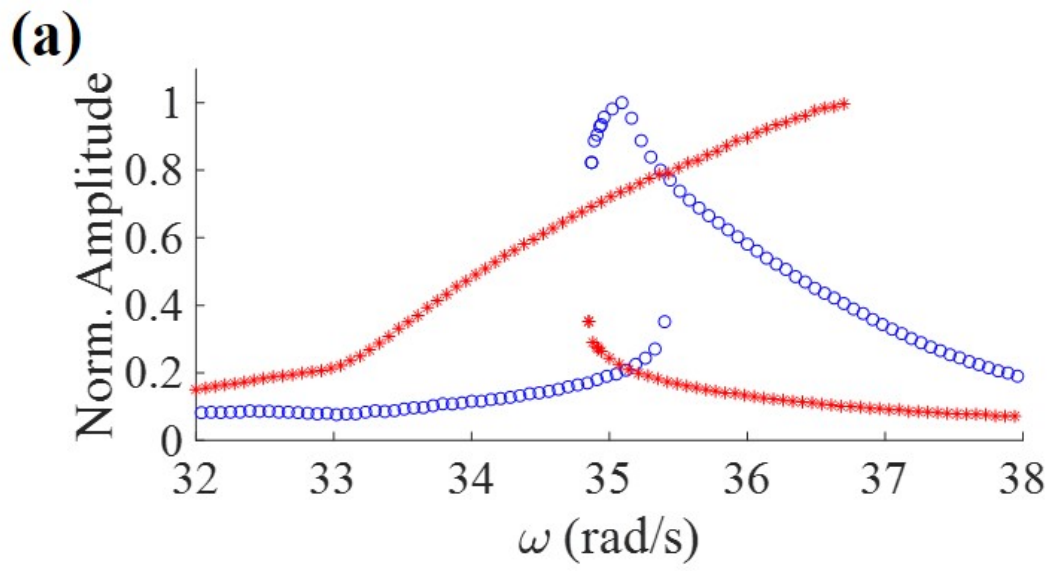


Figure 5.5: Experimental results for noise induced spatial movement of energy in a set of two coupled oscillators: (a) quasi-static frequency sweep for the system and the responses for the first (blue) oscillator and second (red) oscillator, and (b) spatial energy movement from the first oscillator to second oscillator. The dark regions in the horizontal bar on the top in (b) are regions where noise is applied.

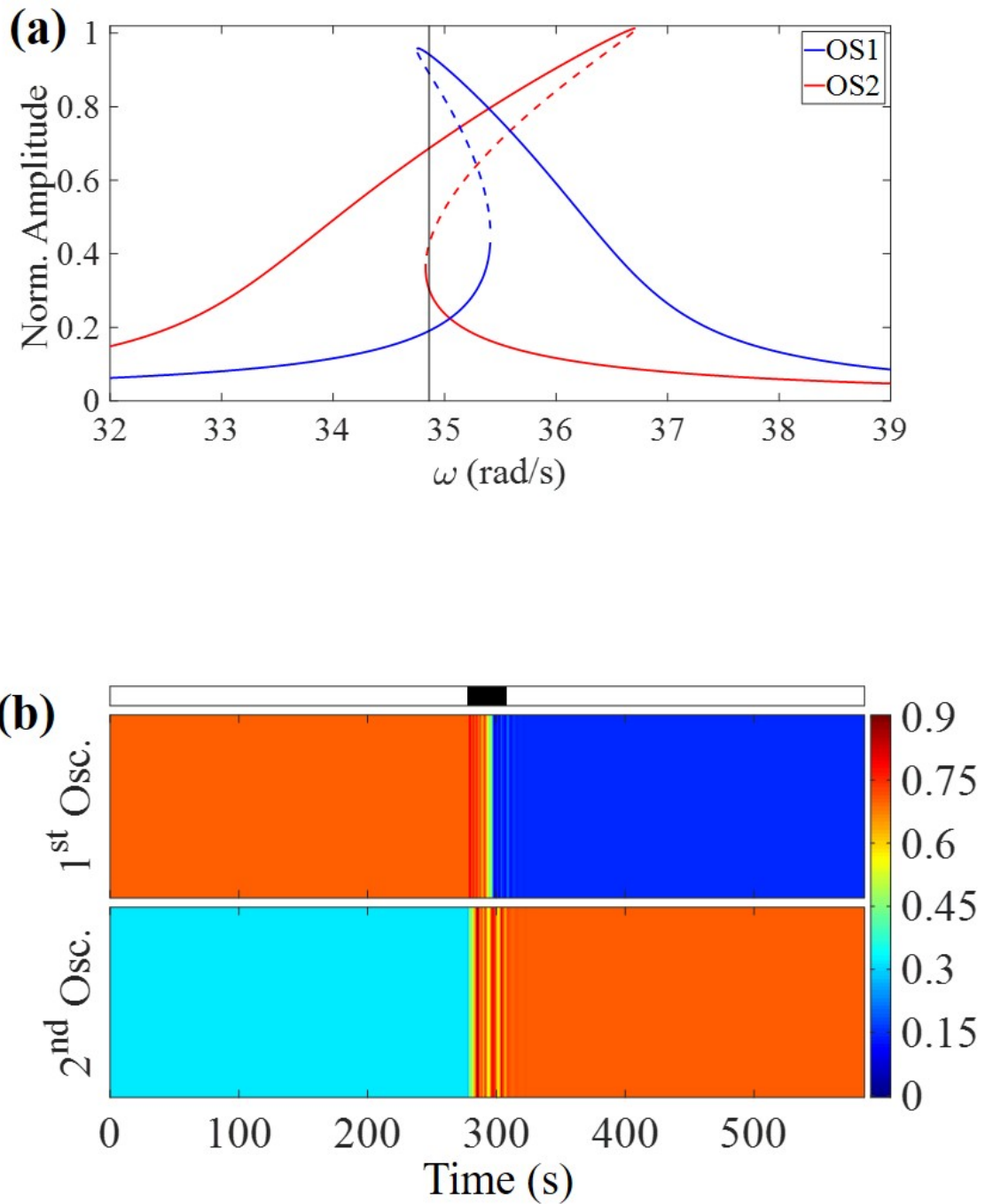


Figure 5.6: Numerical results for noise inducing spatial movement of energy in a set of two coupled oscillators: (a) quasi-static frequency sweep for the system and the responses for the first (blue, OS1) oscillator and second (red, OS2) oscillator, and (b) spatial energy movement from the first oscillator to second oscillator. The dark regions in the horizontal bar on the top in (b) are regions where noise is applied.

the first oscillator and the second oscillator are first obtained from the frequency response curve, which is shown in Figure 5.6 (a), and the corresponding parameter values are listed in Table 2.1. The oscillators are first set to have a LM in the first oscillator. The application of noise results in a change in the spatial location of the LM to the second oscillator, as shown in Figure 5.6 (b).

5.4 Influence of Noise on a Localized Mode and an Anti-localized Mode

For a 21 oscillator array, the influence of noise on a LM and anti-localized mode (ALM) is numerically investigated. All of the oscillators are assumed to be homogeneous with the parameter values listed in Table 2.1. For the LM case, a state of high amplitude oscillations is created at $\omega=34.9$ rad/s near the jump up frequency for the middle oscillator, while all the other oscillators are vibrating in a state of low amplitude oscillations, as shown in Figure 5.7 (a). When noise is introduced, the two neighboring oscillators adjacent to the localized oscillator start to respond and move to a state of high amplitude oscillations. As the noise input is continued, these immediate neighboring oscillators respond and the result is a movement to a state of high amplitude oscillations. This pattern continues resulting in energy cascades until all of the oscillators vibrate in a state of high amplitude oscillations, as shown in Figure 5.7 (b). In Figure 5.8, it is shown that different number of high amplitude oscillations can be obtained by stopping the noise input at different times.

For the ALM, the oscillators are first set to have a low amplitude oscillation

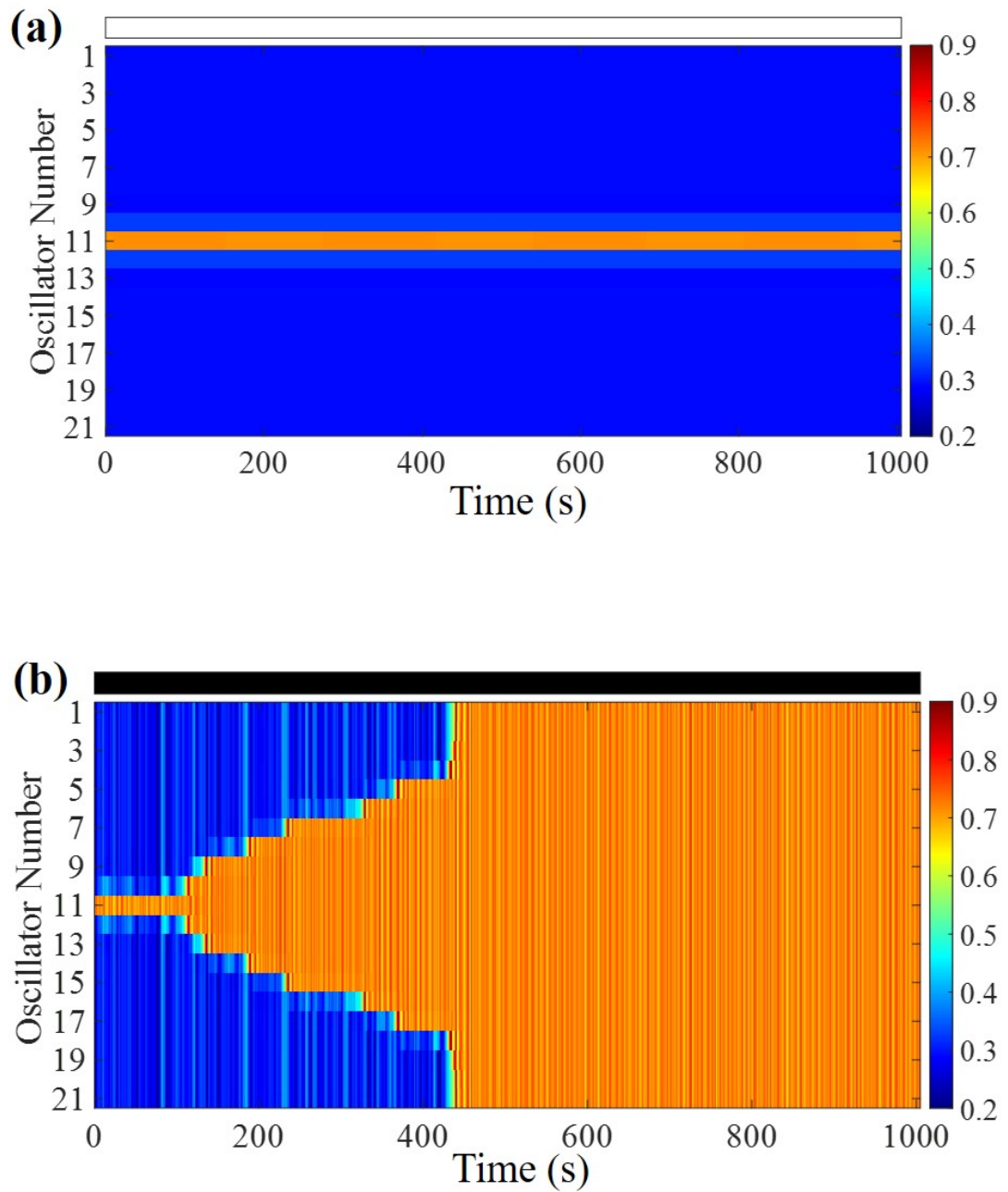


Figure 5.7: Influence of noise on a LM near the left boundary of MR ($\omega=34.90$ rad/s): (a) no noise is applied and (b) $\sigma = 1$ units. In case (b), noise is applied throughout the duration of interest.

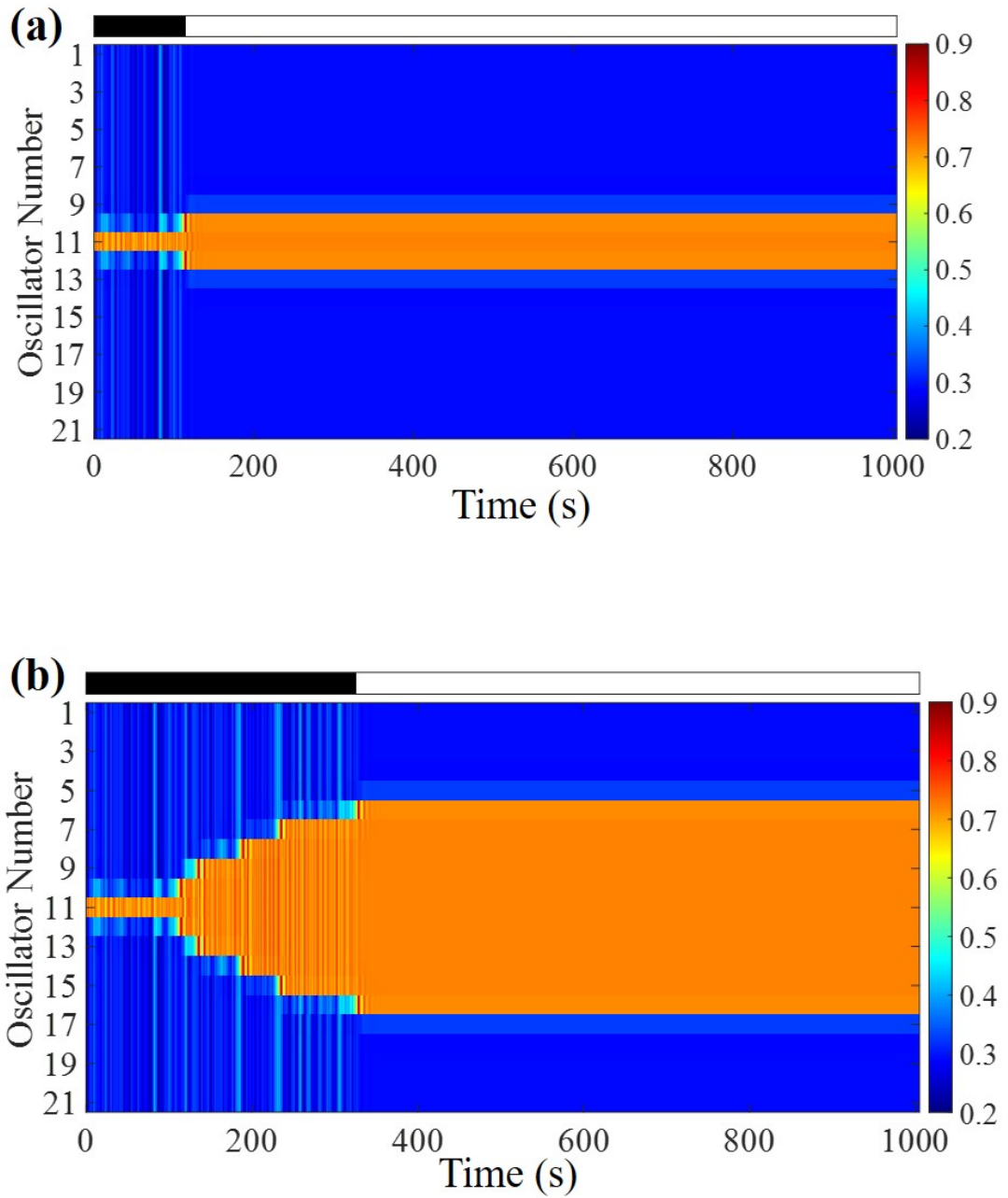


Figure 5.8: Noise is stopped at different time instants in Figure 5.7 inducing increase in the number of oscillators transitioning to a state of high amplitude oscillations from one to three in (a) and eleven in (b). The length of the black horizontal bar corresponds to the duration of the noise input.

only in the middle oscillator at $\omega=36.72$ rad/s near the jump down frequency location, as shown in Figure 5.9. The application of noise shows that there is no transition resulting in drop for the oscillator responses to low amplitude oscillations. Instead, all of the oscillators drop simultaneously to a state of low amplitude oscillations. As such, there is no noise induced transition between different energy branches. Rather, there is only a drop to all low amplitude mode across the array.

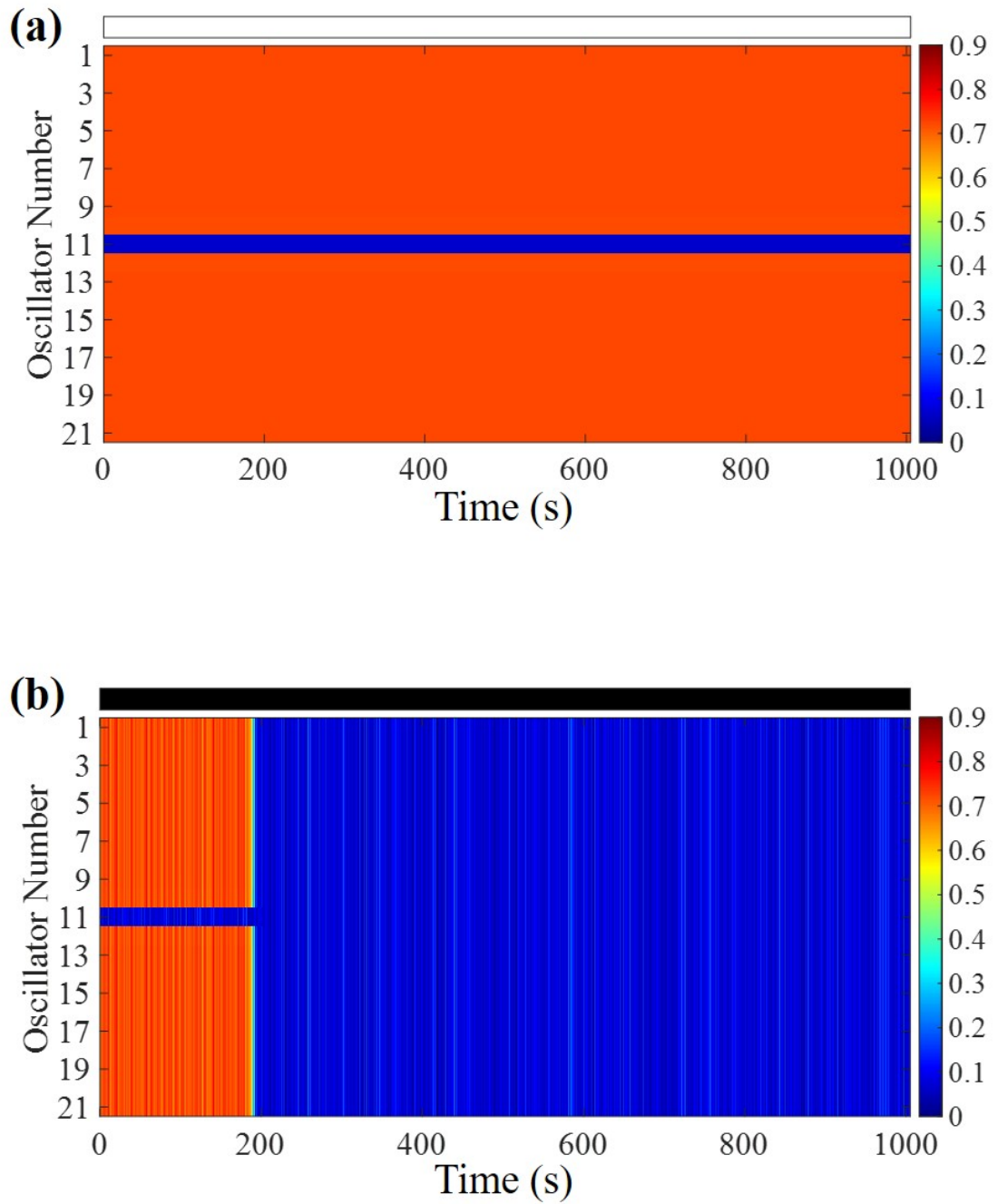


Figure 5.9: Influence of noise on an ALM near the right boundary of MR ($\omega=36.72$ rad/s): (a) no noise is applied and (b) $\sigma = 2$ units. In case (b), noise is applied throughout the considered duration as indicated by the black horizontal bar.

Chapter 6: Summary and Recommendations for Future Work

6.1 Summary

Here, a summary for the dissertation work and the key findings are discussed.

In this work, experimental and numerical studies have been carried out to study the influence of noise on the responses of coupled oscillators arrays. In Chapter 3, as an initial step, responses of an array of two coupled oscillators of the hardening Duffing type are investigated through experiments and numerical studies. Responses to harmonic excitations in the presence and absence of noise in the system input are studied. It has been shown that near the multi-stability region boundaries, the responses of the coupled oscillators arrays are highly sensitive to noise. Close to each boundary, a low level noise intensity is found to induce a change in the system dynamics. As one moves into the center of the frequency range of the considered multistability region, a higher level noise intensity is found to be needed to induce a response change. For the hardening case, near the left boundary of the multi-stability region, the responses of the oscillators tend to move toward high amplitude oscillations, whereas near the right boundary of the multi-stability region, the responses of the oscillators tend to move toward low amplitude oscillations. A method for recognizing how much noise is required to induce a change in

the system dynamics is developed by using the basins of attraction. Starting from a certain response mode, disturbances are applied to all of the oscillators and the resulting steady state responses are tracked and plotted. The size of the initial mode region is found to change with respect to the excitation frequency.

In Chapter 4, the effects of noise on different responses modes of two oscillator and three oscillator systems are discussed. For an array with two homogeneous oscillators, near the left boundary of the considered multi-stability region, the application of noise to a localized mode response is expected to induce a quick change to a state of all high amplitude response modes. Near the right boundary of the considered multi-stability region, the experimental results reveal that the application of noise to a response state with all high amplitudes has discernible influence on the response. The frequency response curves can be used to predict how sensitive each mode is compared to the other modes. While the numerical simulations are found to predict accurately the results close to the left boundary of a multi-stability region, the same is not true near the right boundary of a multi-stability region.

Through different studies in Chapter 4, the effects of coupling strength as well as the number of oscillators are investigated. With regard to the coupling, it has been shown that increasing the coupling facilitates a change in system dynamics under the influence of noise. From the study on the number of oscillators, it is noted that the influence of noise on the response of an oscillator depends highly on the character (i.e., hardening or softening characteristic) of the neighboring oscillators. The oscillators far from the location almost have no effect except for the neighbors.

In Chapter 5, noise input based control of the energy of coupled oscillators

arrays have been discussed. Noise is added to a harmonic excitation to move a high number of oscillators in an array from a high amplitude response state to a low amplitude response state and vice versa. It is shown that noise can be used to gradually move the system response up in the energy branches for an array of non-homogeneous oscillators. Also, the use of noise to transfer the energy from a softening oscillator to a hardening one has been illustrated. An interesting phenomenon for noise assisted shifting of energy from one oscillator to a neighboring has been presented. A cascade of energy increase was shown to be possible by applying noise to a localized response mode, when the excitation frequency is close to the left boundary of a multi-stability region. However, near the right boundary, through the numerical results, it is shown that the application of noise can destroy responses of high amplitude oscillations in all oscillators at once, which is not in conformity with the experimental results. The experimental results presented in the different chapters for noise influenced responses of arrays of coupled nonlinear oscillators are the first of their type.

6.2 Recommendations for Future Work

As discussed earlier, while the system model presented here can be used to accurately predict the experimental behavior near the left boundary of a multi-stability region, the same is not true for the right boundary of a multi-stability region. Thus, a better model is needed to obtain noise influenced responses of coupled oscillators arrays.

The focus of this work has been on arrays with monostable oscillators. However, the system responses can be more complicated if one were to consider other types oscillators, for example bi-stable oscillators. Also, based on few trials in this work, it is found that in the presence of imperfections and/or different types of oscillators in the considered array, one can observe interesting changes in the dynamics. Further studies are recommended to study these aspects, as they would be important for practical systems.

Here, control has been used in a limited sense to illustrate the potential of noise to change the system dynamics. However, one needs to consider the application of control in a broad sense. For example, it is still unclear as to what is the right duration and level of needed noise input to reach the desired final state. This prompts a recommendation to look into this further.

Some methods have been used to explore the possible potential for noise influence, including the basins of attraction and the length of the branches in the frequency-response curves. However, through these methods, one is only accounting for limited information. Work on other methods for high-dimensional systems is recommended.

Finally, different questions also suggest additional directions for future work. For example, how will the system behave with other (practical) noise types than the white noise? How does the system respond to noise when damping coupling is added? How will the results obtained after including the damping nonlinearities in the system model compare with those from the current model? How can one combine noise and controlled imperfections to influence the system dynamics?

Bibliography

- [1] L. Gammaitoni, P. Hänggi, P. Jung, and F. Marchesoni. Stochastic resonance. *Reviews of Modern Physics*, 70(1):223, 1998.
- [2] A. Papangelo, F. Fontanela, A. Grolet, M. Ciavarella, and N. Hoffmann. Multistability and localization in forced cyclic symmetric structures modelled by weakly-coupled duffing oscillators. *Journal of Sound and Vibration*, 440:202–211, 2019.
- [3] E. Perkins and B. Balachandran. Noise-enhanced response of nonlinear oscillators. *Procedia Iutam*, 5:59–68, 2012.
- [4] E. Perkins, M. Kimura, T. Hikihara, and B. Balachandran. Effects of noise on symmetric intrinsic localized modes. *Nonlinear Dynamics*, 85(1):333–341, 2016.
- [5] I. Abed, N. Kacem, N. Bouhaddi, and M. Bouazizi. Multi-modal vibration energy harvesting approach based on nonlinear oscillator arrays under magnetic levitation. *Smart Materials and Structures*, 25(2):025018, 2016.
- [6] A. Vakakis. Dynamics of a nonlinear periodic structure with cyclic symmetry. *Acta Mechanica*, 95(1):197–226, 1992.
- [7] J. Vig and Y. Kim. Noise in microelectromechanical system resonators. *IEEE transactions on Ultrasonics, ferroelectrics, and frequency control*, 46(6):1558–1565, 1999.
- [8] F. Mohd-Yasin, D. Nagel, and C. Korman. Noise in mems. *Measurement Science and Technology*, 21(1):012001, 2009.
- [9] P. Hanggi. Escape from a metastable state. *Journal of Statistical Physics*, 42(1-2):105–148, 1986.
- [10] I. L’Heureux and R. Kapral. White noise induced transitions between a limit cycle and a fixed point. *Physics Letters A*, 136(9):472–476, 1989.

- [11] J. Gao, S. Hwang, and J. Liu. When can noise induce chaos? *Physical Review Letters*, 82(6):1132, 1999.
- [12] C. Du and L. Xie. *Modeling and control of vibration in mechanical systems*. CRC press, 2018.
- [13] S. Crandall and W. Mark. *Random vibration in mechanical systems*. Academic Press, 2014.
- [14] F. Chapeau-Blondeau. Stochastic resonance and the benefit of noise in nonlinear systems. In *Noise, Oscillators and Algebraic Randomness*, pages 137–155. Springer, 2000.
- [15] . Wiesenfeld and F. Moss. Stochastic resonance and the benefits of noise: from ice ages to crayfish and squids. *Nature*, 373(6509):33–36, 1995.
- [16] L. Gammaitoni, P. Hänggi, P. Jung, and F. Marchesoni. Stochastic resonance: a remarkable idea that changed our perception of noise. *The European Physical Journal B*, 69(1):1–3, 2009.
- [17] F. Chapeau-Blondeau and D. Rousseau. Noise improvements in stochastic resonance: From signal amplification to optimal detection. *Fluctuation and Noise Letters*, 2(03):L221–L233, 2002.
- [18] R. Mantegna and B. Spagnolo. Noise enhanced stability in an unstable system. *Physical Review Letters*, 76(4):563, 1996.
- [19] A. Dubkov, N. Agudov, and B. Spagnolo. Noise-enhanced stability in fluctuating metastable states. *Physical Review E*, 69(6):061103, 2004.
- [20] B. Spagnolo, N. Agudov, and A. Dubkov. Noise enhanced stability. *arXiv preprint cond-mat/0405392*, 2004.
- [21] S. Wang, L. Song, E. Lakatta, and H. Cheng. Ca²⁺ signalling between single l-type ca²⁺ channels and ryanodine receptors in heart cells. *Nature*, 410(6828):592, 2001.
- [22] F. Zeng, Q. Fu, and R. Morse. Human hearing enhanced by noise. *Brain research*, 869(1-2):251–255, 2000.
- [23] Z. Long, F. Shao, Y. Zhang, and Y. Qin. Noise-enhanced hearing sensitivity. *Physics Letters A*, 323(5-6):434–438, 2004.
- [24] A. Faisal, L. Selen, and D. Wolpert. Noise in the nervous system. *Nature reviews neuroscience*, 9(4):292, 2008.
- [25] M. McDonnell and L. Ward. The benefits of noise in neural systems: bridging theory and experiment. *Nature Reviews Neuroscience*, 12(7):415, 2011.

- [26] K. Richardson, T. Imhoff, P. Grigg, and J. Collins. Using electrical noise to enhance the ability of humans to detect subthreshold mechanical cutaneous stimuli. *Chaos: An Interdisciplinary Journal of Nonlinear Science*, 8(3):599–603, 1998.
- [27] F. Moss, D. Pierson, and D. O’GORMAN. Stochastic resonance: Tutorial and update. *International Journal of Bifurcation and Chaos*, 4(06):1383–1397, 1994.
- [28] C. McInnes, D. Gorman, and M. Cartmell. Enhanced vibrational energy harvesting using nonlinear stochastic resonance. *Journal of Sound and Vibration*, 318(4-5):655–662, 2008.
- [29] V. Verma and R. Yadava. Stochastic resonance in mems capacitive sensors. *Sensors and Actuators B: Chemical*, 235:583–602, 2016.
- [30] W. Horsthemke. Noise induced transitions. In *Non-Equilibrium Dynamics in Chemical Systems*, pages 150–160. Springer, 1984.
- [31] S. Sinha, J. Cruz, T. Buhse, and P. Parmananda. Exploiting the effect of noise on a chemical system to obtain logic gates. *EPL (Europhysics Letters)*, 86(6):60003, 2009.
- [32] T. Amemiya, T. Ohmori, T. Yamamoto, and T. Yamaguchi. Stochastic resonance under two-parameter modulation in a chemical model system. *The Journal of Physical Chemistry A*, 103(18):3451–3454, 1999.
- [33] H. Dankowicz, X. Zhao, and S. Misra. Near-grazing dynamics in tapping-mode atomic-force microscopy. *International Journal of non-linear mechanics*, 42(4):697–709, 2007.
- [34] W. Chin, E. Ott, H. Nusse, and C. Grebogi. Grazing bifurcations in impact oscillators. *Physical Review E*, 50(6):4427, 1994.
- [35] A. Dick, B. Balachandran, H. Yabuno, M. Numatsu, K. Hayashi, M. Kuroda, and K. Ashida. Utilizing nonlinear phenomena to locate grazing in the constrained motion of a cantilever beam. *Nonlinear Dynamics*, 57(3):335–349, 2009.
- [36] I. Chakraborty and B. Balachandran. Noise influenced elastic cantilever dynamics with nonlinear tip interaction forces. *Nonlinear Dynamics*, 66(3):427–439, 2011.
- [37] L. Meirovitch. *Fundamentals of vibrations*. Waveland Press, 2010.
- [38] K. Furuta, M. Yamakita, and S. Kobayashi. Swing-up control of inverted pendulum using pseudo-state feedback. *Proceedings of the Institution of Mechanical Engineers, Part I: Journal of Systems and Control Engineering*, 206(4):263–269, 1992.

- [39] S. Huang and C. Huang. Control of an inverted pendulum using grey prediction model. *IEEE Transactions on Industry Applications*, 36(2):452–458, 2000.
- [40] M. Levi and W. Weckesser. Stabilization of the inverted linearized pendulum by high frequency vibrations. *SIAM review*, 37(2):219–223, 1995.
- [41] D. Acheson. A pendulum theorem. *Proceedings of the Royal Society of London. Series A: Mathematical and Physical Sciences*, 443(1917):239–245, 1993.
- [42] E. Perkins and B. Balachandran. Noise-influenced dynamics of a vertically excited pendulum. In *ASME 2013 International Design Engineering Technical Conferences and Computers and Information in Engineering Conference*, pages V07BT10A025–V07BT10A025. American Society of Mechanical Engineers, 2013.
- [43] M. Marszal, B. Witkowski, K. Jankowski, P. Perlikowski, and T. Kapitaniak. Energy harvesting from pendulum oscillations. *International Journal of Non-Linear Mechanics*, 94:251–256, 2017.
- [44] C. Gan. Noise-induced chaos in duffing oscillator with double wells. *Nonlinear Dynamics*, 45(3-4):305–317, 2006.
- [45] Y. Xu, R. Gu, H. Zhang, W. Xu, and J. Duan. Stochastic bifurcations in a bistable duffing–van der pol oscillator with colored noise. *Physical Review E*, 83(5):056215, 2011.
- [46] V. Agarwal and B. Balachandran. Noise-influenced response of duffing oscillator. In *ASME 2015 International Mechanical Engineering Congress and Exposition*, pages V04BT04A019–V04BT04A019. American Society of Mechanical Engineers, 2015.
- [47] V. Agarwal, X. Zheng, and B. Balachandran. Influence of noise on frequency responses of softening duffing oscillators. *Physics Letters A*, 382(46):3355–3364, 2018.
- [48] A. Sievers and S. Takeno. Intrinsic localized modes in anharmonic crystals. *Physical Review Letters*, 61(8):970, 1988.
- [49] J. Marin, S. Aubry, and L. Floria. Intrinsic localized modes: discrete breathers. existence and linear stability. *Physica D: Nonlinear Phenomena*, 113(2-4):283–292, 1998.
- [50] A. McGurn. Intrinsic localized modes in nonlinear photonic crystal waveguides. *Physics Letters A*, 251(5):322–335, 1999.
- [51] Y. Kivshar. Nonlinear localized modes in inhomogeneous chains. *Physics Letters A*, 161(1):80–84, 1991.

- [52] A. Lagendijk, B. Van Tiggelen, and D. Wiersma. Fifty years of anderson localization. *Phys. Today*, 62(8):24–29, 2009.
- [53] D. Hundertmark. A short introduction to anderson localization. *Analysis and Stochastics of Growth Processes and Interface Models*, 1:194–219, 2008.
- [54] S. Flach and C. Willis. Discrete breathers. *Physics Reports*, 295(5):181–264, 1998.
- [55] D. Campbell, S. Flach, Y. Kivshar, et al. Localizing energy through nonlinearity and discreteness. *Physics Today*, 57(1):43–49, 2004.
- [56] A. McGurn. Intrinsic localized modes in photonic crystal waveguides composed of a periodic mixed array of linear and kerr nonlinear dielectric media. *Physica D: Nonlinear Phenomena*, 216(1):103–114, 2006.
- [57] M. Sato and A. Sievers. Direct observation of the discrete character of intrinsic localized modes in an antiferromagnet. *Nature*, 432(7016):486, 2004.
- [58] Y. Starosvetsky and A. Vakakis. Traveling waves and localized modes in one-dimensional homogeneous granular chains with no precompression. *Physical Review E*, 82(2):026603, 2010.
- [59] S. Wallen, C. Chong, P. Kevrekidis, and N. Boechler. Discrete breathers in a one-dimensional granular metamaterial: Linear lattice with nonlinear local resonators. In *2014 International Symposium on Optomechatronic Technologies*, pages 15–17. IEEE, 2014.
- [60] M. Porter, P. Kevrekidis, and C. Daraio. Granular crystals: Nonlinear dynamics meets materials engineering. *Physics Today*, 68(LA-UR-15-21727), 2015.
- [61] M. Byrne and M. Porter. *Nonlinear waves in granular lattices*. PhD thesis, University of Oxford, 2009.
- [62] A. Dick, B. Balachandran, and C. Mote. Intrinsic localized modes in microresonator arrays and their relationship to nonlinear vibration modes. *Nonlinear Dynamics*, 54(1-2):13–29, 2008.
- [63] M. Kimura and T. Hikiyara. Experimental manipulation of intrinsic localized modes in macro-mechanical system. *Nonlinear Theory and Its Applications, IEICE*, 3(2):233–245, 2012.
- [64] Q. Chen, L. Huang, Y. Lai, and D. Dietz. Dynamical mechanism of intrinsic localized modes in microelectromechanical oscillator arrays. *Chaos: An Interdisciplinary Journal of Nonlinear Science*, 19(1):013127, 2009.
- [65] M. Sato, B. Hubbard, A. Sievers, B. Ilic, D. Czaplewski, and H. Craighead. Observation of locked intrinsic localized vibrational modes in a micromechanical oscillator array. *Physical Review Letters*, 90(4):044102, 2003.

- [66] M. Kimura and T. Hikihara. Capture and release of traveling intrinsic localized mode in coupled cantilever array. *Chaos: An Interdisciplinary Journal of Nonlinear Science*, 19(1):013138, 2009.
- [67] M. Kimura and T. Hikihara. Coupled cantilever array with tunable on-site nonlinearity and observation of localized oscillations. *Physics Letters A*, 373(14):1257–1260, 2009.
- [68] T. Ikeda, Y. Harata, and K. Nishimura. Intrinsic localized modes of harmonic oscillations in nonlinear oscillator arrays. *Journal of Computational and Nonlinear Dynamics*, 8(4), 2013.
- [69] M. Sato, B. Hubbard, L. English, A. Sievers, B. Ilic, D. Czaplewski, and H. Craighead. Study of intrinsic localized vibrational modes in micromechanical oscillator arrays. *Chaos: An Interdisciplinary Journal of Nonlinear Science*, 13(2):702–715, 2003.
- [70] R. Harne and K. Wang. A review of the recent research on vibration energy harvesting via bistable systems. *Smart Materials and Structures*, 22(2):023001, 2013.
- [71] A. Papangelo, A. Grolet, L. Salles, N. Hoffmann, and M. Ciavarella. Snaking bifurcations in a self-excited oscillator chain with cyclic symmetry. *Communications in Nonlinear Science and Numerical Simulation*, 44:108–119, 2017.
- [72] G. Hunt, M. Peletier, A. Champneys, P. Woods, M. Wadee, C. Budd, and G. Lord. Cellular buckling in long structures. *Nonlinear Dynamics*, 21(1):3–29, 2000.
- [73] O. Batiste, E. Knobloch, A. Alonso, and I. Mercader. Spatially localized binary-fluid convection. *Journal of Fluid Mechanics*, 560:149, 2006.
- [74] C. Beaume, A. Bergeon, and E. Knobloch. Homoclinic snaking of localized states in doubly diffusive convection. *Physics of Fluids*, 23(9):094102, 2011.
- [75] S. Ramakrishnan and B. Balachandran. Energy localization and white noise-induced enhancement of response in a micro-scale oscillator array. *Nonlinear Dynamics*, 62(1-2):1–16, 2010.
- [76] E. Doedel, A. Champneys, T. Fairgrieve, Y. Kuznetsov, B. Sandstede, and X. Wang. Auto 97: Continuation and bifurcation software for ordinary differential equations (with homcont). 1997.
- [77] R. Rosenberg. The normal modes of nonlinear n-degree-of-freedom systems. 1962.
- [78] S. Shaw and C. Pierre. Normal modes for non-linear vibratory systems. *Journal of Sound and Vibration*, 164(1):85–124, 1993.

- [79] S. Karkar, B. Cochelin, C. Vergez, O. Thomas, and A. Lazarus. User guide manlab 2.0. Technical report, Technical report, Laboratoire de Mécanique et d'Acoustique (LMA), CNRS UPR 7051, 2012.
- [80] B. Cochelin, N. Damil, and M. Potier-Ferry. Asymptotic–numerical methods and pade approximants for non-linear elastic structures. *International Journal for Numerical Methods in Engineering*, 37(7):1187–1213, 1994.
- [81] A. Nayfeh and B. Balachandran. *Applied nonlinear dynamics: analytical, computational, and experimental methods*. John Wiley & Sons, 2008.
- [82] D. Higham. An algorithmic introduction to numerical simulation of stochastic differential equations. *SIAM Review*, 43(3):525–546, 2001.
- [83] J. Marin and S. Aubry. Breathers in nonlinear lattices: numerical calculation from the anticontinuous limit. *Nonlinearity*, 9(6):1501, 1996.
- [84] N. Senan. A brief introduction to using ode45 in matlab. *University of California at Berkeley, USA*, 2007.